BINDING MECHANISM OF PHEROMONE-BINDING PROTEINS FROM THE GYPSY MOTH, *LYMANTRIA DISPAR*

by

Yongmei Gong
Bachelor of Science, Peking University 2003

THESIS SUBMITTED IN PARTIAL FULFILLMENT OF
THE REQUIREMENTS FOR THE DEGREE OF

DOCTOR OF PHILOSOPHY

In the
Department of Chemistry

SIMON FRASER UNIVERSITY

Fall 2009

APPROVAL

Name: **Yongmei Gong**

Degree: **Doctor of Philosophy**

Title of Thesis: **Binding Mechanism of Pheromone-Binding Proteins from the Gypsy Moth, *Lymantria dispar***

Examining Committee:

Chair: **Paul C.H. Li**
Associate Professor, Department of Chemistry

_____

Erika Plettner
Senior Supervisor
Associate Professor, Department of Chemistry

_____

David Vocadlo
Supervisor
Associate Professor, Department of Chemistry

_____

Rosemary B. Cornell
Supervisor
Professor, Department of Molecular Biology and Biochemistry/Chemistry

_____

Nancy Forde
Internal Examiner
Assistant Professor, Department of Physics

_____

Dean P. Smith
External Examiner
Associate Professor, Department of Pharmacology, University of Texas Southwestern Medical Center

Date Defended/Approved: September 24, 2009

Declaration of
Partial Copyright Licence

ABSTRACT

Pheromone perception in insects plays important roles for their survival and development. They communicate with the environment through sensing and releasing signal molecules, such as host odors or sex pheromones.

Pheromone-binding proteins (PBPs) are among the indispensable components of the olfactory system in insects. For example, fly mutants lacking a PBP do not respond to a stimulus of pheromone. PBPs bind pheromone. There are accumulating data on the binding strength and structure. Yet, not until recently has the PBP binding been bridged to its function: a PBP mutant locked in the active conformation found in the PBP.pheromone complex has been shown to stimulate the sensory neurons, even in the absence of pheromone.

In this work, I have kinetically dissected the interaction between PBP and ligand, for two PBPs from the gypsy moth, *Lymantria dispar*: PBP1 and PBP2. Starting with PBP2 and its cognate ligand, (+)-disparlure, I have identified a slow process following a fast interaction. A subsequent study with a fluorescent dye has further identified a diffusion-controlled step prior to a unimolecular relaxation process. Both studies suggest that insect PBPs bind ligand progressively. I have proposed a model that PBP and ligand collide to form an encountered intermediate, $P.L_{enc}$, followed by a decay of this species to two stable P.L complexes: external $P.L_{ext}$ and internal $P.L_{int}$. Each of these two binding modes of ligand to PBP may correspond to a different function of the PBP. In addition,

tryptophan quenching experiments have shown different local conformational changes upon ligand binding. Parallel experiments with truncated PBPs lacking the C-terminal peptide have demonstrated the importance of that segment in PBP function.

Efforts have been put to correlate the binding affinity, blend effect and conformation of the LdisPBPs in the presence of synthetic compounds with the effects these compounds have on the electroantennogram (EAG) traces of pheromone stimuli. No correlation was found between affinity of the compounds and short-term/long-term effects of the compounds on the EAG trace. Two subsets of compounds showed a correlation between blend effects and EAG peak broadening. The interpretation is that certain compounds might stabilize the active PBP.L conformation.

Keywords: pheromone-binding protein; insect; gypsy moth; kinetics; interaction mechanism; pheromone selectivity

给我亲爱的父母，龚本君，龚亚萍：

谢谢你们这么多年默默的支持和爱护！

To my dear parents, Benjun Gong and Yaping Gong, for your love and support.

In life's earnest battle they only prevail
Who daily march onward and never say fail.

- Charles Swain (1901)

ACKNOWLEDGEMENTS

In my graduate studies, I have accepted enormous help from many people, especially my senior supervisor, Dr. Erika Plettner. I am very grateful for her complete support in both my research and life. I have learned from her the qualities to be an excellent scientist, as well as a supervisor. I would also like to thank my supervisory committees, Dr. David Vocadlo and Dr. Rosemary B. Cornell, for their guidance, constructive suggestions and discussions. I thank Dr. Paul Li for chairing my defense, Dr. Nancy Forde and Dr. Dean Smith for being my thesis examiners and their valuable comments on my thesis.

I am thankful to Dr. Melanie A. O'Neill and Dr. Steven Holdcroft, for their generosity of letting me use their fluorimeters, and for the time Dr. O'Neill took to help me optimize the experimental conditions. I thank our collaborator Dr. Cornelia Bohne and her graduate students Ms. Tamara C.S. Pace and Mr. Hao Tang, for performing the lifetime measurements of tryptophan and stopped-flow experiments, as well as their valuable comments. Many thanks to Ms. Jane Huang, for the peptide mapping analysis, Ms. Regine Gries, for performing the EAG tests, Mr. Duncan Napier, for conducting the light-scattering experiments, Mr. Benjamin Hon, for teaching me the usage of the CD instrument, and Dr. Andrew Lewis, for testing the NMR of fluorinated disparlure. I also thank Mr. Qi Yang, for the help with mathematics on page 83.

Help and support from Plettner group are much appreciated. I especially thank Dr. Nicolette Honson for her generous help to me to start my study at SFU. She has set up an example for me in many ways. Ms. Ewa Sokolow, Ms. Jie Zhang and Dr. Carlos Castillo are thanked for preparing the proteins. I would like to thank all the past and present group members, for their precious friendship, Dr. Adina Rojuabally, Ms. Taraneh Lajevardi, Mr. Martin Mwangi, Ms. Sheila Smith, Dr. Ranjeet Nair, Dr. Srinivas Nagabandi, Dr. Anoma Mudalige, Dr. Peggy A. Paduraru, Dr. Hao Chen, Dr. Yang Yu, Mr. Richard T.W. Popoff, Ms. Brinda Prasad, and all the lovely co-op students.

I am indebted to Mr. Xu Han, for proofreading of my thesis, for preparing cover images for the chapters, and for all the other supports.

TABLE OF CONTENTS

LIST OF FIGURES

LIST OF TABLES

LIST OF ABBREVIATIONS

Abbreviation	Meaning
3D	Three dimensional
9-ODA	(E)-9-oxodec-2-enoic acid
ABSF	4-(2-aminoethyl)benzenesulfonyl fluoride
AC	Adenylyl cyclase
AMA	1-aminoanthracene
ANS	8-anilino-1-naphtalenesulphonic acid
Asp	Aspartate
AU	Arbitrary unit
cAMP	Cyclic adenosine monophophate
CD	Circular dichroism
CHAPS	3-[(3-Cholamidopropyl)dimethylammonio]-1-propanesulfonate
cVA	*cis*-vaccenyl acetate (11(Z)-octadec-11en-1-yl acetate)
Cys/C	Cysteine
DMSO	Dimethyl sulfoxide
DNS	Dansyl
DTT	Dithiothreitol
EAG	Electroantennogram
EDTA	Ethylenediaminetetracetic acid
EtOH	Ethanol
FID	Flame-ionization detector
FPLC	Fast protein liquid chromatography
GC	Gas chromatography
GDP-β-S	Guanosine- 5'- O- (2- thiodiphosphate)
GOBP	General odorant-binding protein
GPCR	G-protein-coupled receptor
H3B2	3-hydroxyl-2-butanone

HEK	Human embryonic kidney
IPTG	Isopropyl-β-D-thiogalactopyranoside
K_d	Dissociation constant
kDa	Kilodalton
K_i	Dissociation constant for inhibitor binding
LTI	Long-term inhibition
Lys/K	Lysine
MALDI	Matrix assisted laser desorption ionization
MES	2-(N-morpholino)ethanesulfonic acid
nBBSA	n-Butyl benzenesulfonamide
NMR	Nuclear magnetic resonance
NPN	N-phenyl-1-naphthylamine
OBP	Odorant-binding protein
OR	Odorant receptor
PAGE	Polyacrylamide gel electrophoresis
PB	Peak broadening
PBP	Pheromone-binding protein
PCR	Polymerase chain reaction
PDB	Protein data bank
PDE	Pheromone-degrading enzyme
PMSF	Phenylmethylsulfonyl fluoride
SDS	Sodium dodecyl sulfate
SNMP	Sensory neuron membrane protein
STI	Short-term inhibition
TFA	Trifluoroacetic acid
Trp/W	Tryptophan
Tyr/Y	Tyrosine
Val/V	Valine
ε	Extinction coefficient

CHAPTER 1 INTRODUCTION

1.1 Olfaction Pathway of Insects

Olfaction (the sense of smell) plays an important role in insects. They rely on olfaction for searching for food, finding a prospective mate and communication with each other. Insects interact with the environment by sensing and emanating semiochemicals, chemical messages, which are composed of volatile organic molecules. There are two parts of the insect olfactory system: one for general odorant detection and one for pheromone detection. The second one is highly specifically tuned for each species and will be my focus in this work.

1.1.1 An Overview of Various Pheromonal Compounds

Pheromones are a subclass of semiochemicals used for communication within species [1]. This subclass can be further divided by function, such as sexual pheromones, aggregation pheromones and alarm pheromones. Semiochemicals used for interspecific communication are called allelochemicals. They are composed of three classes of chemicals based on the costs and the benefits to signaller and receiver. The semiochemicals that benefit the receiver at the cost of the signaller are kairomones; allomones are the other way around, and synomones benefit both sides. Overall, semiochemicals are signal molecules released by one individual, detected by a second individual, and they elicit characteristic behavior (releasers) or long-term physiological changes (primers)[2,3].

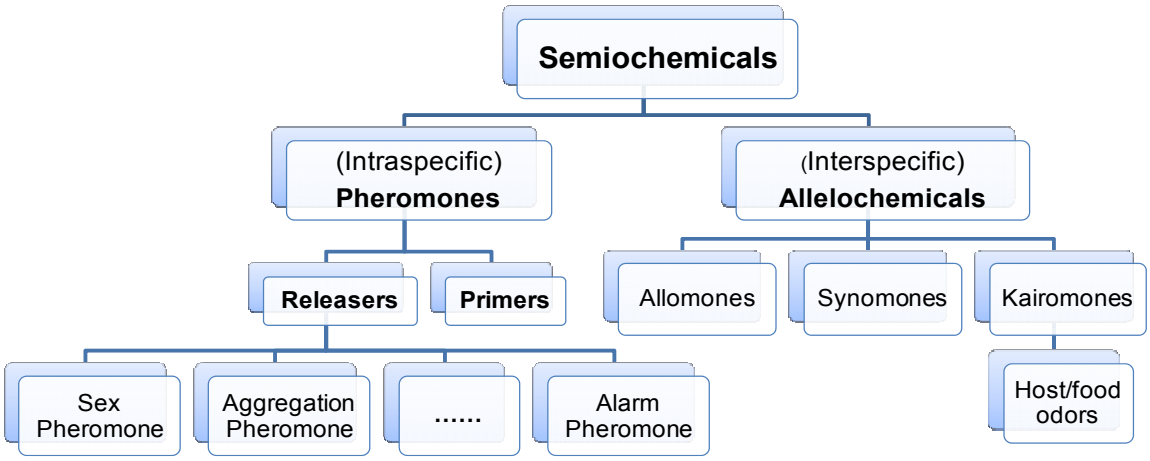

It was long before the first pheromone was discovered that people had already realized the importance of chemical cues in insect communication. In the 19th century, the French naturalist Jean-Henri Fabre found that a virgin female emperor moth (*Saturnia pavonia*) could attract many males even though it was covered [1]. One hundred years later, in 1959, the first pheromone, (E,Z)-10,12-hexadecadien-1-ol (bombykol) (1) was purified from 500,000 female silk moths (*Bombyx mori*)[4]. After that, pheromone blends of ants, bees, beetles, cockroaches, flies, grasshoppers, moths and termites have been identified and used to underline their importance in insects' sexual and social communication. We use the term "pheromone blends", because most commonly, insects use a unique blend of compounds to achieve specificity. For example, the wild silk moth, *Antheraea polyphemus*, uses a mixture of 90% (E, Z)-6,11-hexadecadien-1-yl acetate (2) and 10% (E, Z)-6,11-hexadecadienal as the sex pheromone [5]. The male cockroach, *Nauphoeta cinerea*, uses a mixture of 2-methyl thiazolidine (3) and 4-ethylguaiacol (4), 7:1 ratio, to attract the females from a distance, and

another compound, 3-hydroxy-2-butanone (H3B2) (5), at close range to keep the female in the vicinity of the male [6].

Pheromone components have diverse structures (Figure 1-1)[7]. Many moth pheromones usually have a long hydrocarbon chain, often with some oxygen containing functional group, such as epoxide or aldehyde, and one or two unsaturated bonds or methyl branches, to cover certain range of active conformations [8-10]. Cockroach pheromones often have a more complex variation of the basic structural motif. For example, the brownbanded cockroach (*Supella longipalpa*) uses 5-(2R,4R-dimethylheptanyl)-3-methyl-2H-pyran-2-one (supellapyrone) (6) as the sex pheromone [11,12].

Closely related species employ different pheromone blends in a subtle way. For example, (7R, 8S)-*cis*-2-methyl-7, 8-epoxyoctadecane ((+)-disparlure) (7) is the major component of the sex pheromone of the gypsy moth, *Lymantria dispar*. A closely related moth species, nun moth (*L. monacha*), uses a mixture of (±)-disparlure and (±)-monachalure (7,8-epoxyoctadecane) (8) as the sex pheromone [13]. The (-)-disparlure is neither attractive nor repellent to gypsy moth by itself, but when presented simultaneously with (+)-disparlure, it cancels upwind flight behavior in the males [14]. *Heliothis* species have the same unsaturated aldehyde as the major pheromone component but different proportions of the minor components [7].

The extreme sensitivity and specificity of the insect olfactory system becomes apparent when we notice the subtle differences in the pheromone structures and compositions. Regardless of the difference in the components of

the pheromone blends, insects are capable of discriminating different stereoisomers and the chirality of the pheromone compounds plays a significant role in insect olfactory discrimination [15]. Besides gypsy moth, another example of enantiomers being used as the sex pheromone is in olive fruit flies, *Dacus oleae*. During the mating season, the females emit racemic 1,7-dioxaspiro[5.5]undecane (olean) (9). Interestingly, the (R)-isomer attracted the males in both laboratory and field tests and the (S)-isomer induced responses of the females only in the laboratory tests. The (S)-isomer may act as a short-range arrestant and an aphrodisiac in the process of mating [16].

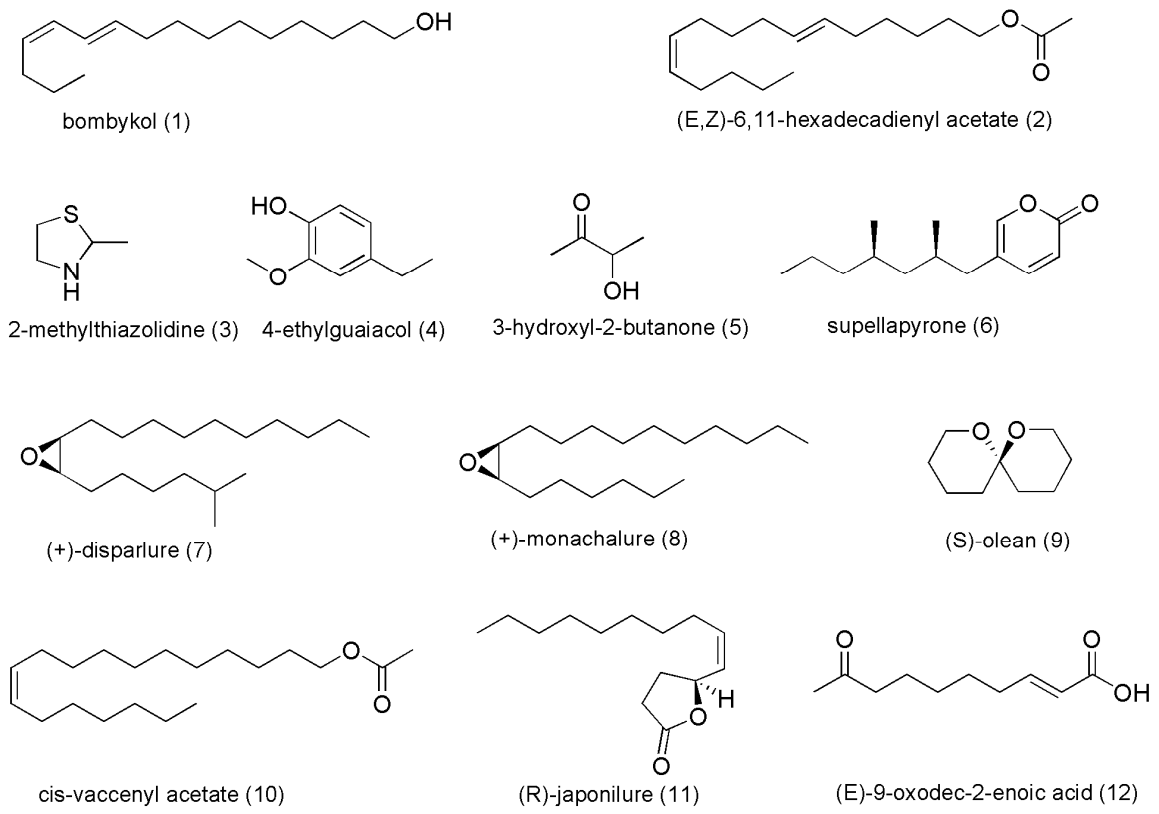

Figure 1-1 Structures of various pheromones mentioned in Chapter 1.

It is remarkable how insects achieve such a simple, yet highly effective communication system. Key components of this system are the biosynthesis of semiochemicals by the emitter and the detection of the signals by the receiver. In the past few decades, numerous fundamental studies of semiochemical detection have been done, initially on the moth antennal olfactory system, because moths have large antennae. Recently, groundbreaking discoveries have been made in *Drosophila melanogaster* because their genome [17], brain[18] and the antennal/mouthparts [19,20] are well characterized. Another developing field that is based on the highly selective and sensitive communication system of insects, is the growing number of applications of insect pheromones in pest management, including mating disruption and monitoring with traps [21,22].

1.1.2 Antenna: Perireceptor Events

The insects have developed a highly sensitive and selective pheromone perception system. A male moth can follow the chemical cues up to miles to locate the source [23,24]. The silk moth responds to a behavioral threshold concentration of the pheromone of ~1 pM/s [25]. An antenna is the place where the chemical messages carried by the pheromone ligands are collected, classified and transformed into an ion gradient potential signal that will be recognized and integrated by the central nervous system. The antennae of insects have evolved to be powerful chemoreceptors. For example, studies with moths have shown that the antenna acts as sieve for catching up to 30% of the pheromone

molecules in a stream of air [26]. The highly branched feather-like antennae are densely covered with sensory hairs (sensilla) and the pheromones are detected by specific olfactory neurons in the long hairs on the antenna, which are called *sensilla trichodea*. The hollow cuticular long *sensilla trichodea* are usually innervated by two to three unbranched dendrites of olfactory neurons and are filled with the sensillum lymph, a solution rich in proteins (pheromone-binding proteins (PBPs) and pheromone-degrading enzymes (PDEs)) and fatty acids, such as palmitic acid (0.19 M), linoleic acid (1.31 M) and stearic acid (0.09 M) [27]. PBPs are small, acidic, soluble proteins of ~13-16 kDa, that bind pheromone components (also see section 1.2). PBPs are the most abundant protein in the sensillar lymph (Figure 1-2). This is the environment in which the perireceptor events of pheromone detection take place.

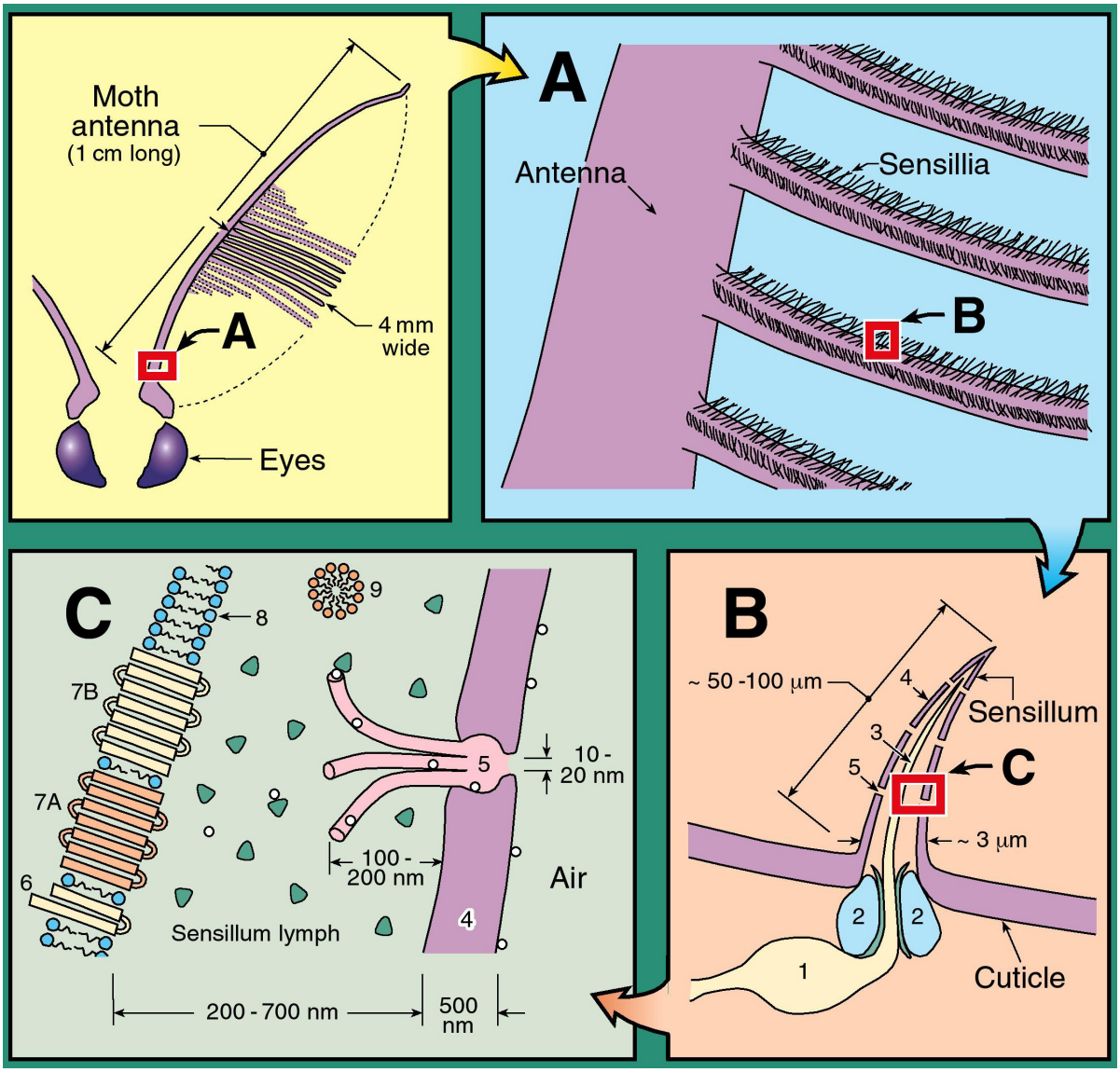

Figure 1-2 Schematic illustrations of the moth olfactory system.

(A). A close view of the hairy branches of moth antenna. (B). Diagram of the olfactory sensillum (1. olfactory receptor neuron; 2. auxillary supporting cells; 3.dendrite of an olfactory receptor neuron projecting into the hollow space of the sensillum; 4. cuticle wall of the hair; 5. cuticular pores). (C). The peripheral components of the sensillum trichodeum (6. sensory neuron membrane protein (SNMP); 7. olfactory receptor and co-receptor; 8. phospholipid bilayer of the neuronal membrane; 9. micelles formed by fatty acids. Δ: pheromone-binding proteins (PBPs); o: pheromone molecules). The pheromone molecules adsorbed on the cuticle wall of the sensillum migrate along the surface into the pore canal penetrating the cuticle and diffuse through the pore tubules into the sensillum lymph. PBPs come to interact with the ligands. The pheromone molecule may diffuse by itself through the barrier to associate with the membrane protein and then activate the receptor[28]. Alternatively, ligand can either activate the PBP[29] or be delivered by the micelles[27]. Adapted from (Gong et al., 2009) [30] with permission.

A perireceptor event was first suggested in the vertebrate olfaction system to describe all the biophysical and biochemical processes in the nasal mucus, the aqueous interface surrounding the olfactory receptor neurons (ORNs)[31]. Later, perireceptor events were invoked for the invertebrate system, to explain interactions between an odorant molecule and other sensillum lymph components before it reaches the ORNs [32]. When a pheromone molecule is trapped on the surface of the antenna, it hardly desorbs to any measureable extent for the first few seconds [26]. The adsorbed molecule then diffuses along the surface to the pores that penetrate the sensory hair, through the pore tubules and into the interior. The pore tubules are mechanically stable structures that may or may not be in direct contact with the sensory neuron dendrite [33,34] (Figure 1-2C). The pore tubules are assumed to be composed of lipids and proteins but this assumption has not been verified [33]. From here, there are different hypotheses regarding the pathway of pheromone reception, from the cuticle to the dendrite of the neuron (Figure 1-2).

As we know, a hypothesis consists either of a suggested explanation for an observable phenomenon or of a reasoned proposal predicting a possible causal correlation among multiple phenomena. The phenomena we have observed or the phenomena a successful hypothesis has to satisfy in the understanding of insect pheromone perception include three aspects: first, efficiency in pheromone detection and signal inactivation; second, slow degradation of pheromone molecules *in vivo* and third, rapid degradation of pheromone molecules by PDEs. In odorant-mediated flights, insects can respond

to a signal lost in 0.1-0.5 s [35]. They must reset their olfactory systems quickly to detect intermittent signals encountered while flying. Electroantennogram (EAG) studies have revealed rapid decay of the receptor potential of the neurons after a stimulus[26]. Therefore, the message carried by a pheromone needs to be delivered quickly and terminated quickly. Once a pheromone has activated the sensory neuron, it should be degraded or removed to avoid reactivation. Male antenna-specific PDEs have been proposed as good candidates to explain the rapid cessation of the pheromone signal. For example, ApolPDE can degrade the pheromone at a half-life rate of less than 15 ms [36]. However, this seems contrary to the observation that pheromone degradation on whole antennae is very slow, with half-lives uniformly detected in minutes for several moth species (*B. mori*, *A. polyphemus* and *L. dispar*) [37-39]. One explanation for this inconsistency is the slow migration of the pheromone into the interior of the sensory hair and the possibility that not all of the pheromone molecules adsorbed on the antennae can reach the sensillum lymph in a short time. Another option is that PBPs are somehow involved in signal termination.

Two hypotheses to explain pheromone transport and removal/deactivation in the perireceptor space have been proposed: 1) that PBPs deactivate pheromone non-enzymatically or 2) that PBPs actively transport hydrophobic pheromones to the dendrite. The first hypothesis was articulated by Kaissling in 1974 when the PBPs were not discovered yet. In this model, the pheromone molecules crossed the sensillum lymph via the lipophilic pore tubules (as suggested by Steinbrecht and Muller in 1971 [40]), activated the sensory neurons

and then were quickly deactivated through non-enzymatic degradation process [41]. These non-enzymatic processes were later suggested to be assisted by PBPs [42,43]. In the second hypothesis, it was suggested that PBPs acted as a solubilizer to assist the pheromone transport through the sensillum lymph to the sensory neurons. The pore tubules provided a larger surface in this case to facilitate the interactions between the PBPs and the pheromone molecules [34]. In addition, PBPs were suggested as a protector of the pheromone molecules, to prevent them from competing enzymatic degradation by lymph PDEs [44]. The last model was based on ester pheromones (such as (2) in *A. polyphemus*), which are rapidly degraded by lymph esterases after the stimulation of the odorant receptors [36].

All models of PBP function are based on one fact: PBPs can bind pheromone ligands and other small molecules. Back to 1970s, when little was known about the pheromone structures, Riddiford first successfully demonstrated the interaction between the radiolabeled pheromone from the female *A. pernyi* and the male specific antennal protein (later renamed as AperPBP) [45]. Since then, numerous studies have built up the ligand-binding database of PBPs from different species, with either radioactive ligand techniques, fluorescence titration assays, or gas chromatography (GC) [46]. PBPs can selectively bind many compounds, which will be discussed in Section 1.2. However, the proposed functions of PBPs seem contradictory: hypothesis one suggests that PBPs act as deactivators and hypothesis two suggests that PBPs act as transporters and activators of pheromone responses. The seemingly contradictory functions have

been recently reconciled in a third hypothesis that different conformational or binding states can serve the two opposite functions. In a specific, ligand-bound conformation, the PBP.ligand complex, PBP.L, activates the neuronal dendrite [29], while in non-activating conformations, PBP.L effectively removes the ligand. The latter scavenging function may prevent saturation of receptors at high ligand doses [47]. The former function has been elegantly demonstrated recently, with a PBP from *D. melanogaster* (LUSH) and an aggregation pheromone, (Z)-11-octadecenyl-1-*acetate* (*cis*-vaccenyl acetate, (cVA)) (10). The LUSH.cVA complex can present itself as a ligand to stimulate the odorant receptor [29].

As another important sensillum component, PDE did not draw as much attention as the PBP since the first PDE, a sensilum esterase, was co-identified with the PBP from the *A. polyphemus* in 1981 [48]. A PDE is an enzyme that has selectively evolved to degrade pheromone molecules and resides in a space that is relevant to pheromone detection [49]. PDEs degrade the pheromone quickly. In *A. polyphemus*, which has a two-component pheromone consisting of 9:1 ratio of acetate: aldehyde [5], ApolPDE selectively degrades the acetate component with an estimated *in vivo* half-life of 15 ms [36]. ApolPDE was isolated, cloned and expressed recently, showing a much faster catalyzing rate (k_{cat} = 127 s^{-1}) compared to the native enzyme isolated directly from gels (k_{cat} = 0.033 s^{-1}) [50]. The next identified PDE was an antenna-specific aldehyde oxidase from *Manduca sexta*. The *in vivo* half-life of its pheromone components that were exclusively aldehydes was estimated at around 0.6 ms in the presence of MsexAOX [51]. Many species use pheromone components with chemically diverse

functional groups, therefore, they presumably require multiple PDEs. Similar oxidases were identified in antennal extracts from *A. polyphemus* and *B. mori*. Both of them were able to degrade bombykal (the aldehyde form of bombykol and the minor component of *B. mori* pheromone) and were abundant in both male and female antennae [52]. Another characterized PDE was from the Japanese beetle, *Popillia japonica*. *P. japonica* females release (R,Z)-5-(-)-(1-decenyl)oxacyclopentan-2-one ((R)-japonilure) (11) as the attractant [53]. (S)-japonilure is the behavioral antagonist to *P. japonica* but is used by a related species Osaka beetle, *Anomala osakana*, as the sex pheromone [54]. Recombinant PjapPDE, an esterase, is able to selectively degrade (R)- and (S)-japonilure with half-lives of 30 and 81 ms, respectively [55]. ApolPDE and PjapPDE have similar molecular weight of around 60 kDa [48,55]. MsexAOX is relatively larger as of 295 kDa [51]. In addition to the soluble PDEs, there are other types of enzymes, such as the antennal specific epoxide hydrolase from *L. dispar*, which might be membrane-bound [56,57].

These PDEs, and the PBPs must somehow interact in the sensillar lymph, to balance enzymatic pheromone degradation with the transport, activation and scavenging functions proposed for PBPs. How PDEs and PBPs interact is not known. As a first step, it was important for my work to understand the kinetic mechanism of PBP-pheromone interaction.

1.1.3 Neurons: Receptor Events

In insects, each olfactory sensory neuron expresses one to three ligand-binding members of the olfactory receptor gene family, along with the highly conserved and broadly expressed Or83b family subunit. Studies have shown that functional odorant receptors (ORs) are heteromeric complexes composed of at least one variable odorant binding subunit and one Or83b family subunit (Figure 1-2C). The stoichiometry of each subunit remains unknown. Insect ORs have seven transmembrane domains and were initially assumed to be G-protein-coupled receptors (GPCRs), like ORs in vertebrates. A classical GPCR can activate the G-protein and trigger the production of the second messenger through conformational changes induced by a functional ligand. However, there is little homology between insect ORs and those of other species. After the OR genes were first identified in the rat in 1991 [58], for almost a decade there was no success in identifying the insect homologs of vertebrate ORs with the method of polymerase chain reaction (PCR) cloning. Until 1999, putative insect ORs were identified in *Drosophila* based on a bioinformatics scan [59-61].

The insect olfactory system may use a distinct signalling mechanism. It has been found that the *Drosophila* ORs not only share no apparent sequence similarity to ORs in vertebrates, but also adopt a different membrane topology with the N-termini and the most conserved loops within the cell and the C-termini at the external cell surface (Figure 1-3) [62], while for classical GPCRs, it is vice versa. Recently, it has been demonstrated from two groups that the insect ORs act as odorant-gated non-selective ion channels [63,64]. Coexpression of the

Drosophila tuning OR and Or83b in vertebrate cells confers odor-sensitive ion currents and the currents have been detected by outside-out patch-clamp recordings, possibly produced directly by the insect ORs. However, it is still controversial whether a G-protein-coupled-pathway is involved or not [65]. Wicher and colleagues have found an increase in the intracellular cAMP concentration upon odorant stimulation of the OR complex. The increased level of cAMP indicates a G-protein-coupled pathway. In addition, G proteins from the G_q family have been localized by microscopy to the dendrites of moth sensilla [66]. In Wicher's study (2008), a membrane permeable cAMP analogue was able to induce a similar current in cells expressing Or83b alone but not the tuning OR, indicating that the cAMP mediates gating of the OR complexes through Or83b (Figure 1-3). The application of the G-protein inhibitor, GDP-β-S, reduced the OR sensitivity by a factor of ~100. Therefore, these researchers have proposed a dual mode of OR activation: a slow but highly sensitive pathway via G-protein-coupled signal amplification at low ligand concentrations and a very rapid pathway through direct ligand activation at high ligand concentrations [64]. However, the cAMP sensitivity was not observed by Sato and colleagues. They propose that the insect OR complexes are ligand-gated ion-channels (Figure 1-3, path 2), while Wicher et al. suggest that, in addition to that, the OR complexes are also ion channels activated by cyclic nucleotide (path 1). More experiments would be required to make this clear.

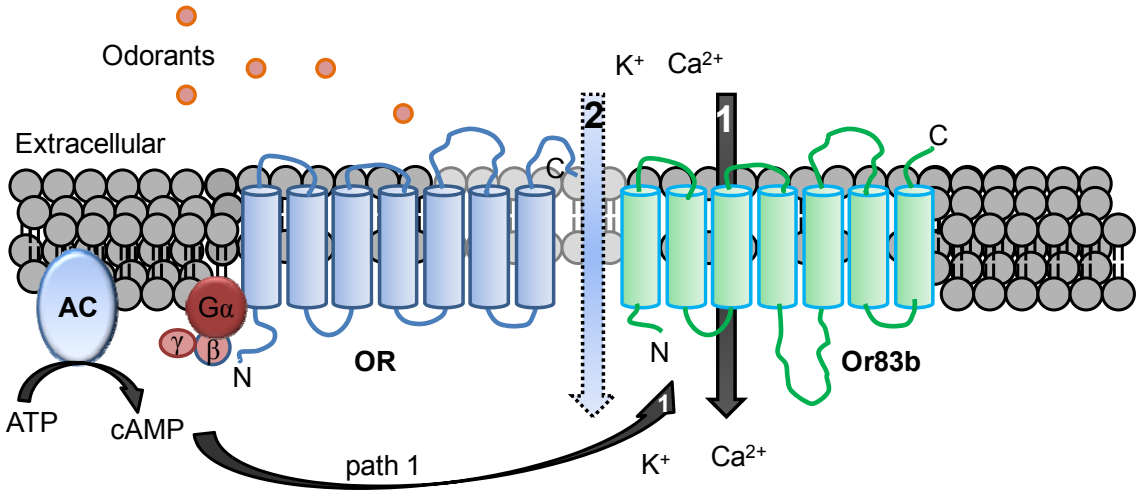

Figure 1-3 Proposed model for the cation channel function of insect odorant receptors.

Path 1: Odorant activation of the OR triggers the G-protein-coupled signalling pathway. The cyclic nucleotide activates Or83b and leads to the cation influx. Path 2: Odorant activates the OR-Or83b complex directly leads to inward flow of cations. (AC, adenylyl cyclase) Compiled from results given in [63,64].

Functional studies of ORs have shown that an OR can recognize multiple odorants, and that individual odorants are recognized by multiple ORs. In the generalist neurons, a combinatorial receptor code mediated by broadly tuned ORs is employed to discriminate odorants through a distinct area in the brain [67,68]. Different from that, the specialist neurons are projected into the macroglomerular complex in the male brain where the pheromone information is further integrated [69,70]. The male-specific ORs expressed in the specialist neurons are narrowly tuned to their ligand. For example, the long sensilla trichodea of *B. mori* house two olfactory receptor neurons, one specifically tuned to bombykol and the other to bombykal [71]. One male-specific OR, BmorOR1 and a broadly expressed OR, BmorOR2 (member of Or83b family) were co-expressed in one neuron and conferred the response to bombykol. The combination of BmorOR2 with another male-specific OR, BmorOR3 elicited a response to bombykal. BmorOR1 and

BmorOR3 were not co-localized and were exclusively expressed in two adjacent OR neurons [72]. This suggests the specificity of the ORs in pheromone detection. However, ORs by themselves expressing in exogenous cells have rather unspecific responses to pheromone molecules. The HvirOR (HR13) did not show statistically different responses to different pheromone components [73]. BmorOR1 can be activated by both bombykol and bomykal when the ligands were dissolved in DMSO [74].

The Or83b subunit in an OR complex is essential for its function but does not participate directly in pheromone binding. OR83b family proteins are specific to insect OR neurons and broadly expressed on the antenna [61,75,76]. They may act in concert with both the conventional ORs and the pheromone ORs to respond to many different odorants or pheromones. OR neurons lacking Or83b have shown no odorant-evoked action potential and also little spontaneous activity [76]. BmorOR2 was found to be essential for the expression of the sex-pheromone receptor proteins [72]. Thus, Or83b protein has been suggested to act as a co-receptor for ligand detection, a chaperone that ensures the functional expression of the ORs, a link to the signal transduction cascade of the OR neurons, or a combination of all of these functions [76].

Another important membrane-bound component in the pheromone signal transduction pathway is the sensory neuron membrane protein (SNMP), which is the insect-specific sub-group of the CD36 family in vertebrates. CD36 is a scavenger receptor that binds a variety of ligands such as lipoprotein [77] and long-chain fatty acids [78]. SNMPs have been suggested to have two transmembrane

domains as CD36 (Figure 1-2). Recent research from two different groups has shown with the SNMP mutant flies, that SNMP is required in the OR neurons for the pheromone-evoked electrophysiological responses and acts downstream of the PBP in the pheromone reception pathway [28,79]. Two suggested functions of SNMPs in *Drosophila* are: first, facilitation in the capture of pheromone molecules and in transfer of these molecules to the OR complex [28]; second, an inhibitor of the activity of OR neurons in the absence of the pheromone cVA [79]. *Drosophila* SNMP, together with other SNMPs from moths (SNMP1 and SNMP2), fall into the same group of insect SNMP/CD36 gene family, which are classed into three major groups based their sequence similarity, gene structure and history of gene duplication [80]. It has been shown that moth SNMP1 and SNMP2 were expressed differentially in olfactory sensilla in *A. polyphemus* and *H. virescens*, with SNMP1 uniquely expressing in one of the neurons of trichoid sensilla [81,82] and SNMP2 expressing in support cells [83]. *Drosophila* SNMP was found predominantly expressed in the OR neurons of trichoid sensilla as well as in support cells throughout the antenna [28]. Therefore, moth SNMP1 subgroup may have similar functions as *Drosophila* SNMP, but the functions of SNMPs in the support cell still need to be elucidated. Also, the functional interactions between neuronal SNMP, the ORs and the PBP still need to be elucidated.

1.2 Insect PBPs

1.2.1 General Aspects about PBPs

PBPs are small (~15 kDa), extracellular proteins that are members of the insect odorant-binding protein (OBP) family. Two other members of this family are general odorant-binding proteins (GOBP1 and GOBP2) [84-86], which are involved in the detection of food and plant volatiles. PBPs were typically identified by tissue specificity and N-terminal sequence, including several criteria such as the ability to bind pheromone and the preservation of six conserved cysteines. To date, PBPs have been sequenced and studied in 39 species, spanning 7 orders (Appendix A). Most of the species only express one PBP in their antennae except for several moth species such as *A. polyphemus*, *L. dispar* and *Mamestra brassicae* [87-89]. The first PBP was identified from *A. polyphemus* [48]. By homogenizing the antennae, as well as other tissues (wings, head, legs, etc.) from both male and female, and comparing the proteins in each tissue, Vogt successfully found an abundant soluble protein unique to male antennae. The binding ability of that protein with the pheromone ligand was confirmed by incubating the homogenates with radio-labeled pheromone followed by gel electrophoresis, and from there came the name: pheromone-binding protein. The concentration of ApolPBP in the sensilla was originally estimated to be 20 mM [48]. The largely quoted concentration for ApolPBP was 10 mM from Klein's work [90] and a similar value of 6.7 mM was reported for LdisPBPs [89]. Honson in our group has carefully reanalyzed the *in vivo* concentrations of LdisPBP1 and LdisPBP2

with both FPLC and immunoblotting techniques. Smaller (200-1200 μM) but still significantly high concentrations were revealed [27].

In general, PBPs range between 120 and 150 amino acids long and have been categorized recently into three structural groups: long, medium and short, differing mainly in the length of their C-terminal segment [91]. These proteins all appear to have compact structures composed of six α-helices interlocked with three disulfide bridges. Details are listed in the following section.

1.2.2 Structural Studies of PBPs

1.2.2.1 Overview of the Tertiary Structure

The 3D structures of five insect PBPs have been reported to date, either with or without ligand, and including two NMR structures of apo protein. When BmorPBP was co-crystallized with the species-specific pheromone bombykol, it was possible for the first time, to gain an insight into the tertiary structure of PBPs [92]. Consistent with previous observations from CD spectra, BmorPBP is formed by six α-helices that are arranged roughly in a conical shape (Figure 1-4). The helix α3 is rigidly fixed in position by two disulfide bonds to the flanking helices α1 and α6. A third disulfide bridge links helices α5 and α6. This is consistent with the profile determined by peptide mapping that the first cysteine residue is connected to the third one, the second to the fifth and the fourth to the sixth (Cys(I)-Cys(III), Cys(II)-Cys(V), Cys(IV)-Cys(VI)) [93-96]. Four antiparallel helices α1, α4, α5 and α6

converge to form the binding pocket at the narrow end of the cavity, with the opposite end capped by helix α3 (Figure 1-4).

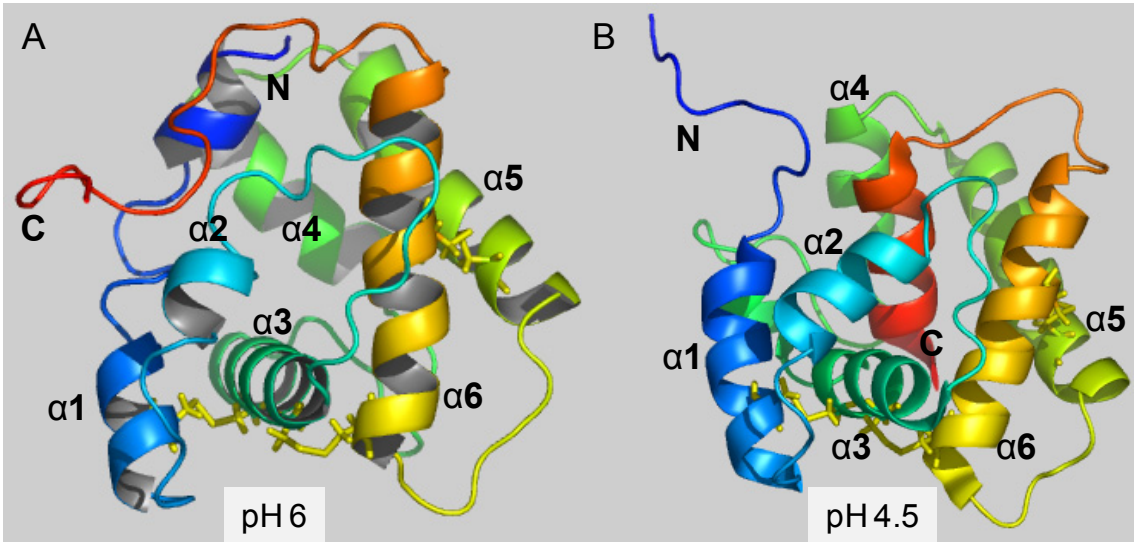

Figure 1-4 Distinct NMR structures of BmorPBP at neutral and acidic pH.

(A) at pH 6 (PDB: 1LS8); (B) at pH 4.5 (PDB: 1GM0). The N-termini of the structures are coloured blue and the C-termini are red. Three disulfide bridges are visible from this angle shown in yellow. The helix α3 is horizontal at the bottom and locked by two disulfide bridges to helices α1 (left) and α6 (right). At pH 4.5, the C-terminal peptide forms the 7th α-helix and inserts into the helix bundle. At the same time, the N-terminal peptide unwinds.

BmorPBP was crystallized as an asymmetric dimer [92]. This phenomenon was observed in the crystal structures of all subsequently determined PBPs from other insects, namely AmelPBP (ASP1) from honeybee *Apis mellifera* [97], LUSH from fruit fly *D. melanogaster* [98], and LmaPBP from cockroach *Leucophaea maderae* [99] (Figure 1-5). The interactions between monomers in a dimeric unit might include hydrophobic interactions and electrostatic interactions between surface ion pairs. However, some researchers believe that the dimer is not biologically relevant because of the overall small interface surface observed [97,99]. A similar conclusion has been made from the study of the crystal structure of one

OBP from the mosquito *Anopheles gambiae*. This structure was also a dimer but with a much larger interface [100]. The major concern in the latter study was the weak hydrophobic interactions between monomers. PBP dimers have also been observed frequently with gel filtration and native gel electrophoresis of antennal extracts and expressed PBPs from many species [101-104]. It has been suggested that the equilibrium of monomer/dimer is shifted towards the dimer at pH > 6 [105]. Fluorescence anisotropy experiments, designed to study the oligomerization state of the PBP, also support the existence of PBP dimers in solution [30]. However, it is still unclear whether the dimerization is biologically relevant or not.

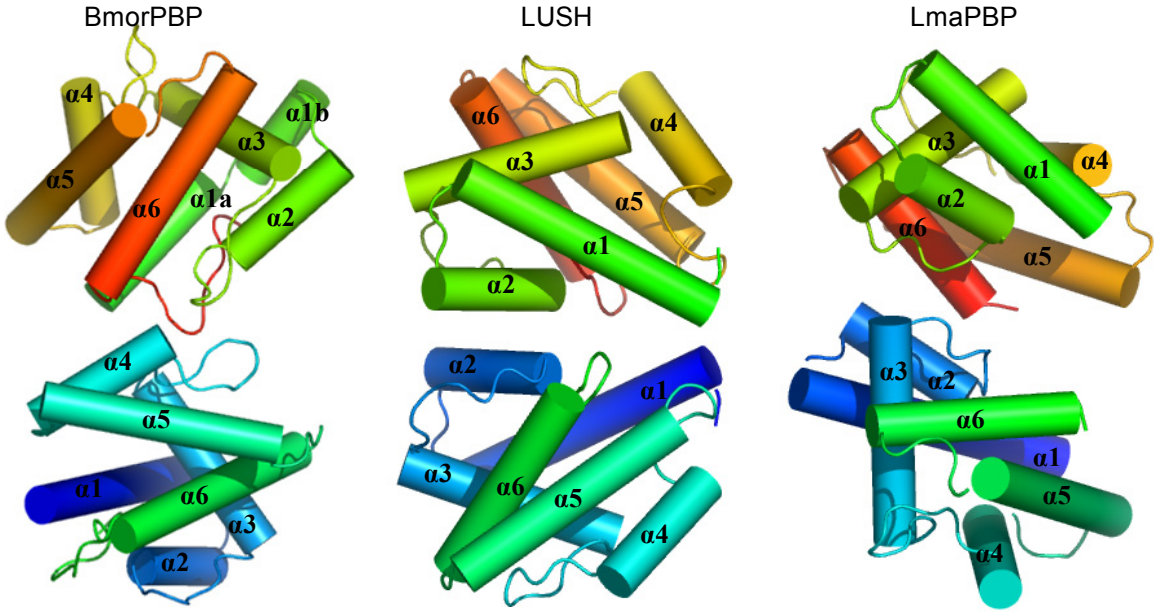

Figure 1-5 Dimeric crystal structures of representative PBPs.

Long-chain PBP: BmorPBP (1DQE); Medium-chain PBP: LUSH (1T14); Short-chain PBP: LmaPBP (1P28).

The NMR structure of BmorPBP obtained at physiological pH exhibited a nearly identical fold to the crystal structure of the polypeptide chain in the BmorPBP-bombykol complex, with an average backbone rmsd value of 1.00 Å [106]. The NMR structure has revealed two flexible regions on the protein, the C-terminal segment and the loop between helices α2 and α3. The NMR structure of ApolPBP at pH 6.3 revealed 9 α-helices, with the first and the third helices from the BmorPBP structure split into three and two short helices, respectively [107]. Its C-terminus is also unstructured, extending into the solvent, and the overall structure exhibited increased mobility and slightly differed from the NMR structure of BmorPBP (rmsd = 4.6 Å). A significant difference between structures was observed in the NMR structure of BmorPBP at pH 4.5, in which the C-terminal segment was found inside the binding pocket as a well defined α-helix (Figure 1-4B) [108].

1.2.2.2 The C-terminal Segment of PBPs

Insect PBPs have been classified into three groups based on the primary sequence length: long (~160 residues), medium (~120 residues) and short (~110 residues) [91]. The three classes share similar folds, but the major difference between the groups is in the C-termini (Figure 1-6).

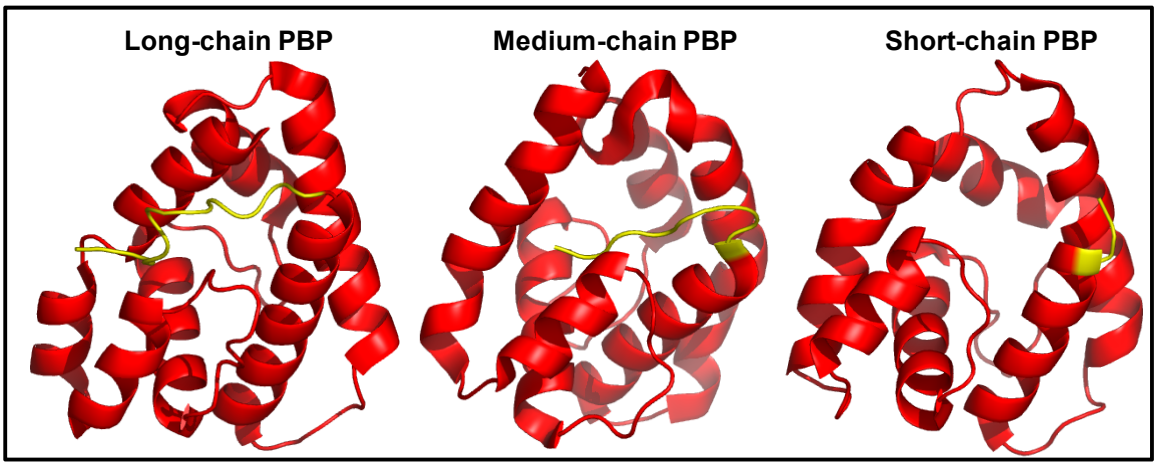

Figure 1-6 Different PBP classes have various lengths of the C-terminal segment.

An overview of the conformations of the C-terminal peptide (yellow) in long-, medium- and short-chain PBPs. Left: BmorPBP (long, 1DQE); middle: LUSH (medium, 2GTE); right: LmaPBP (short, 1P28).

In the long-chain PBPs, represented by the lepidopteran PBPs BmorPBP and ApolPBP, the C-terminus (>12 a.a.) was flexible and unstructured in most of the structures [92,106,107,109,110], except for three examples. These included two apo-BmorPBP structures. One was determined by NMR at acidic pH [108] and another was a crystal structure at pH 7.5 [111]. In both, the C-termini formed the 7th helix of the protein, and this helix was inserted into the hydrophobic binding pocket, obstructing the site normally occupied by pheromone ligand (Figure 1-4B). It is striking to see such a dramatic change, as it is rare for a protein to involve significant global conformational changes upon ligand binding [112]. However, if one assumes that there is a sufficient decrease in the local pH near the neuron membrane, then the pH induced conformational change could have a functional significance. This fits into the model in which the PBP acts as a carrier that needs to specifically take up ligand at the pores and then release the ligand in the vicinity of the membrane (Figure 1-7). The cycle of pheromone ligand binding and

releasing is thus built on the competition between the C-terminus and the ligand to occupy the binding pocket. The insertion of the C-terminus at low pH is postulated to help release, or eject the ligand, and a ligand will replace the C-terminus at higher pH in the bulk sensillum lymph [111].

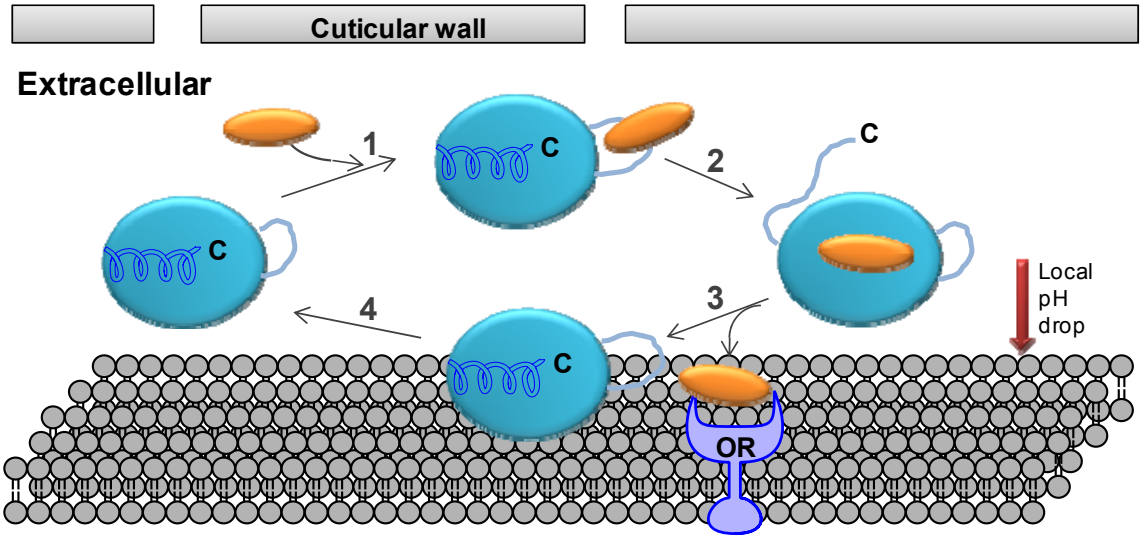

Figure 1-7 One model for ligand uptake and release.

A histidine-rich loop was proposed as a lid to open and let the ligand enter the binding pocket (1), the ligand competes with the α-helix formed by the C-terminal peptide (2). Then, a local pH decrease near the neuron membrane favours the formation of the α-helix of the C-terminal peptide and leads to the release of the ligand (3). The free PBP diffuses away from the membrane (4).

Experimental data consistent with this model include the incapability of BmorPBP to bind a ligand at acidic pH [113], under which the binding pocket should be occupied by the C-terminus. ApolPBP only binds the acetate pheromone at pH above 6 as well [114]. Its C-terminus was determined originally as unstructured in the acidic form (pH 5.2), indicating that the winding and unwinding of the C-terminal peptide into the binding pocket was not a universal feature of lepidopteran PBPs [110]. However, it was re-determined two years later and found

to present the same acidic form as BmorPBP [115]. Therefore, it was suggested that the mechanism of ligand binding and release involving the insertion of the C-terminus into the binding pocket might be generally valid for moth PBPs of the "long" category.

The concentrations of ions should change dramatically near a phospholipid bilayer [116], because of electrostatic interactions with the phosphate groups. Studies of the effects of pH and salt on binding properties of LdisPBPs have revealed that high concentrations of KCl caused stronger binding of pheromone to the PBPs. This effect counterbalances the dissociation of the ligand from the PBP induced by the decrease in pH. Therefore, the positive ion gradients near the membrane of sensory neurons may not be responsible for the release of pheromone [117], but protonation of side chains on the PBP leading to a PBP conformational switch at the C-terminus is likely to explain pheromone release at the membrane. While there have been a lot of debates about pH changes in long-chain PBPs, it is relatively easier to explain the behavior of the C-terminal peptide in the other two types of PBPs, because the medium and short PBPs may not have a long enough C-terminal peptide to form a helix. The C-terminus of the medium-chain PBPs folds back in the protein core and forms one of the walls of the binding cavity [97,98], while the short-chain PBPs, based on the only one example from LmaPBP, do not have the hydrophobic C-terminal peptide at all (Figure 1-6) [99].

Apart from the above observations, the C-terminus of PBPs has been the focus of recent new insights. In 2008, two different groups working with medium-

chain PBPs, LUSH and ASP1, have noticed a subtle difference in the C-terminal conformation of PBPs between the apo/nonpheromonal-ligand-binding form and the pheromone-binding form [29,91]. In the study of LUSH, the authors have carefully compared the crystal structure of LUSH-cVA with those of apo-LUSH and LUSH-butanol (LUSH is required for the avoidance of *Drosophila* to high concentrations of short-chain alcohols [118]). They have found two distinct binding modes of cVA to LUSH that do not result in one unique protein conformation. The cVA interacts with the C-terminal residue Phe121 differently in the two conformations, but both have induced a pheromone-specific conformational change of the C-terminal peptide (residues 116-124) that results in the disruption of a salt-bridge between Asp118 and Lys87 that is usually present in the apo-LUSH and LUSH-butanol structures (Figure 1-8A). A mutant, $LUSH^{D118A}$ which does not inherit the salt-bridge, stimulates the sensory neurons in the absence of pheromone [29]. Thus, PBPs function as a protein ligand that can be activated by the relevant pheromone ligand and transmit the message of pheromone binding through the conformational changes in the C-terminal region [29].

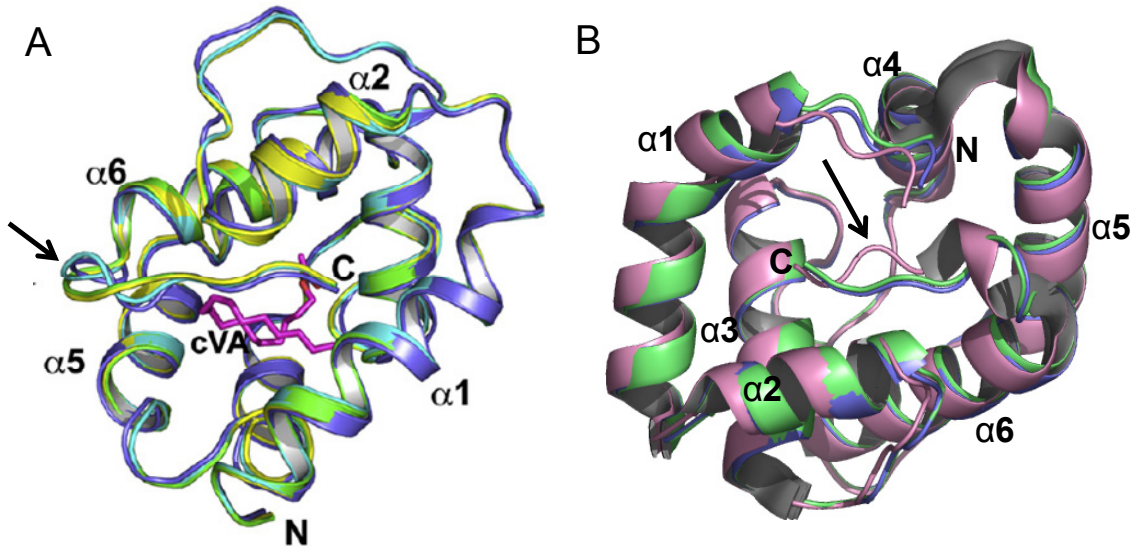

Figure 1-8 The conformations of the C-terminal peptide of medium-chain PBPs exhibit subtle differences in different PBP.ligand complexes. (A). Ribbon diagram comparing one monomer from the asymmetric unit of the LUSH.cVA complex (blue) with the LUSH^{D118A} (cyan), apo-LUSH (green), and LUSH.butanol complex (yellow)*. (B). Diagram comparing the ASP monomer in apo-ASP (pink, 2H8V) with that in the ASP.9-ODA (blue, 3BFA) and ASP.C15-COOH (green, 3BFH) complexes. The differences are indicated with arrows.

In the study of ASP1, unfortunately, the structures are only reported as a monomer, so we cannot tell if there are two binding modes of the ligand as well. Pesenti et al. have followed the idea that the ligand binding and pH change interplay to orchestrate the cycle of ligand uptake and release in the sensillum lymph [91]. They have compared the structures of ASP1 in complex with different ligands, natural (pheromone, (E)-9-oxodec-2-enoic acid (9-ODA), (12)) or unnatural (plasticizer, n-Butyl benzenesulfonamide (nBBSA) and fatty acids), and have studied the pH effect on the protein structure. Different C-terminal conformations have been observed with different ligands but it does not seem to be highly ligand-specific, because 9-ODA and the C15 carboxylic acid have both

* Reprinted from Cell, 133 (7), Laughlin, J. D. et al., Activation of pheromone-sensitive neurons is mediated by conformational activation of pheromone-binding protein, p. 1255, Copyright (2008), with permission from Elsevier.

induced similar C-terminal conformational change. However, this conformation does differ significantly from that of the apo-ASP1 (Figure 1-8B). The authors postulate that the change is regulated by the hydrogen bond forming or breaking between Asp35 side chain and the main chain of the last residue Val118 [91].

1.2.2.3 Properties of the Binding Cavity

The binding cavity of PBPs can hold a wide variety of substances, from pheromones to general odorants, and even to non-natural compounds such as fluorescent reporter compounds and plasticizers [91,99,109]. Most of the time, there is only one ligand bound per monomer, with a few exceptions in which two molecules are detected in the pocket. For example, two bell pepper odorant molecules are modelled in the pocket of BmorPBP [109], and one 9-ODA and one glycerol molecule are co-crystallized in the ASP1 structure [91]. The cavity has variable volumes in different complexes. The cavity in the ASP1.9-ODA complex has a volume of 1577 $Å^3$, of which only a small portion is occupied by the ligand. This cavity is 35% larger than that of the complex with nBBSA (plastic) and similar in size to that of the complex with hexadecanoic acid [91]. Binding with the fluorescent reporter, 8-anilino-1-naphtalenesulphonic acid (ANS) has yielded a volume increase of ~50% for LmaPBP [99]. The volume of the pocket for BmorPBP in complex with bombylkol is small, 167 $Å^3$ [111]. From the available structures of PBP.ligand complexes, BmorPBP and LUSH can completely envelop the ligand, leaving small openings to the surface. The cavity looks pretty much like a flask. In the other two cases, for ASP1 and LmaPBP, there are broad openings that can

be easily observed and are proposed as the entrance for the ligand (Figure 1-9) [91,99].

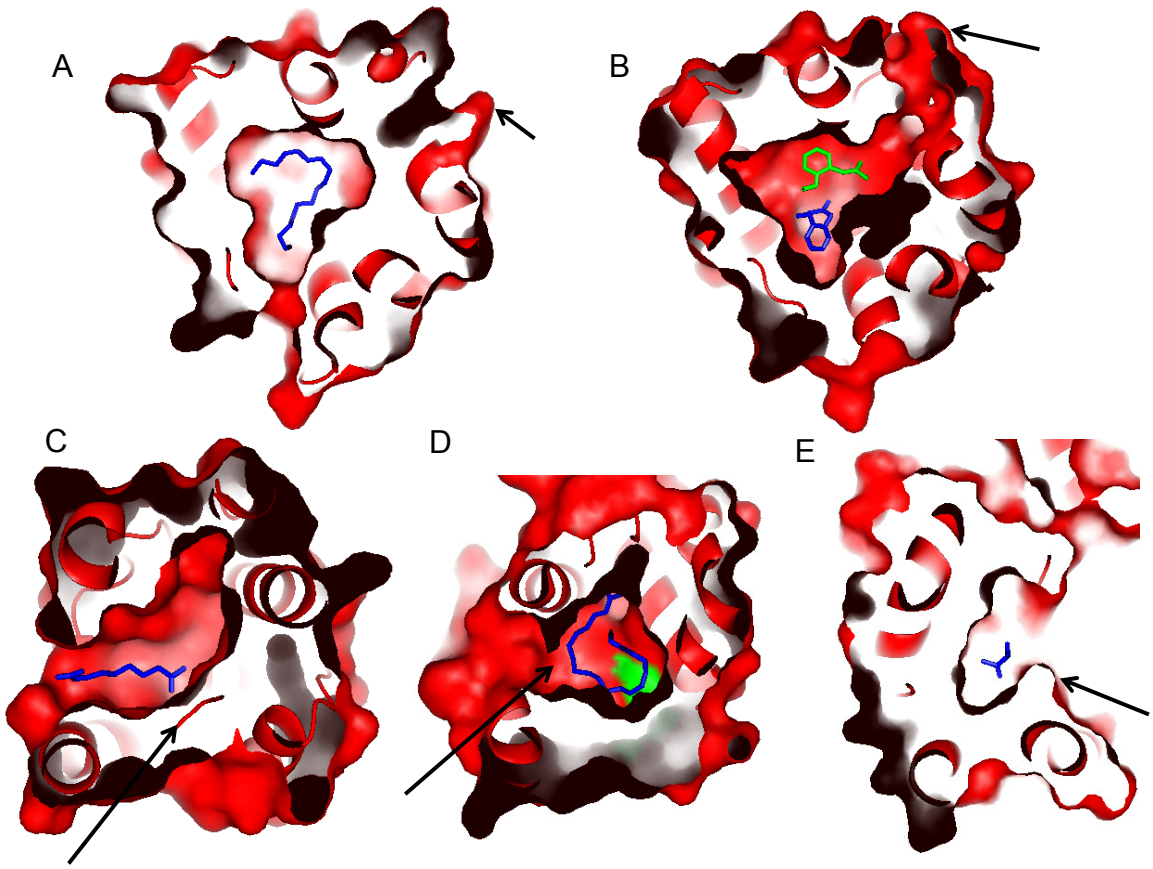

Figure 1-9 The binding cavities of different PBP.ligand complexes with variable openings. (A) BmorPBP with its cognate ligand bombykol. (B) BmorPBP with two bell pepper odorant molecules. (C) ASP1 with the major component of the pheromone, 9-ODA. (D) LUSH with cVA. (E) LmaPBP with H3B2. Arrows indicate the C-terminal region of the protein. This region could be at the bottom (A), on one side of the wall (C, D) or at the opening (B, E) of the binding pocket.

1.2.3 Binding Affinities with Various Ligands

PBPs are named after their ability to bind a pheromone. The first PBP was identified by incubating the ^{3}H labeled pheromone of *A. polyphemus* with its antennal homogenates, running a native gel and then looking for a protein band

that bound the pheromone [48]. After that, the first set of binding experiments was developed, based on the radiolabeled ligand and native gel electrophoresis [89,119]. The disadvantages of that method are: 1) the difficulty to synthesize and store the radiolabeled ligand and 2) the limitation of gel electrophoresis to quantitatively detect the binding. To date, a variety of methods to measure quantitatively the binding affinities of PBPs with the ligands have been developed. They fall into two groups: direct measuring and indirect measuring.

Direct measuring means to measure directly the quantity of the ligand that is bound to the protein. This would need a technique to first separate the unbound ligand from the bound. Our group has developed a method to achieve this purpose with a size-exclusion mini-column [104]. W. Leal's group has used Microcon YM-10 centrifugal filter [113]. The bound ligand is then quantified by liquid scintillation counting for the radiolabeled ligands or extracted with organic solvent and quantified with GC for the non-radiolabeled ligands.

Indirect measuring uses the changes of fluorescence intensity of a fluorophore upon PBP ligand binding to indicate the magnitude of binding. The fluorescence of either the intrinsic tryptophan or an extrinsic fluorescent compound that acts as a non-natural ligand can be utilized. The first method has been used on ApolPBP and LdisPBPs binding studies [47,120]. Some ligands tested quenched the tryptophan fluorescence and some enhanced it. The change in fluorescence was relatively small, giving rise to great errors when determining dissociation constants. The second method needs fluorescent reporters (Figure 1-10), such as 1-aminoanthracene (AMA, 13), ANS (14) or N-phenyl-1-

naphthylamine (NPN, 15). The first report of this method used AMA to test the binding properties and specificity of MbraPBP1, ApolPBP, BmorPBP, and a mutant of MbraPBP1 [121]. When the AMA was titrated into the protein solution, its fluorescence intensity increased and when AMA was displaced by a second ligand, the fluorescence intensity decreased. However, AMA turned out not to be a general probe for all PBPs since only some of them are capable of binding AMA [121,122]. After this study, other probes have been utilized in fluorescence displacement assays [122-124]. The major problem with this method is the difficulty in evaluating the impact of the competition of the probe itself on ligand binding. The probe may have a synergistic or antagonistic effect on PBP binding with the ligands of interest ((Honson et al. 2003) [47] and Chapter 4). Honson has developed a method to covalently attach a dansyl group to a thiol group produced by the disulfide bridge reduction and followed the fluorescence change of the dansyl group [47]. However, the dansylated protein is short-lived probably due to the preference of forming the original disulfide bridge [27].

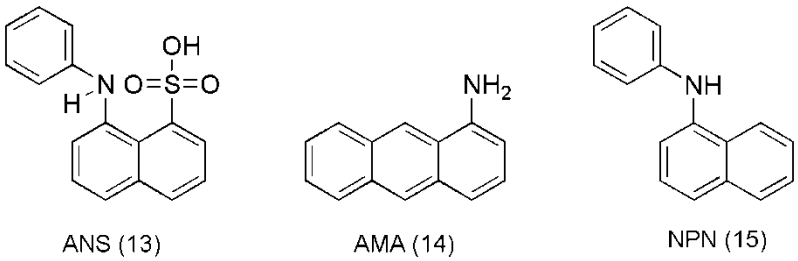

ANS (13) AMA (14) NPN (15)

Figure 1-10 Structures of fluorescent reporters.

The binding affinity of a ligand is represented by the dissociation constant of the PBP.ligand complex (K_d). The dissociation constant is obtained from either Eq. (1.1) or Eq. (1.2), based on the method used.

$$\boldsymbol{K_d = \frac{P_{free} \times L_{free}}{P.L}} \quad \textbf{(1.1)}$$

$$\boldsymbol{P.L = \frac{P.L_{max} \times L_{free}}{K_d + L_{free}}} \quad \textbf{(1.2)}$$

P_{free} and L_{free} represent the concentrations of apo-PBP and free ligand, respectively. P.L and $P.L_{max}$ represent the concentration and the maximal concentration of the PBP.ligand complex.

Overall, the K_d values for PBPs with various ligands are in the range of μM and they show difference between ligands [46]. For example, LdisPBP1 binds (-)-disparlure more strongly than (+)-disparlure with K_ds of 2.2 and 7.1 μM, respectively [104]. ApolPBP has a K_d of 0.64 μM for its pheromone binding and a K_d of 21 μM for binding with (4E, 9Z) tetradeca-4,9-dien-1-yl acetate [125]. This difference leads to the conclusion that insect PBPs help to discriminate ligands and they preferentially deliver the ligand to the ORs based on the binding strength. However, PBPs bind non-biological ligands with comparable strengths as the pheromone compounds. The K_d for ApolPBP with AMA is 0.95 μM [121] and for LdisPBP1 with NPN is 1.3 μM (Chapter 3). It is also noticed that the binding affinities themselves do not correlate with either the EAG or the behavioral response of the ligand [47].

1.3 Biological Functions of PBPs

Pheromone perception in insects is highly sensitive and selective. The binding of a pheromone molecule to the PBP may contribute to either the sensitivity or the selectivity or both.

There are three observations that suggest PBPs may enhance the sensitivity of the insect olfaction. First, the addition of a PBP into the pheromone-detecting sensilla lowers the response threshold for pheromone ~100 times [126]. This suggests that PBPs somehow enhance the efficiency of pheromone detection. Second, *Drosophila* expressing BmorOR1 and devoid of BmorPBP show low sensitivity to the pheromone [127]. Third, LUSH increases the sensitivity of T1 neurons to cVA over 500-fold [29], when comparing the responses of sensilla devoid of LUSH and sensilla that express LUSH.

Three observations indicate that PBPs are related to the olfaction selectivity. First, modified mammalian HEK cells that express BmorOR1 respond to both bombykol and bombykal when the ligand is delivered with DMSO, but the specificity is altered when BmorPBP is involved [74]. Second, odorant receptors show different activity profiles for a set of ligands in the presence of different PBPs either delivered to cells expressing an OR [73], or delivered through the recording electrode into a sensillar preparation [128]. Third, a LUSH mutant, in which the conformation of the C-terminal segment has been locked into the active conformation by substitution of Asp118 to Ala (D118A LUSH), induced electrophysiological activity in T1 sensilla in the absence of pheromone [29]. This activity correlates to specific aggregation behaviors of the flies induced by cVA.

However, there are also other studies indicating that PBPs are not essential for ligand specificity of the receptors. *Xenopus* oocyte cells expressing BmorOR1 only respond to bombykol [127]. Several other *lepidopteran* sex-pheromone receptors are narrowly tuned to their ligands [129].

It is clear though that PBPs are essential for pheromonal signal transduction. For example, LUSH was specifically required for cVA sensitivity of T1 neurons. Fly mutants lacking LUSH had a complete loss of sensitivity to cVA, consistent with the behavioral insensitivity to this pheromone. Transgenic expression of LUSH restored the function [130]. Other possible functions for PBPs include: First, they can transport hydrophobic odorants across the lymph to the receptors [131] (Figure 1-2). Second, the OBPs have been shown to be necessary for both neuronal background activity and odor-evoked activity [28,29,73,130]. Third, PBPs may act as scavengers, buffering high doses of odorant and thereby preventing the neurons from saturating [47,132]. The cVA sensitivity of fly mutants lacking LUSH could not be restored by a moth PBP [130]. This and the presence of multiple PBPs [88,89,133] indicates that these proteins may also take part in the olfactory coding or signal filtering.

1.4 Aim and Scope of this Work

Communication with species-specific signal chemicals (pheromones) plays an important role in insect reproduction. For example, in the case of moths, the female releases the pheromone, and the males detect and follow the

pheromone plume upwind to mate. A smart design of an inhibitor of the pheromone perception of pest insects can interrupt the communication between insects and therefore to control their population. In order to do so, it is important to understand the molecular mechanism underlying the sensitivity and specificity of pheromone perception in insects.

My work attempts to understand this mechanism by kinetically studying PBPs. PBPs are the most abundant extracellular proteins in the sensory hairs of insects and these proteins are important for pheromone detection. Most of the published work on PBPs focuses on the ligand binding affinities of PBPs or the investigation of the 3D structures of apo- and ligand-bound PBPs. However, PBP-ligand interactions require > 30 min to establish equilibrium [104], whereas a moth responds to the pheromonal stimulus in milliseconds; thus, the interactions between the olfactory components (PBPs, ligands, and ORs, etc.) may not be under thermodynamic control. The purpose of this work is to provide a dynamic perspective of the PBP-ligand interactions and to link these to the functions of PBPs.

Through the kinetic studies, I have built up a three-step pathway for PBP-ligand interaction. The major scenario is that the ligand is taken into the binding pocket step by step and each step is in a different time regime. More work needs to be done to explore whether or not a specific function of PBP is associated with the ligand-interaction in each step. My results also indicate that the ligand sensitivity and specificity of pheromone perception in insects do not correlate to PBP-ligand binding in a straightforward manner. The ligand selectivity may arise

from subtle conformational changes of the protein upon ligand binding or from a downstream olfactory component, for example, OR.

In detail, I started with one PBP, LdisPBP2, from the gypsy moth, which was found to bind ligand relatively slowly and I built a two-step model to explain the kinetic interactions between a PBP and the ligand (Chapter 2). Then, I expanded the view of PBP-ligand interaction kinetics, based on the proposed model. With a different methodology using a fluorescent compound as a model ligand, I studied the kinetics with stopped-flow fluorescence of both LdisPBP1 and LdisPBP2, and the truncated forms of both PBPs without the C-terminal peptide. I have also developed a method to investigate local conformational changes of interest by quantifying the quenching of tryptophan fluorescence (Chapter 3). At the end, in order to link the *in vitro* protein studies to the behavioral responses induced by a ligand, I studied the binding of a series of derivatives of general odorant compounds synthesized in our group, to PBPs. A major breakthrough came from a series of compounds that cause a delayed activation of the antenna, concurrent with an antagonism of the antennal depolarization. The structure-activity relationship in this series of compounds correlates with the binding behavior in LdisPBP1 (Chapter 4). However, I can hardly find other correlations between PBP binding and the antennal responses of a ligand.

CHAPTER 2 LIGAND-BINDING MECHANISM OF LDISPBP2

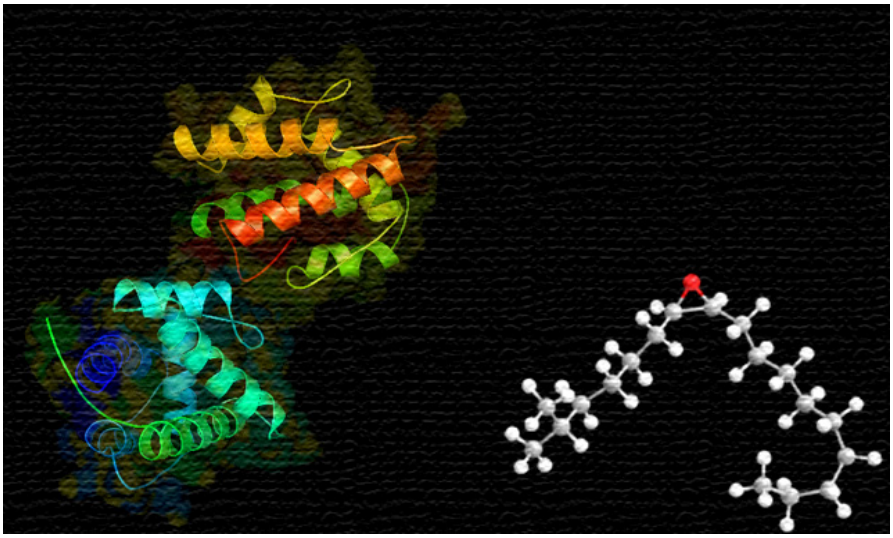

- The results of this chapter are adapted from the published paper in Chemistry & Biology with permission [30].
- A slow interaction process between PBP2 and (+)-disparlure was discovered and carefully examined.
- PBP2 in solution exhibited an equilibrium of monomer/multimer. Ligand binding shifted the equilibrium to the multimer slowly.
- This chapter is intended to explain the purpose of the kinetic study and how the binding mechanism was established. This is the foundation for future, more specific studies on PBP binding mechanisms.

2.1 Introduction to the Gypsy Moth and Its PBPs

The gypsy moth, *L. dispar* is a notorious forest pest that originally ranged from Europe to Asia. It was accidentally introduced to North America in 1868 and has caused severe infestations. Its caterpillars defoliate deciduous and evergreen trees and shrubs, and make them more vulnerable to diseases and other insects.

The female gypsy moths emit (+)-disparlure as the main sex attractant pheromone component [134-136]. The enantiomer, (-)-disparlure, is a behavioral antagonist of upwind flight in gypsy moth males [137]. The male moth antenna has separate sensilla populations specialized on (+)-disparlure or on (-)-disparlure, but not both [138]. The gypsy moth has two known PBPs: LdisPBP1 and LdisPBP2 (PBP1 and PBP2 from here on). The sexual dimorphism, ontogeny [89] and ligand binding affinities of these PBPs have been studied. PBP2 binds (+)-disparlure and PBP1 binds (-)-disparlure slightly more strongly than the other enantiomer [104]. Binding enhancement has been observed when (+)-disparlure or (-)-disparlure is mixed with (Z)-2-methyloctadec-7-ene [47]. The alkene is a strong antagonist in the gypsy moth [13] but a synergist in the closely related species, nun moth [139]. Binding decrease has been observed when (+)- and (-)-disparlure are mixed [104]. The reason for these “blend” effects is not clear yet. Studies of the pH effects on the pheromone binding to PBP1 and PBP2 have revealed a dramatic increases in the binding affinities at pH > 6, similar to other PBPs. The weak binding at low pH can be counterbalanced by high salt concentration [117]. PBP1 and PBP2 are also able to bind variable pheromone analogs or aromatic compounds with slightly

different binding constants [47,122,140]. However, the time scale of PBP-ligand equilibration is much slower than the time scale at which individual insect sensilla are activated after the onset of a stimulus. Thus, kinetic studies are necessary to understand the mechanism of ligand binding and the biological function of PBPs.

2.2 Experimental Procedures

2.2.1 Preparation and Characterization of Dansylated PBP2 (DNS-PBP2)

PBP2 was expressed and purified as previously described [104] and stored at -37 °C in 20 mM pH 7.4 Tris-HCl buffer. Before the reaction, 10 mL of 30 to 50 μM PBP2 solution was dialyzed against 2 × 1 L 20 mM $NaHCO_3$ pH 10.3 buffer overnight at 4 °C, to replace the Tris. Two times excess of 53.0 mM fresh dansyl chloride (DNS-Cl) in EtOH was slowly added to the protein solution every half hour. The reaction was conducted at room temperature on a stirring plate and stopped after 1 h by running the crude product on preparative 12% native PAGE gels directly. Fluorescent fractions were pooled together and dialyzed against 20 mM pH 7.4 Tris-HCl buffer. The dansylation was confirmed by MALDI mass spectrometry, and the composition, with respect to the number of dansyl groups attached, was evaluated by FPLC (Figure 2-1). For the analysis, 50 μL of the concentrated DNS-PBP2 samples would be run through the FPLC (BioLogic DuoFlow™ Chromatography System, Bio-Rad Laboratories, Hercules, CA), which was fitted with a UNO Q-1 anion exchange column. Sample was eluted

using an increasing salt gradient consisting of two buffers: Buffer A is 20 mM Tris pH 7.4 and Buffer B is 20 mM Tris, 1.0 M NaCl pH 7.4.

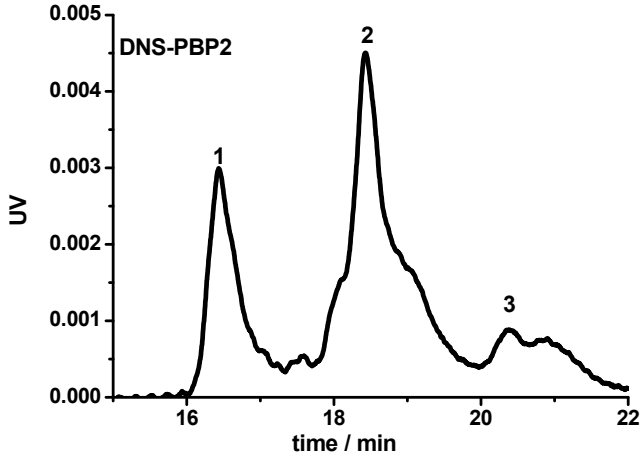

Figure 2-1 FPLC trace reveals the composition of DNS-PBP2.

Each peak was identified by MALDI (1: nonmodified PBP; 2: monodansylated PBP; 3: didansylated PBP). The integration area for each peak was used for calculating the DNS-PBP composition, as shown in Table 2-3

The attachments sites of DNS were identified by peptide mapping with the help of Ms. J. Huang from Dr. Agnes lab (Department of Chemistry, SFU) (Figure 2-2, Table 2-1 and Table 2-2). CNBr digestion and chymotrypsin digestion were performed separately on both DNS-PBP and non-dansylated PBP samples. For CNBr digestion, 1 mg of the protein was dissolved in 200 µL 70% trifluoroacetic acid (TFA) solution and then reacted with 1 mg CNBr at room temperature for 24 h. The sample was speed vacuum dried and dissolved in 100 µL 0.1% TFA. For chymotrypsin digestion, 50 µg protein in 50 µL buffer (100 mM NH_4HCO_3, 2 mM $CaCl_2$, pH 8) was added to 10 µg chymotrypsin dissolved in 2 µL of the same buffer. The mixture was sonicated for 10 min in a water bath and then incubated at 37 ˚C for 24 h. The reaction was terminated by flash freezing the sample with

liquid nitrogen. Peptides were analyzed by MALDI with a sinapinic acid matrix (Figure 2-2).

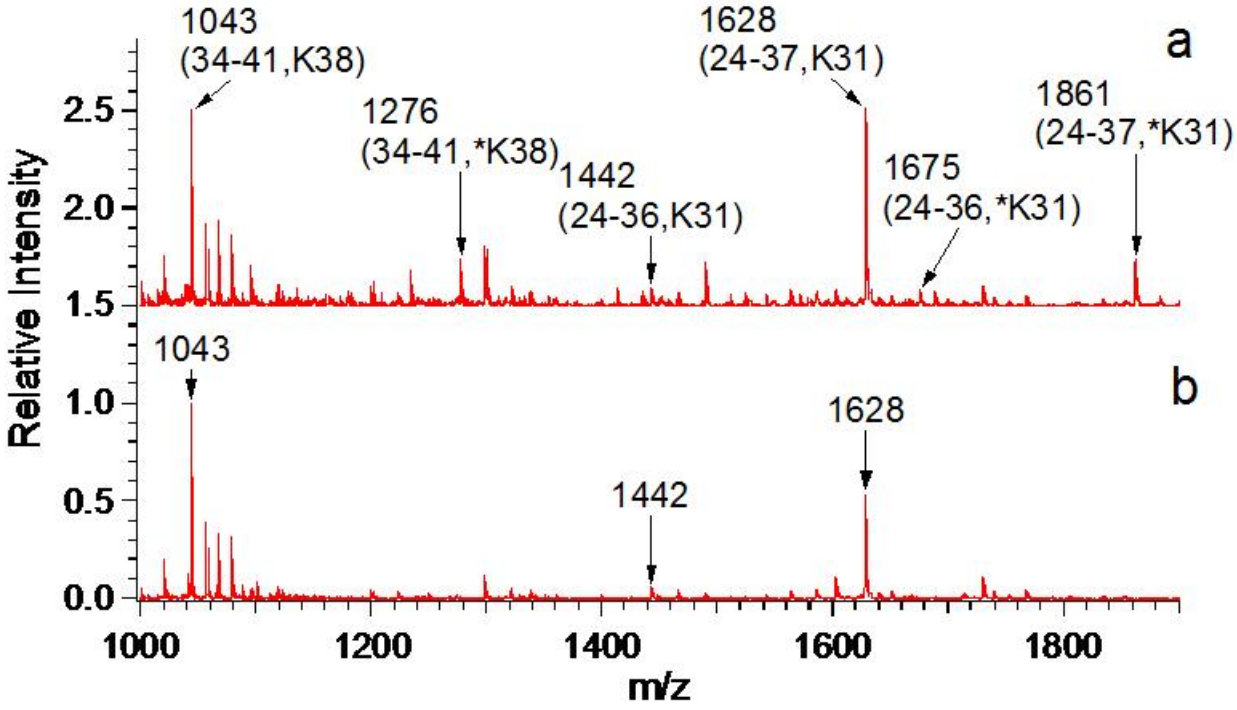

Figure 2-2 MALDI mass spectra containing Lys Chymotryptic peptides of PBP2 and DNS-PBP2. (a) Peptides of DNS-PBP2; (b) Peptides of PBP2. An asterisk denotes the modified peptides.

Table 2-1 Detected peptides containing Lysine from PBP2, digested with CNBr and chymotrypsin.

Peptide	Lysine Position	Theoretical $[M+H]^+$	Unmodified Observed $[M+H]^+$	Mass Error (ppm)
34 – 41	K38	1043.4838	1043.5100	25
24 – 36	K31	1441.6851	1441.9824	206
24 – 37	K31	1627.7644	1628.1437	233
121–127	K121, 126	832.5157	832.8712	427
53 – 61	K58	1122.5725	1122.7478	156

121–129	K121, 126	1132.6380	1133.0921	401
1 – 12	K2, 11	1466.7136	1465.9584	-515
11 – 23	K11, 14, 17	1602.9042	1602.0740	-518
42 – 61	K44, 58	2504.1877	2503.8274	-144
*58 – 66	K58	971.5413	971.0537	-502
*67 – 86	K78	2078.9684	2078.9395	-14

An asterisk * denotes the peptides from CNBr digestion.

Table 2-2 Detected Lysine-containing peptides from DNS-PBP2, digested with CNBr and chymotrypsin.

Peptide	Lysine In peptide	Unmodified Theoretical $[M+H]^+$	Unmodified Observed $[M+H]^+$	Modified Theoretical $[M+H]^+$	Modified Observed $[M+H]^+$	DNS Modified Lysine residue
34 – 41	K38	1043.4838	1043.5764	1276.5348	1276.8391	K38
24 – 36	K31	1441.6851	1442.0824	1674.7361	1675.2621	K31
24 – 37	K31	1627.7644	1628.2544	1860.8154	1861.4426	K31
121–127	K121, 126	832.5157	832.9108	1065.5667 1299.6177	- -	- -
53 – 61	K58	1122.5725	1122.5869	1355.6235	-	-
121–129	K121, 126	1132.6380	1133.4921	1365.6890 1598.7400	- -	- -
1 – 12	K2,11	1466.7136	1466.1423	1699.7646 1932.8156	- -	- -
11 – 23	K11,14, 17	1602.9042	1602.0189	1835.9552 2069.0062 2302.0572	- - -	- - -
42 – 61	K44,58	2504.1877	2503.4990	2737.2387 2970.2897	- -	- -
*58 – 66	K58	971.5413	971.0178	1204.5923	-	-
*67 – 86	K78	2078.9684	2078.5017	2312.0194	-	-

An asterisk * denotes the peptides from CNBr digestion. A (-) indicates no peptides detected.

The apparent molecular weights of the protein samples were calculated according to their compositions. Extinction coefficients at 280 nm, ε_{280}, evaluated

from known quantities of pure non-dansylated and dansylated PBP2 compare well to calculated estimates, which are based on the amino acid composition of the PBP2 [141] and the absorbance of DNS group at 280 nm (ε_{280} =1920 $M^{-1}cm^{-1}$ for dansyl t-butylamine):

$$\varepsilon(280)(M^{-1}cm^{-1}) = 5500\times(\#Trp) + 1490\times(\#Tyr) + 125\times(\#Cystine) + 1920\times(\#DNS)$$

(#Trp = 2, #Tyr = 2, #Cystine = 3, #DNS = $\sum_0^i a_i(\#DNS)_i$)

The experimentally measured ε_{280} values were used to evaluate protein concentration. Results were summarized in Table 2-3. All protein samples used for the experiments were in 20 mM pH 7.4 Tris-HCl buffer unless otherwise indicated.

Table 2-3 Physical parameters of DNS-PBP2

Protein	Composition (0:1:2) DNS	ε_{280} ($M^{-1}cm^{-1}$)		M_w apparent	Modification sites
		a	b		
DNS-PBP2	3:7:2	13700 ± 800	16119	16497.4	K31, K38
PBP2	N/A[c]	14300 ± 700	14730	16147	N/A

[a]. ε_{280} measured directly; [b]. ε_{280} calculated from the amino acid composition [141]
[c]. N/A = not applicable

2.2.2 Construction, Expression and Purification of C-terminally Truncated PBP2 (T-PBP2)

C-terminally truncated PBP2 was constructed by Dr. E. Plettner (Department of Chemistry, SFU), by a PCR based approach to delete the C-terminal fragment that starts at Trp129 and goes to Gln 145. A forward primer with a Nco I site (5′ GATGGCCATGGAGAATTCGAAGGATGTAATGC 3′) and

reverse primer with a Hind III site (5´ CCGCAAGCTTAGTTTAGTTTGTGTACGTG 3´) amplified the PBP2 gene lacking 51 nucleotide residues corresponding to the last 17 amino acids from the C terminus. After restriction enzyme digestion, the amplicon was ligated into corresponding sites in the multiple cloning region of the pET-22b(+) vector (Novagen). The construction was transformed into JM109 and selected by PCR. Plasmids from positive clones were isolated and the gene sequence confirmed from both ends using the T7 promoter and T7 terminator primers.

Plasmids containing the T-PBP2 gene were transformed into *E. coli* BL21(DE3) and grown in LB + ampicillin (50 mg/L) medium at 37°C. Overnight 50 mL cultures were harvested and the pellet resuspended in 1 L of fresh medium. The culture was grown with good shaking (250 rpm) until it reached an OD590 0.6 - 1, then cells were pelleted again and resuspended in fresh medium containing 200 mg/L of IPTG to induce expression for 4 - 4.5 h at 27°C. Protease inhibitors ABSF (0.5 mg) and PMSF (20 mg) were added prior to harvesting the cells to prevent proteolysis in subsequent steps. Pellets were washed three times in 100 mM Tris buffer (pH 7.0) then resuspended in 300 mL of Lysis buffer (80 mM Tris HCl, 200 mM NaCl, 1 mM EDTA, 4% Glycerol, pH 7.2, containing 100 µg lysozyme, 200 µg leupeptin and 200 µg aprotinin) and stirring in a cold room for 2 hours. Bacterial cells were lysed by sonication (duty 50', output 10') three times per 10 minutes. After centrifugation the pellet was resuspended in wash buffer (0.2% Triton-X-100 in 50 mM Tris(OH), pH 6.8) and passed through a tissue homogenizer three times. The harvested pellet was denatured in 45 mL 8N

guanidinium HCl, passed through the homogenizer and added to 20 mL reducing solution (10 mM DTT in 200 mM Tris HCl, pH 8.0 plus 50 µL β-mercapthoethanol) and stirred for 2 hours on ice under constant sparging with argon. The solution was then renatured in 500 mL of 5 mM cysteine in 100 mM Tris, pH 8.0, adding 10 mL of 200 mM cystine in 0.5N NaOH. After centrifugation the supernatant was concentrated down to 40 mL in Ultrafiltration Amicon Cells (Millipore) with a 10 kDa NMWL membrane. The solution was dialyzed overnight against 20 mM Tris pH 7.4 and then concentrated further to 5 - 8 mL with a 5 kDa NMWL membrane.

The renatured T-PBP2 protein was purified by large 12% native PAGE. Proteins were eluted at constant current (200 mA) for 1 hour with the Whole Gel Eluter (Bio-Rad). Fractions were quantified by UV-VIS at 280 nm and those with the highest ODs were analyzed by SDS-PAGE. Proteins with the expected molecular weight were confirmed by Western blotting against PBP2 antiserum and the mass spectra of the pooled fractions were obtained on a MALDI/TOF mass spectrometer. The antiserum was raised against pure recombinant PBP2 [104].

For the experiments, 500 µL of T-PBP2 protein was further purified by FPLC using a UnoQ column, dialyzed overnight against 20 mM Tris pH 7.4, concentrated in NANOSEP™ Microconcentrations (Pall Filtron) with a 3 kDa molecular weight cut off and delipidated by incubation with buffered charcoal. The final concentration was calculated using the OD at 280 nm and an ε value of 8480 $M^{-1}cm^{-1}$. The truncated protein used in all assays was produced by Dr. C. Castillo.

2.2.3 Binding Affinity Validation of the Fluorescent Proteins

I incubated 2 µM PBP2 and DNS-PBP2 with 4 µM and 20 µM (+)-disparlure overnight, respectively. The protein-bound ligand was separated from the free ligand by P2 gel filtration and then was quantified by GC. PBP2 and DNS-PBP2 showed comparable binding affinities to (+)-disparlure (Figure 2-3).

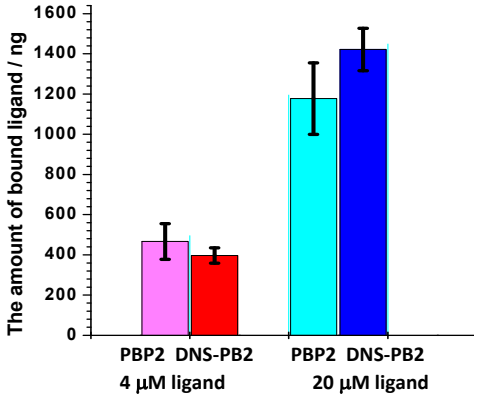

Figure 2-3 PBP2 and DNS-PBP2 bind (+)-disparlure with similar affinity.

Protein concentration was 2 µM. P values from t-test were 0.46 and 0.23, respectively. This means values do not differ significantly since P > 0.05.

To compare the dissociation constant, K_d, of the modified and nonmodified protein with (+)-disparlure, GC binding assays were performed with a Varian 3400 gas chromatograph (GC), operated in splitless mode and fitted with a flame-ionization detector (FID). For incubation replicates, the protein (DNS-PBP2 or PBP2) was diluted to 2 µM and a final volume of 1.5 mL. The ligand, (+)-disparlure was added in EtOH (0.6 µL of a 10 mM stock solution) to give a final concentration of 4 µM. This mixture was incubated overnight at 4 °C. Protein-bound and free pheromone were separated by gel filtration on small (0.3 g)

columns of Bio-Gel P2 (BioRad, 2 kDa exclusion limit) in a 1000 µL pipette tip with a cotton plug [104]. The eluate, which contained the protein·(+)-disparlure complex, was extracted with 3 × 500 µL hexane: ethyl acetate (1:1). The organic extracts were combined and run through the GC. The control assay without protein has revealed a 96% filtration efficiency of the column, which was taken into consideration later in calculations.

In the case of T-PBP2, the incubation mixture and separation procedure was modified by Dr. C. Castillo because of its weaker affinity to (+)-disparlure. A solution of 400 µL, 2 µM T-PBP2 was incubated with 4 µM (+)-disparlure and 320 µM of CHAPS (3-[(3-Cholamidopropyl)dimethylammonio]-1-propanesulfonate) on ice for 3 hours. The detergent was included to minimize ligand adsorption on the glass vial. Half of the solution was passed though a Bio-Gel P2 (0.08 g) column in a 200 µL tip. Half was transferred to a new glass vial. Both solutions were extracted with 2 x 100 µL hexane : ethyl acetate (1:1). In all cases, a control assay with the same amount of ligand but no protein was conducted in parallel.

2.2.4 Optical Properties of DNS-PBP2

For initial trials, both DNS and Trp (λ_{ex} = 295 nm) fluorescence intensities were measured for each protein sample. No fluorescence resonance energy transfer from Trp to DNS was detected. As in PBP2, the Trp fluorescence in DNS-PBP2 did not change upon ligand addition, but the fluorescence of DNS group decreased significantly (Figure 2-6A and B). Therefore, subsequent kinetic measurements were made by exciting at 340 nm and following DNS fluorescence.

All the fluorescence measurements were done with a PTI fluorometer equipped with a 710 photomultiplier detection system.

To convert the measured decrease in DNS intensity to changes in protein-ligand complex concentration, I performed the following correlation. A series of mixtures with a total protein concentration of either 2 µM or 4 µM, and varying proportions of PBP·ligand complex were prepared. The DNS-PBP·ligand complex was obtained by incubating DNS-PBP with 10 × excess of ligand overnight at 4 °C. The protein with bound ligand was separated from the free ligand by gel filtration on small columns of Bio-Gel P2 (0.3 g) in a 1000 µL pipette tip. The filtrate containing the PBP·ligand complex solution was aliquoted and flash frozen with liquid N_2. Aliquots were thawed immediately before measurement. The percentage of the total PBP-ligand complex in each aliquot, p, was evaluated by a parallel extraction of the aliquot and quantification by GC. For the assays, fresh DNS-PBP stock, which never came in contact with any ligand, was added to obtain a constant total protein concentration, $[P]_{total}$. In each series, the concentration of the ligand-containing protein ranged from 0 to ($[P]_{total}$ × p) µM.

2.2.5 Association of DNS-PBP2 with (+)- and (-)-Disparlure

Ligand association with DNS-PBP2 was investigated at a constant protein concentration (2 µM) with varied ligand concentrations (0.6 - 8 µM), and also at a constant ligand concentration (excess, 10 µM) with varied protein concentration (1 - 8 µM). Each protein sample was equilibrated in the fluorescence cuvette for

at least two minutes before ligand addition, and all measurements were made at 20 °C. At least four replicates were performed. Controls, in which the same volume of EtOH was added to the protein as that of the ligand stock were performed in parallel. Samples were excited at 340 nm, and the emission of DNS-PBP2 was monitored at 522 nm one point per second for at least 90 s.

To validate the optical measurements, I have performed a second series of experiments, in which the protein concentration was varied and the ligand concentration was constant and in excess using a GC assay. In this assay, 100 µL PBP2 samples of 1, 2, 4 and 8 µM were incubated with 10 µM (+)-disparlure (1 µL of 1 mM ethanol stock) for various lengths of time (5 to 90 s), and each point was tested in triplicate. Pheromone bound to PBP was separated from the free pheromone by gel filtration on small columns of Bio-Gel P2 (0.06 g) in a 200 µL pipette tip. The filtrate was extracted with 2 × 50 µL hexane: ethyl acetate (1:1) mixture and the recovered ligand was quantified by GC (Figure 2-4).

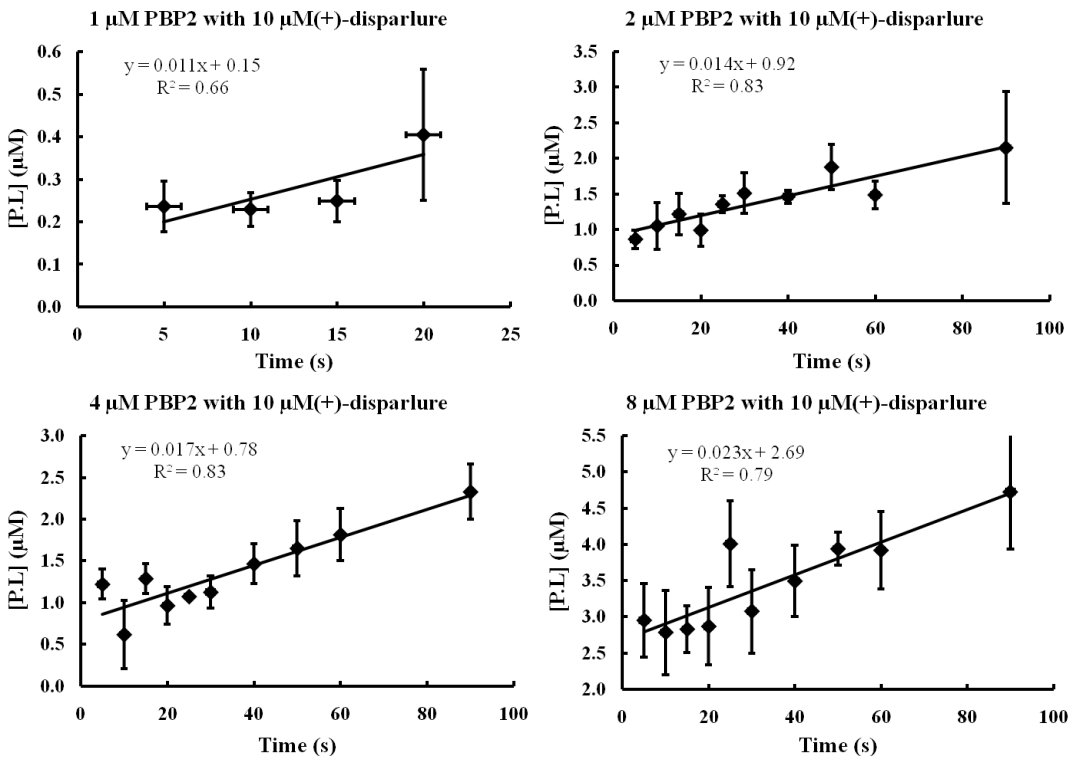

Figure 2-4 The association process of PBP2 with (+)-disparlure from the GC assay. Each point represents the average of three replicates (±S.E.). The slope represents the initial association rate.

2.2.6 Association of T-PBP2 with (+)-Disparlure

The association progress curve of T-PBP2 with (+)-disparlure was first performed with 100 µL solution (2 µM protein and 10 µM ligand), for various lengths of time (1, 5, 10, 15, 20, 25, 30 and 40 min), four to eight replicates for each point. The same gel filtration approach as for PBP2 association kinetics was used here. There was very good linearity up to 40 min. Later, tests were done for the association of 2 µM protein with varied ligand concentrations (0.5, 1, 1.5, 4 and 6 µM), at 15 and 40 min (Figure 2-5). There were at least four replicates for each point. Due to the small amount of ligand bound to the T-PBP2, 500 µL of

protein solutions were used and the protein-ligand complex was separated by larger P2 columns (0.35 g/tip). The filtrate was extracted with 2 × 200 µL hexane: ethyl acetate (1:1) mixture. Then, the organic extract was concentrated down to constant volume and the condensed extract was used for GC quantification.

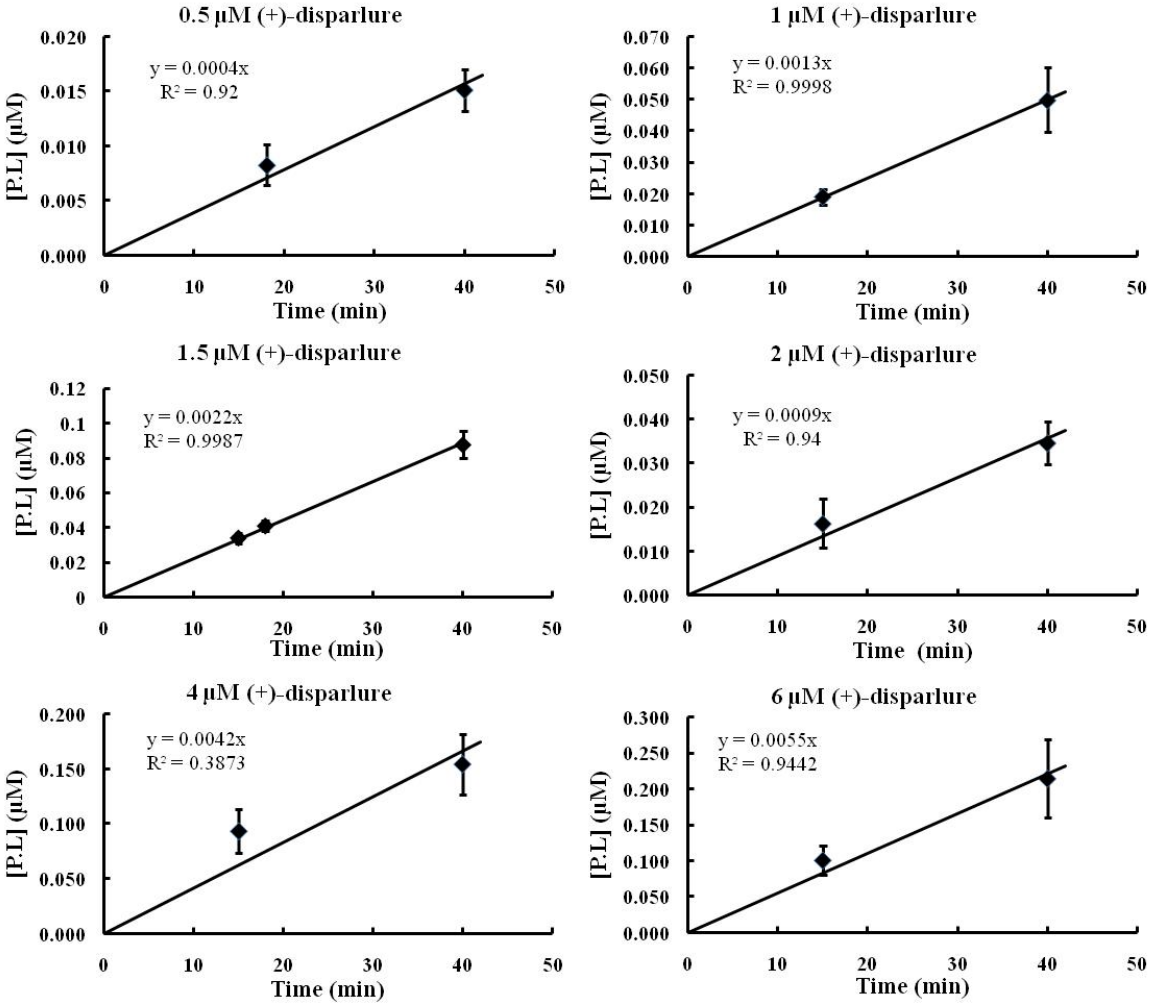

Figure 2-5 The association of 2 µM T-PBP2 with (+)-disparlure from the GC assay.

Each point represents the average of at least four replicates (±S.E.). The slope of the line through the origin represents the initial association rate.

2.2.7 Dissociation of DNS-PBP2 with (+)- and (-)-Disparlure

The DNS-PBP·ligand complexes were obtained following an overnight incubation as described above, and diluted to the desired concentration of 2 μM. The DNS fluorescence intensity was monitored immediately after preparation for about 3 h at 20 °C. Dissociation rate constants were obtained by fitting the data to an exponential decay.

2.2.8 Molecular Size Determination by Tryptophan Anisotropy

The Perrin equation,

$$r = \frac{r_0}{1 + \tau/\phi} \quad \textbf{(2.1)}$$

describes the relationship between the fluorescence anisotropy, r and the fluorescence lifetime, τ, and the rotational correlation time, ϕ, of a fluorophore (r_0 is the limiting anisotropy in the absence of diffusion). The rotational correlation time can also be expressed by the Stokes-Einstein-Debye equation,

$$\phi = \frac{\eta \cdot V}{k \cdot T} \quad \textbf{(2.2)}$$

where η is the solvent viscosity, k is the Boltzmann constant, T is the absolute temperature and V is the volume of the rotating particle. Combining Eq. (2.1) and Eq. (2.2) and rearranging,

$$\frac{1}{r} = \frac{1}{r_0}(1 + \frac{\tau \cdot k \cdot T}{V} \cdot \frac{1}{\eta}) \quad \textbf{(2.3)}$$

By measuring the fluorescence anisotropy as a function of viscosity at constant temperature, one may obtain the hydrodynamic volume of the rotating particle from the slope of a plot 1/r vs. 1/η [142,143].

To evaluate the extent of PBP multimerization, it is necessary to estimate the hydrodynamic volumes of the monomeric PBP. The hydrodynamic volume of a solvated macromolecular particle of arbitrary shape can be expressed as follows:

$$V_h = \frac{M_W}{N_a}\left(v_2 + \delta \cdot v_1^0\right) \quad \textbf{(2.4)}$$

where v_2 is the partial specific volume of the macromolecule, v_1^0 is the specific volume of water, δ is the hydration factor of the protein and N_a is the Avogadro constant [144].

Both v_2 and δ values can be estimated from the amino acid composition of the protein [145,146]. An average value of 0.037 of the positive error between the calculated and experimental hydration factors from 6 proteins was taken into account [145]. In my case, v_2 = 0.736 cm^3/g, and δ = 0.343 g H_2O/g protein. At 20 ºC, v_1^0 = 1.0018 cm^3/g, the reciprocal of the density of water.

2.2.8.1 Tryptophan Anisotropy Measurements

Samples (20 mM Tris buffer, pH 7.4) were prepared as described in (Flecha et al., 2003) [142], and sample viscosity was varied with glycerol, using the

same composition for each set of samples (four replicates). The viscosity of each sample was calculated from the concentration of glycerol [142]. Two protein concentrations (2 and 10 μM) were chosen. Experiments were conducted without ligand and with 10 μM of the most strongly bound ligand for each protein. Ligand-containing samples were measured after 3 min and again after overnight incubation. Tryptophan was excited at 280 nm and its emission monitored at 335 nm (20 °C) using a HORIBA Jobin Yvon SPEX spectrofluorometer (Fluorolog-3) equipped with Glan-Thompson autopolarizers (5 nm bandwidth). Reported anisotropy values, determined from the intensity of the horizontally (H) and vertically (V) polarized emission components according to Eq. (2.5), are averages of at least three measurements. G factor is defined as the ratio of sensitivities of the detection system for the vertically and horizontally polarized light [147].

$$r = \frac{I_{VV} - G \cdot I_{VH}}{I_{VV} + 2 \cdot G \cdot I_{VH}}, \text{ with } G = \frac{I_{HV}}{I_{HH}} \quad \textbf{(2.5)}$$

2.2.8.2 Lifetimes of Tryptophan in PBP2

Fluorescence lifetime measurements were performed by Ms. T. C. S. Pace in Dr. Bohne lab (Department of Chemistry, University of Victoria), with an Edinburgh Instruments OB 920 single photon counter. The excitation wavelength was 300 nm, while the emission was measured at 340 nm. The bandpass for the excitation and emission monochromators was ca. 16 nm and the number of counts collected at the maximum intensity was 2,000. The instrument response

function was recorded using Ludox to scatter light at the excitation wavelength and the instrument response function was deconvoluted from the fluorescence decay curve when fitting the decays to the sum of two exponentials. The quality of the fit was judged by analyzing the χ^2 values (0.96 – 1.11) and by visual inspection of the residuals and the autocorrelation.

Amplitude average lifetimes were calculated using the equation (2.6), where τ_i are the lifetimes and A_i the pre-exponential factors. The sum of all pre-exponential factors is unity:

$$\langle \tau \rangle = A_1 \tau_1 + A_2 \tau_2 \qquad \textbf{(2.6)}$$

The tryptophan lifetimes were measured for 2 and 10 μM protein solutions. Tests were conducted with the ligand-free protein and with protein that had been incubated with 10 μM ligand overnight. The same combinations of PBP and ligand as in the anisotropy tests were used. In the absence of ligand the lifetimes and pre-exponential factors do not depend on the protein concentration (τ_1 = 6.09 ± 0.09, A_1 = 0.57 ± 0.3, τ_2 = 3.4 ± 0.1, A_2 = 0.44 ± 0.03), while in the presence of ligand the lifetimes and pre-exponential factors change continuously with the increase in the protein concentration.

2.3 Results

2.3.1 Ligand Binding Affinities of the Dansylated PBP2 and of the C-terminus truncated PBP2

The average amount of disparlure bound to dansylated PBP2 (DNS-PBP2)

was compared to that bound to unlabeled PBP2. The result showed no statistically significant difference (6 independent replicates, t-test, $P > 0.05$, Figure 2-3), and that the two proteins have very similar dissociation constants (Table 2-4). Therefore, the DNS modification did not affect the binding affinities of PBP2. This might be explained by the modification sites, K31 and 38 being on the surface of the homology-modeled PBP2 structure. However, the C-terminally truncated PBP2, T-PBP2, exhibited a significantly reduced thermodynamic binding affinity towards (+)-disparlure (Table 2-4). Two observations suggest similar secondary structures for PBP2 and T-PBP2: 1) T-PBP2 reacts with antiserum raised against PBP2 and 2) both proteins have similar far-UV CD spectra (Figure 3-5).

Table 2-4 The comparison of the dissociation constants between PBP2, DNS-PBP2 and T-PBP2 with (+)-disparlure by GC assay.[a]

Protein	$[P]_{total}$ (μM)	$[L]_{total}$ (μM)	$[L]_{bound}$ (μM)	$K_d=[L]_{free}[P]_{free}/[L]_{bound}$ (μM)
PBP2	2	4.7 ± 0.3	1.1 ± 0.2	3 ± 1 [b]
DNS-PBP2	2	3.8 ± 0.6	1.5 ± 0.5	3 ± 2 [b]
T-PBP2	2	0.6 ± 0.1	0.07 ± 0.01	16 ± 3 [b]

[a] Means ± S.E. of 6 replicates. [b] Values represent the average of K_ds calculated from individual samples.

2.3.2 Optical Properties of DNS-PBP2

When excited at 295 nm, DNS-PBP2 gives two emission peaks, assigned to Trp at 327 nm and DNS at 520 nm. The intensity of each is designated as I_{trp} and I_{dns} respectively (Figure 2-6A). The I_{dns}/ I_{trp} ratio decreased significantly (>

20%) upon ligand binding, dominated by a decrease in I_{dns}. With increasing concentration of ligand-bound protein, both I_{dns} and I_{trp} are observed to decrease linearly, although the change in I_{trp} is substantially smaller (Figure 2-6B). For this reason, subsequent experiments were conducted with selective excitation of DNS at 340 nm. The correlation between the change in I_{dns} and the concentration of ligand-bound protein is not dependent on total protein concentration; I_{dns} is observed to decrease with the same slope for either 2 or 4 μM protein (Figure 2-6C). Similar results were obtained using either (+)-disparlure, (-)-disparlure, or the racemic mixture (data not shown). Since I_{dns} is more sensitive than I_{trp} to ligand binding I have used I_{dns} to monitor the kinetics of protein-ligand association and dissociation.

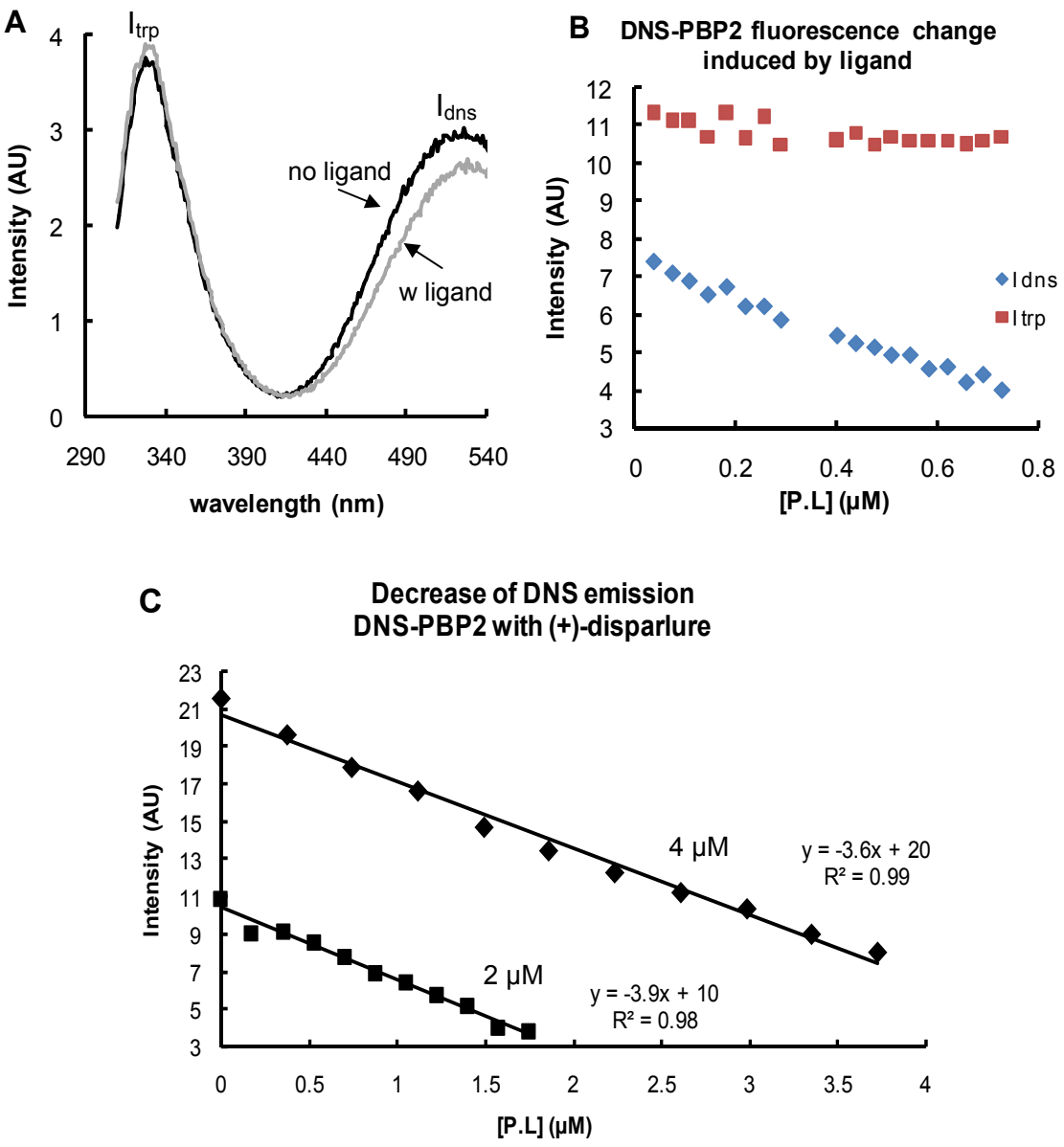

Figure 2-6 The optical properties of DNS-PBP2 related to ligand binding.

A. DNS-PBP2 emission spectra at excitation wavelength of 295 nm (black: without ligand; pale: with ligand). B. An example to show the I_{trp} and I_{dns} change in tryptophan and dansyl fluorescence intensity, with increasing concentration of the protein·ligand complex for DNS-PBP2·(+)-disparlure, when the total protein concentration was kept at 2 μM. Samples were excited at 295 nm. C. I_{dns} decreased linearly, corresponding to the increase in the concentration of ligand-bound protein. Samples were excited at 340 nm, for two different total protein concentrations (squares: 2 μM; diamonds: 4 μM).

2.3.3 Kinetic Studies

2.3.3.1 Association of DNS- PBP2 with (+)- and (-)-Disparlure

I have observed a slow association of ligands to PBP2 and DNS-PBP2, in seconds (Figure 2-4 and Figure 2-7A), and an even slower association to T-PBP2, in minutes (Figure 2-5 and Figure 2-7B). I consistently observed in both fluorescence and GC assays a non-zero physical quantity at time 0, which suggested some kinetic behavior of the protein that was not resolved on the experimental timescale (~ 5s). This is clearly visible in the fluorescence assay (Figure 2-7A) where ~ 50% of the total fluorescence quenching associated with ligand binding is static. Similar behavior is detected in the GC-based assay. The shortest feasible incubation time for GC-based assays is similar to the time resolution of the fluorescence experiments. Within this time window, I also observed by GC that ~ 40% of the total concentration of PBP2-ligand complexes (monitored over 100 s) had already formed (Figure 2-4). I am unable to resolve the kinetics of PBP2 with (+)-disparlure in < 5s with the current methods. However, I have carefully validated the measurements with different methods for the slower (>5s) kinetic behavior and the results are consistent (see Chapter 3).

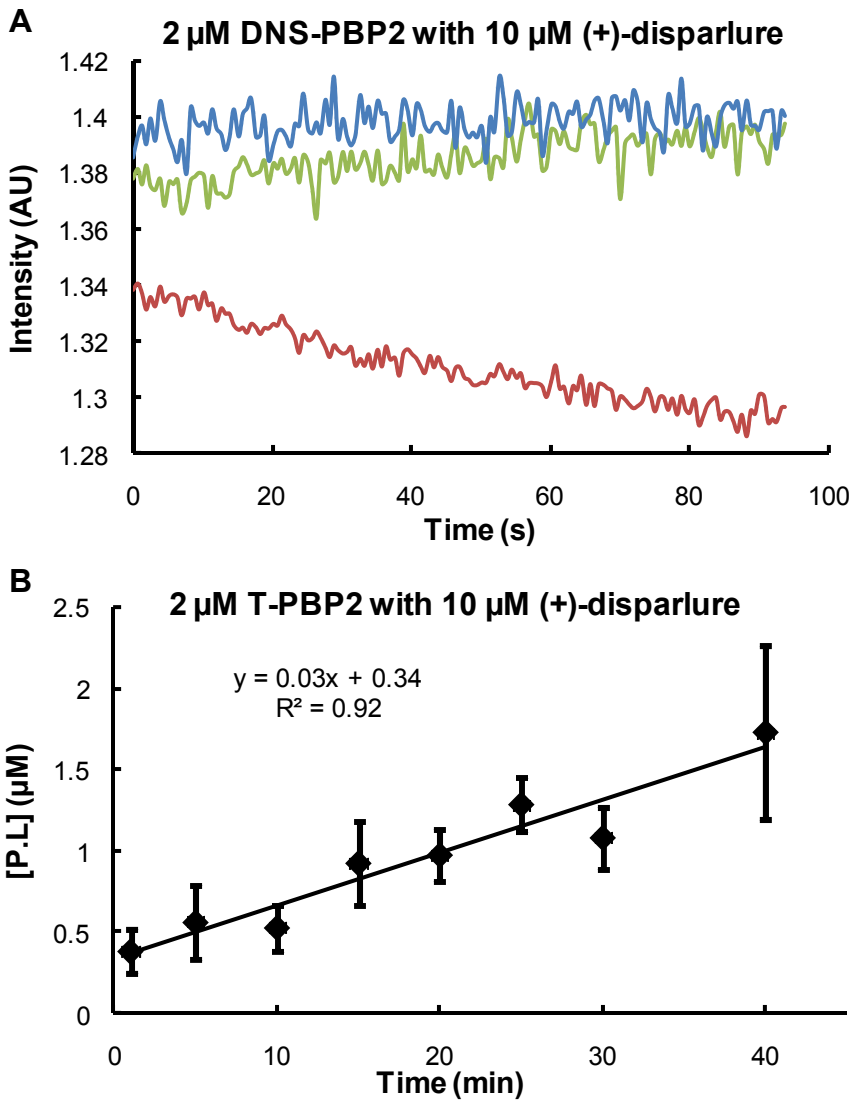

Figure 2-7 The slow association of DNS-PBP2 and T-PBP2.

A. I_{dns} decreased with time upon ligand addition (red line) while the solvent for the ligand, EtOH, showed no effect (green line). The DNS fluorescence was stable with time when there was no treatment (blue line). B. The association of 2 μM T-PBP2 with 10 μM (+)-disparlure determined by a GC assay. Each point represents the average of at least three replicates, bars indicate the S.E.. The slope represents V_0, the initial binding velocity used in the determination of the order in Figure 2-9. T-PBP2 shows much slower kinetics when compared to PBP2 (Figure 2-4).

In this work, I have probed the slow association by measuring the initial binding rate as a function of ligand concentration according to Eq. 2.7,

$$V_0 = k_{on}[P]_0^m[L]_0^n \quad \textbf{(2.7)}$$

where V_0 is the initial linear rate of the slow phase, k_{on} is the association constant, P_0 is the initial protein concentration, L_0 is the initial ligand concentration, and m and n reflect the reaction order of the protein and ligand, respectively. With increasing ligand concentration in the low concentration regime where ligand is limiting ([L] ≤ 2 μM, 2 μM DNS-PBP2), the initial rate increased linearly. From the slope I have obtained the k_{on} values for both ligands (Figure 2-8A). The reaction order, n for ligand, was obtained from the slope of a plot of $\log V_0$ vs. $\log[L]_0$ (Table 2-5). At ligand concentrations exceeding that of protein, V_0 becomes independent of ligand concentration. This result is very important. It indicates that PBP2 becomes saturated with excess ligand and reaches its maximum association velocity, which is independent of the ligand concentration. I have observed an offline point at 2 μM of ligand for both ligands, in both methods. This is consistent with the previous observation that binding affinity is related to the protein: ligand ratio [47]. One explanation is that PBP acts differently at high and low ligand concentration and that 2 μM, corresponding to 1:1 PBP: ligand ratio in this case, is a switch point for different PBP functions.

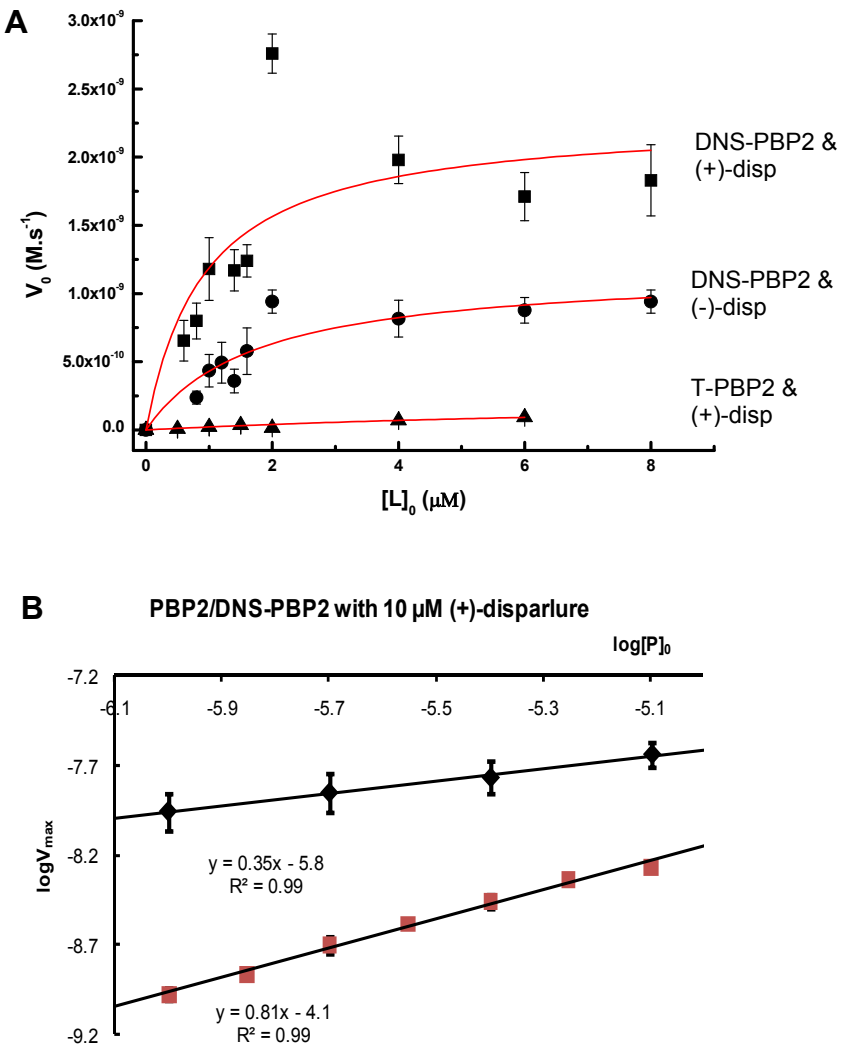

Figure 2-8 Binding rates of PBP2 with (+)- or (-)-disparlure.

For DNS-PBP2, rates were obtained by excitation at 340 nm and following changes in DNS fluorescence on addition of ligand. For PBP2 and T-PBP2, rates were extracted from the GC-based data in Figure 2-4 and Figure 2-5. Bars indicate S.E. for fluorescence-based data and fitting errors for GC-based data. A. The plot of V_0 against L_0 when the protein concentration was 2 μM and the ligand concentration was varied from 0.6 μM to 8 μM. V_{max} is the maximal rate of ligand binding at ligand saturation. Curves are fitted to Michaelis-Menten equation (squares: DNS-PBP2 and (+)-disparlure; circles: DNS-PBP2 and (-)-disparlure; triangles: T-PBP2 and (+)-disparlure). B. Based on Eq. 2.7, the plot of $\log V_{max}$ against $\log P_0$ when the ligand concentration was held constant at 10 μM and protein concentration was varied from 1 μM to 8 μM (diamonds: PBP2; squares: DNS-PBP2). The slopes give the reaction orders in protein, which are both smaller than 1 (see text).

In a second series of experiments, the protein concentration was varied from 1 - 8 μM while the ligand concentration was in constant excess (10 μM). The initial rates thus obtained correspond to the maximum at each protein concentration. These are shown in Figure 2-8B derived from fluorescence and GC assays. These data may be fit to Eq. 2.8,

$$\log V_{\max} = \log k + m \log P_0 \quad \textbf{(2.8)}$$

where m represents the general "association" order of the protein, while the parameter k typically represents the rate constant. The meaning of this parameter for PBP2 ligand binding will be discussed below. The association orders for PBP2 from either fluorescence (0.81 ± 0.03) or GC (0.35 ± 0.02) assays are both smaller than 1 (Table 2-5).

The association curve of T-PBP2 with (+)-disparlure is very similar to that of PBP2 (Figure 2-8A), except that the binding is much slower.

Table 2-5 Summary of ligand binding kinetics and thermodynamics for PBP2.

Measurement			Ligand	
			(+)-disparlure	(-)-disparlure
k_{on} ($M^{-1}s^{-1}$) [a]	DNS-PBP2		$(4.8 \pm 0.4) \times 10^2$	$(1.6 \pm 0.2) \times 10^2$
	T-PBP2		$(0.12 \pm 0.01) \times 10^2$	N.D.[e]
k_{off} (s^{-1}) [a]	Flu.		$(4.7 \pm 0.4) \times 10^{-4}$	$(5.0 \pm 0.2) \times 10^{-4}$
	Radio [b]		1×10^{-4}	3.3×10^{-5}
n			1.1 ± 0.2	1.3 ± 0.3
K_d (μM)	Flu.	k_{off}/k_{on}	1.0	3.1
	Radio [b]		1.8	3.2
K_d' (μM) [c]	DNS-PBP2		0.9 ± 0.5	1.6 ± 0.6
	T-PBP2		10 ± 3	N.D.
k_2 (s^{-1}) [d]	DNS-PBP2		4.3×10^{-4}	2.6×10^{-4}
	T-PBP2		1.5×10^{-4}	N.D.
m	Flu.		0.81 ± 0.03	N.D.
	GC		0.35 ± 0.02	N.D.

[a] $V_{on} = k_{on}[P]^m[L]^n$; $V_{off} = k_{off}[P \cdot L]$

[b] Assays with radio labeled disparlure [46,104].

[c] The dissociation constant of the hypothetical intermediate $P \cdot L_{ex}$ from the fitting of PBP2 association data (Figure 2-8A) with Michaelis-Menten equation.

$$K_m = \frac{k_{-1} + k_2}{k_1} \approx \frac{k_{-1}}{k_1} = K_d'$$

[d] $k_2 = K_d' \times k_{on}$ (Scheme 1)

[e] N.D. = not determined

2.3.3.2 Dissociation of DNS-PBP2 Ligand Complexes

Dissociation of DNS-PBP2·ligand complexes (Figure 2-9) follows an apparent first-order exponential decay (Eq. 2.9, derived in section 2-6),

$$\chi = Ae^{-k_{app}t} \quad \textbf{(2.9)}$$

where χ represents the amount of complex dissociated, and k_{app} is the apparent dissociation rate constant, k_{off}. DNS-PBP2 complexes with either (+)- or (-)-disparlure dissociate with similar, extremely slow, kinetics (Table 2-5). The rate constants for ligand binding and release yield dissociation constants ($K_d = k_{off}/k_{on}$,

Table 2-5), that compare well to literature values of 1.8 and 3.2 μM for (+)- and (-)-disparlure, respectively [104]. The slight selectivity between these two ligands was preserved. That is, PBP2 binds (+)-disparlure more strongly than (-)-disparlure, either in equilibrated conditions or as indicated from the derived kinetic constants. These results are important, as they indicate that the processes I am following represent the rate-limiting steps for binding and dissociation.

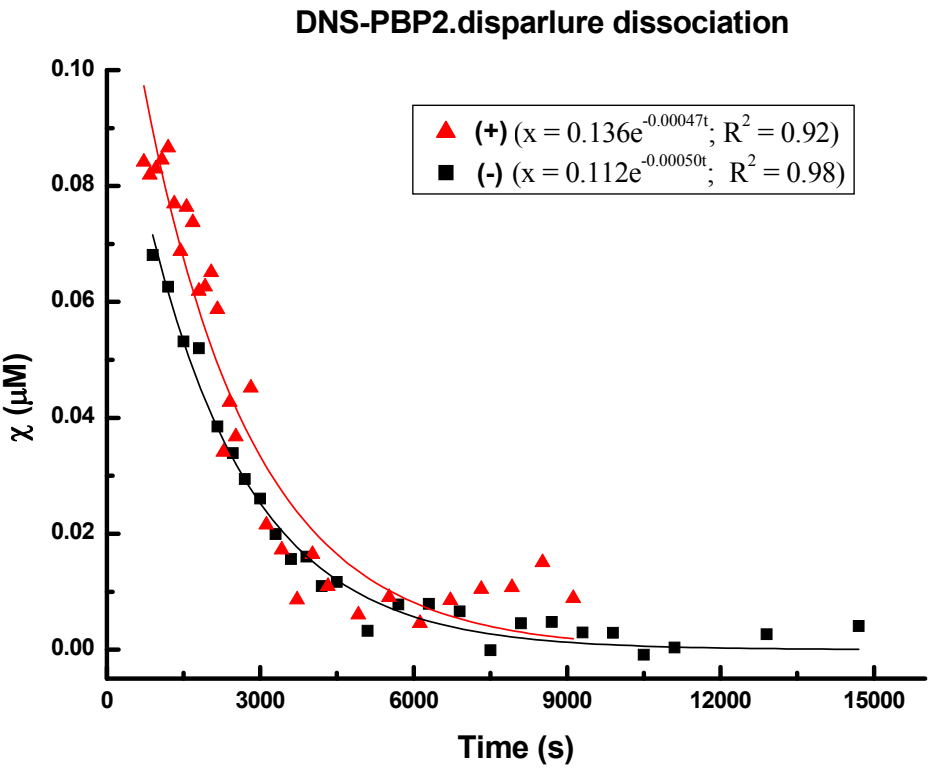

Figure 2-9 The dissociation of DNS-PBP2.ligand complexes with time.

The amount of the complex dissociated plotted against time (Eq. 2.8). Fitting of the data to the first order exponential decay presented the apparent dissociation rate constant, which is 4.7 x 10^{-4} s^{-1} for (+)-disparlure (triangles) and 5.0 x 10^{-4} s^{-1} for (-)-disparlure (squares). Fitting results are listed on the top right corner.

2.3.4 Molecular Size of Ligand-PBP2 Complexes Evaluated by Tryptophan Anisotropy

I have measured the Trp fluorescence anisotropy of unlabeled PBP2 and its ligand complexes, as a function of solvent viscosity in order to evaluate their hydrodynamic volumes, and, correspondingly, their degree of multimerization. Double reciprocal plots of anisotropy versus viscosity are linear as predicted by Eq. 2.3 (Figure 2-10). To extract the volume, V, from these data, we require also the limiting anisotropy (r_0), and fluorescence lifetime (τ) of Trp in each sample and the hydrodynamic volume of monomeric PBP. The former, r_0 was obtained from the linear fitting of the data (Figure 2-10) and τ (Table 2-6) has been measured experimentally. The hydrodynamic volume of monomeric PBP2 is estimated to be 29 nm^3 according to Eq. 2.4. Based on crystallographic data, the approximate dimensions of the BmorPBP (15.9 kDa, 142 a.a) are 40 x 35 x 30 Å [92]. Its corresponding volume, approximating an ellipsoid, is 22.0 nm^3. Considering that PBP2 (16 kDa, 145 a.a) is longer by 3 amino acids than BmorPBP, the calculated 29 nm^3 volume for PBP2 monomer is reasonable.

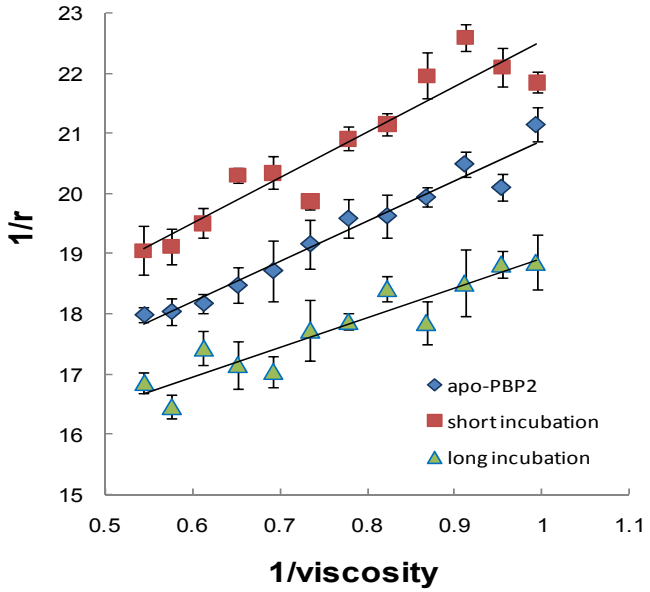

Figure 2-10 Change of the tryptophan anisotropy with viscosity reveals changes in volumes upon interaction with ligand. [PBP2] = 2 µM, [(+)-disparlure] = 10 µM, λ_{ex} = 300 nm (Eq.2.3). The concentrations of glycerol used ranged from 0 to 22% p/p, corresponding to the viscosity from 1 to 1.8 mPa.s. Each point represents the average of three replicates.

Hydrodynamic volumes of PBP2 and its complexes are evaluated according to Eq. 2.4, yielding values ranging between ~ 40 and 90 nm^3 depending on protein concentration and ligand incubation time (Table 2-6). Within experimental error (± 5 nm^3) the average hydrodynamic volume of apo-PBP2 was independent of protein concentration between 2 and 10 µM, and the averaged volume for an overall population of PBP2 (free and ligand-bound forms) was unchanged by short incubation with ligand. A consistent increase in volume was detected following overnight incubation with ligand.

Table 2-6 Trp anisotropy parameters for PBP2 and PBP2·(+)-disparlure complexes following different incubation conditions.

Conditions	2 μM PBP			10 μM PBP		
	w/o ligand	3 min [a] incubation	overnight	w/o ligand	3 min [a] incubation	overnight
r_0	0.08	0.07	0.07	0.04	0.05	0.07
τ / ns [b]	4.95	4.39 [c]	3.82	4.83	4.79 [c]	4.74
V / nm^3	52.6	54.7	67.1	44.9	43.0	87.5
# of monomer [d]	1.8±0.1	1.9±0.01	2.3±0.2	1.5±0.3	1.5±0.2	3.0±0.8

[a] Protein samples were incubated with 10 μM (+)-disparlure.
[b] Amplitude average lifetime
[c] Average of the lifetimes obtained without ligand and incubated with ligand overnight.
[d] $V_{sample}/V_{monomer}$

In all cases, the numbers of monomers in each rotational unit (evaluated as $V_{sample}/V_{monomer}$) are non-integral. This is not surprising given that I am measuring the average molecular volume of an equilibrium population of PBP2 species, e.g., monomer and dimer. I further note the errors associated with these measurements, and the theoretical approximations made, including modeling the rotating particle as a sphere. However, in all cases the number of monomers is greater than unity, largely between 1-2 within experimental error. This consistently suggests that PBP2 does not exist as homogenous monomers in solution, either with or without ligand; instead, an equilibrium population of monomers and dimers is the simplest explanation for my data. The change of the multimerization equilibrium induced by ligand was significantly slower than the binding kinetics. Therefore, the change in multimer states during the time window of the binding kinetics was insignificant and this simplified data analysis.

2.4 Discussion

2.4.1 Fluorescent PBP2 Mimics Wild-Type Protein

As confirmed by the GC assay, PBP2 and DNS-PBP2 have the same dissociation constants within experimental error (Table 2-4); the modification does not change the binding affinities of PBP2. It is therefore likely that the binding pocket and corresponding ligand interactions are unaffected by the fluorophore, consistent with the labeling sites (Lys31 and/or Lys38) being on the surface of the protein. Furthermore, two different methods, GC and fluorescence, gave fractional association orders, m, for PBP2 with (+)-disparlure (Figure 2-8B), and K_d values estimated from k_{on} and k_{off} for both ligands are close to those previously reported (Table 2-5). Thus, the fluorescent-labeled PBP2 is a valid mimic of wild type protein, and provides a method for measurements of native ligand binding kinetics.

2.4.2 Kinetic Pathway for PBP2- Ligand Interaction

Previous studies have found that a decrease of the pH can induce a significant conformational change on the C-termini of long-chain PBPs [108,115,148]. However, from a more recent study, it seems that a small local conformational change of the PBP (not caused by pH changes), is sufficient to trigger the receptor response [29]. I did not investigate the pH effect on PBP-ligand interaction kinetics in this paper. Based on the behaviors of PBP2 under physiological pH I have found here, I propose an alternative pathway of ligand binding and releasing, without invoking a significant conformational change of the C-terminus

induced by a pH decrease.

Based on the measured association and dissociation kinetics of DNS-PBP2 with (+)- and (-)-disparlure, I propose that the ligand associates with PBP2 first at a peripheral site, equilibrating with the rate constants k_1 and k_{-1} for the forward and reverse interactions, respectively (Scheme 1). The PBP2·ligand complex intermediate, $P{\cdot}L_{ext}$ may then be transformed to the specific complex P·L, by properly orienting the ligand and docking it into the inner binding pocket. The rate constant for this step is designated as k_2. Complex P·L dissociates to the intermediate $P{\cdot}L_{ext}$ with a very small rate constant, k_{-2} (Scheme 1). The rate-limiting step for binding is internalization of the initially associated ligand, while exhalation of the bound ligand to the peripherally-associated species rate limits the dissociation process ($k_1 \gg k_2$, $k_{-1} \gg k_{-2}$).

Scheme 1.

$$P + L \underset{k_{-1}}{\overset{k_1}{\rightleftharpoons}} P.L_{ext} \underset{k_{-2}}{\overset{k_2}{\rightleftharpoons}} P.L$$

The proposed intermediate in the binding pathway is necessary to rationalize the saturability of the association curves observed in both fluorescence and GC-based assays (Figure 2-8A). Two-phase binding kinetics have been observed during earlier work on PBPs [46,113], and a similar ligand-binding pathway has been observed for human cytochrome P450 3A4 [149], for which substrate binds to a peripheral site before entering the catalytic pocket. Here I find that the initial association proceeds at a fast rate, which can not be

resolved on the timescale I am using, suggesting that it is more easily accessed by ligand. I propose that this first binding site is a hydrophobic patch on the protein surface, specifically a site near the C-terminus of the PBP. This model is based on several facts. First, the C-terminus is sufficiently hydrophobic to accommodate the aliphatic chain of the ligand (Figure 2-11). Second, the flexibility of the C-terminus provides a greater opportunity for protein-ligand collision than the less flexible core of the protein. Third, the C-terminus, the N-terminus and the loop between α-helices 2 and 3 comprise an opening of the binding pocket with considerable mobility [107,110]. My proposed model is also supported by two other pieces of experimental data. First, in the photoaffinity labeling of ApolPBP with an analogue of its pheromone, the exclusively labeled residue (Thr44) is located on the α2/α3 loop in a conformation pointing outward relative to the binding pocket [107,125]. Second and most importantly, the ~40× slower kinetic behavior of T-PBP2 (this study) indicates damage to the association phase when the C-terminus is missing (Table 2-5).

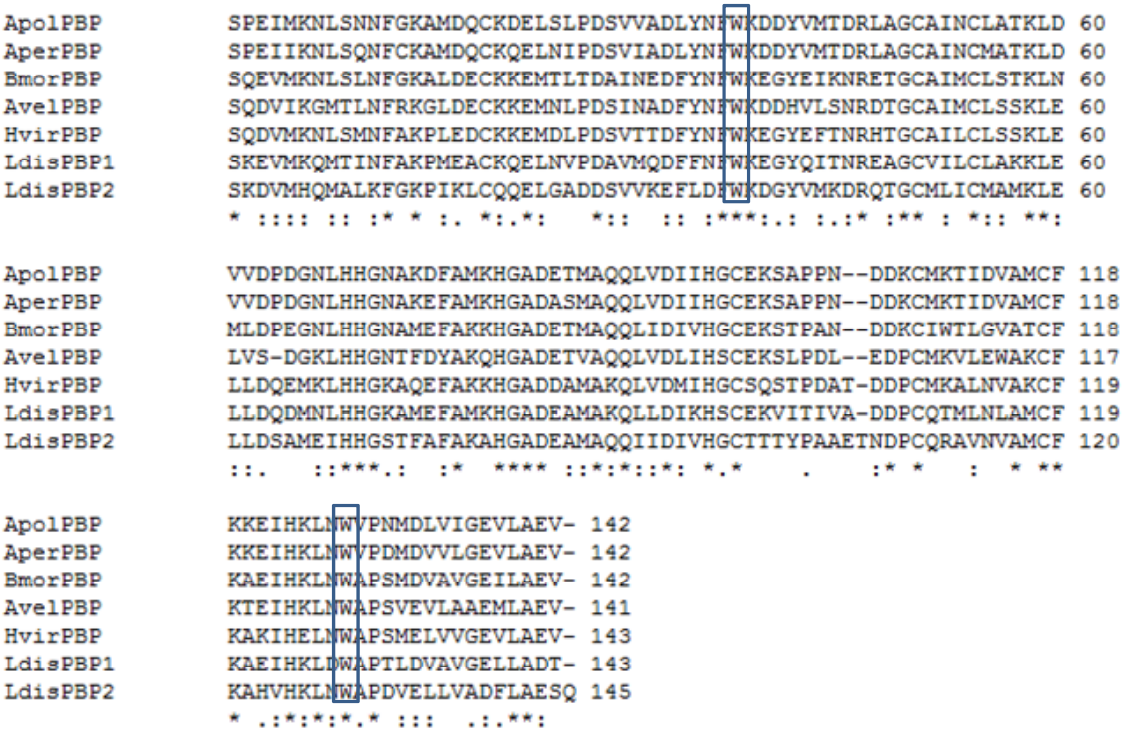

Figure 2-11 Sequence alignments of moth PBPs.

Apol*: A. polyphemus,* Aper: *A. pernyi,* Avel: *A. velutinana,* Bmor: *B. mori,* Hvir: *H. virescens and* Ldis: *L. dispar*. The symbol '*' indicates a fully conserved residue, ':' specifies strongly conserved residues, while '.' indicates a weakly conserved residue. Overall, the C-termini of the long-chain PBPs, starting from the second framed Trp, share high similarity and are considerably hydrophobic.

I also suggest that the external binding site possibly involves Trp37 which is highly conserved in all long-chain PBPs and is in the α2-α3 loop (Figure 2-11 and Figure 2-12). Assays of ligand binding based on changes in Trp fluorescence are consistent with the proposed two-step binding model. Binding of bombykol, the cognate ligand for BmorPBP, was shown to quench the intrinsic Trp fluorescence of BmorPBP in milliseconds with no spectral shift [113]. Also, titration of ligand into ApolPBP elicited a change of the Trp37 fluorescence intensity with no shift in emission wavelength [120]. These changes in Trp fluorescence intensity

with no spectral shift appear to be characteristic of a rapid interaction between a ligand and the external binding site.

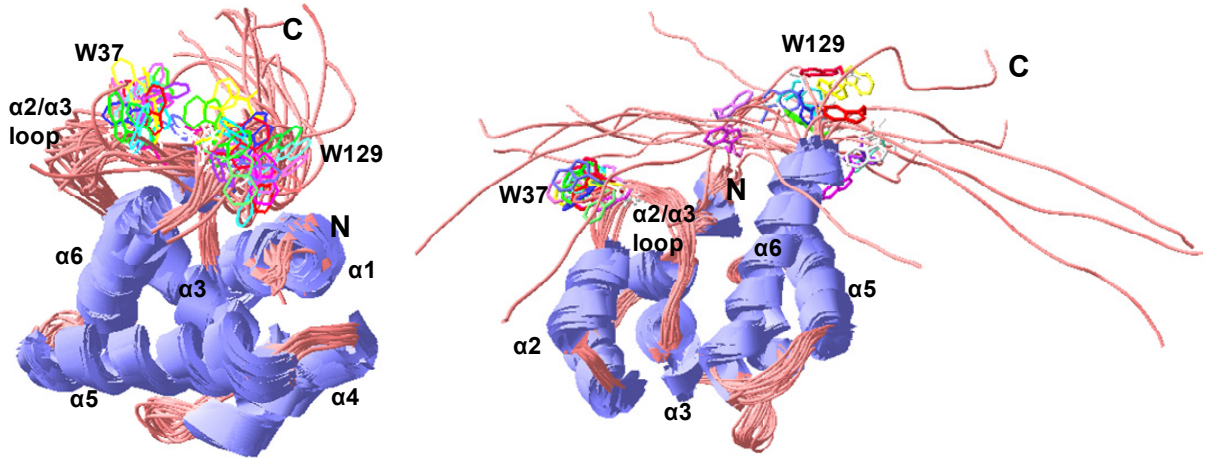

Figure 2-12 The threading structures of PBP2 on 20 NMR structures show flexible regions. Left: on BmorPBP (PDB ID: 1LS8) (Lee, et al., 2002); Right: on ApolPBP (PDB ID: 1QWV) (Mohanty, et al., 2004). Trp37 and Trp129 are shown. The C-terminus and the loop between α-helices 2 and 3 present multiple conformations. Models were prepared with Spdb-viewer.

The process of ligand translocation from the external, peripheral site, to the internal binding pocket has been the focus of this chapter. I will discuss the first step in detail in the next chapter. With DNS-PBP2 and disparlure, I could not separate the initial association from the translocation process. However, the overall binding process is saturable (Figure 2-8A), meaning that a steady-state population of the intermediate ($P.L_{ext}$) builds up rapidly, and that the externally adsorbed ligand is then slowly internalized. The k_{on} values obtained represent the overall rate constant for both steps. The overall process (Scheme 1) is analogous to a pathway for one-site enzyme catalysis. A plot of the initial rate against ligand concentration at constant protein concentration may thus be fit to the Michealis-Menten equation to estimate the K_m value. This will be close to the dissociation

constant, $K_d^{'}$ of the intermediate when $k_{-1} \gg k_2$ (Table 2-5). This is related to the concentration of the intermediate, Eq. 2.10

$$[P.L_{ext}] = \frac{[P][L]}{K_d^{'}} \approx \frac{[P][L]}{K_m} \quad \textbf{(2.10)}$$

and, correspondingly, to the overall rate constant for ligand binding, k_{on}, Eq. 2.11

$$V_{on} = \frac{d[P.L]}{dt} = k_2[P.L_{ext}] \approx \frac{k_2}{K_m}[P][L] = k_{on}[P][L] \quad \textbf{(2.11)}$$

The values of $K_d^{'}$ for (+)- and (-)-disparlure with DNS-PBP2 are similar, (0.9 ± 0.5) μM and (1.6 ± 0.6) μM, respectively. However, the binding affinity of (+)-disparlure at the peripheral site of T-PBP2 is 10× weaker ($K_d^{'}$ = 10 μM). This agrees well with the hypothesis that the C-terminus is the major component of the peripheral binding site. The translocation rate constant k_2, as a product of $K_d^{'}$ and k_{on}, is a first order rate constant with the unit of s^{-1}. The k_2 values show slight difference between ligands (4.3×10^{-4} s^{-1} for (+)-disparlure and 2.6×10^{-4} s^{-1} for (-)-disparlure), suggesting that the slow second translocation step is ligand selective. This value for T-PBP2 with (+)-disparlure is smaller (1.5×10^{-4} s^{-1}), which means that the loss of the C-terminus affected the internalization of the ligand to some extent (Table 2-5).

The dissociation of the P·L complex is extremely slow. This is likely caused by complete enclosure of the ligand in the binding pocket, such as bombykol in BmorPBP and cVA in LUSH (Figure 1-9) [29,92]. Furthermore, my observation that T-PBP2 dissociates from ligand more easily (larger K_d, Table 2-4), indicates that

the removal of the C-terminus has lowered the barrier to dissociation. Based on my study, I propose that the C-terminus and the other components of the external binding site may act as a “gate” that the ligand has to pass to enter or exit the binding pocket.

2.4.3 Monomer and Multimer Equilibrium in Solution

Aggregation of OBPs in solution has been reported several times [47,102,104,105], and has been observed directly in the solid state by x-ray crystallography [29,92,97-100]. Since the oligomeric state of the proteins may affect the interactions with ligand, I need to understand the aggregation forms of the PBP under the kinetic test conditions. I propose that in solution, the PBP monomer exists in equilibrium with at least one other population of higher-order aggregate, most likely a dimer under my experimental conditions. This proposal is supported by values for PBP2 hydrodynamic volumes, estimated by Trp fluorescence anisotropy, that are intermediate between monomeric and dimeric forms, even at a low concentration of 2 μM (Table 2-6).

Additional evidence for protein multimerization comes from measurements of the initial association rate of PBP2 with an excess of ligand, which provides the maximum rate, V_{max}, at that protein concentration (Figure 2-8B). I found that V_{max} is proportional to $[P]^m$, $m<1$(Table 2-5), which means that $V_{max}/[P]$ will decrease with increasing protein concentration. Since V_{max} represents the maximum number of ligand molecules that can be bound to the protein per second, $V_{max}/[P]$ represents the maximum number of bound ligand molecules per protein molecule

per second, in other words, the binding capacity of the PBP per second. At increased protein concentration, this binding capacity decreases. One explanation is that, at high protein concentration, the aggregated protein blocks the binding of ligand to some extent. If there are two populations of protein in the solution (Figure 2-13), they may or may not have the same conformation. One population of PBP can bind ligand directly (A in step b1 and b3), while another, whose binding pocket is blocked in the multimeric form, needs to dissociate first (B in step b2). The monomer-multimer equilibrium will shift towards multimer with increasing protein concentration (step a), accounting for the decreased per second binding capacity in the higher protein concentration regime.

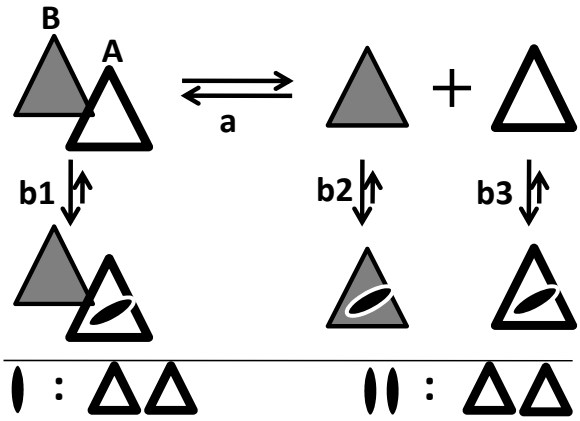

Figure 2-13 Model of the equilibrium between the PBP dimer and monomer.

Addition of ligand or high protein concentration favors the formation of dimers (step a), in which two populations of PBP exist (type A and type B). Type B PBP has a more blocked ligand entrance to the inner binding site. The binding process of PBP molecules is labeled as step b. Dimeric PBP has smaller binding capacity (1 ligand per two proteins) than the monomeric PBP (1 ligand per protein) (ellipses: ligand; triangles: PBP). The binding capacity is shown schematically below the line.

Consequently, I suggest addition of another component to the core PBP2 kinetics scheme, namely, equilibrium between monomeric and dimer/multimeric

forms of PBP2. The shift of this equilibrium induced by ligand is slow and therefore will not interfere with the PBP-ligand interaction kinetics. Steady-state kinetics do not resolve the equilibrium distribution; my measurements reflect the population-weighted average kinetic properties of all PBP2 species, of which only ligand-binding competent type A are represented by P in Scheme 1.

The maximal initial velocity measured by both fluorescence and GC methods (Figure 2-8B) corresponds to the $P_A \cdot L_{ex}$ concentration at its maximum. In excess ligand, the concentration of the intermediate $P_A \cdot L_{ex}$ is proportional to the concentration of P_A, which is linked to the initial protein concentration P_0, and the dimer-monomer equilibrium constant. Since I have no information on the latter, I make no attempt to derive or solve an expression for the parameter k in Eq. 2.8. Considering the high concentration of PBPs in the sensillum lymph (average about 600 μM for LdisPBPs [27]), it is unlikely that PBP will reach maximum velocity at odorant doses encountered in typical plumes. These doses range from 10 molecules$\cdot s^{-1} \cdot$sensillum^{-1} (17 pM) to about 10^8 molecules$\cdot s^{-1} \cdot$sensillum^{-1} (170 μM) (estimated by Dr. E. Plettner).

2.5 Summary

The pheromone-binding proteins (PBPs), which exist at a high concentration in the sensillum lymph surrounding olfactory neurons, are proposed to be important in pheromone detection and discrimination in insects. In this chapter, I present the first systematic study of PBP-ligand interaction kinetics. I find that PBP2, from the gypsy moth *L. dispar*, associates and dissociates

slowly with its biofunctional ligands, (+)- and (-)-disparlure. My study has revealed an important role for the C-terminus of long-chain PBPs and I hypothesize that it acts as a gate and as part of a path for the ligand. Tryptophan anisotropy measurements detect PBP multimers in solution, and an increase in the multimeric state of the protein upon long exposure to ligand. I propose a kinetic model which includes monomer/multimer equilibria and a two-step binding process: 1) external binding of the pheromone assisted by the C-terminus of PBP2, and 2) slow embedding of the pheromone into the internal pocket. This experimentally-derived model sheds light on the potential biological function and mechanism of PBPs as ligand scavengers. Once internalized, the ligand is unlikely to exchange with other components in the sensillum lymph.

2.6 Supporting Information

2.6.1 Dissociation of DNS-PBP2 with (+)- and (-)-Disparlure

The dissociation process is very complicated. Since DNS-PBP2.ligand complexes do dissociate slowly, when I was following the dissociation, the free protein and ligand started to bind to each other again. The association process counteracted part of the dissociation effect. Considering that the dissociation of the DNS-PBP2.ligand complex will reach equilibrium at the end, I took the dissociation as a reverse disturbance of equilibrium.

$$P + L \underset{k_{off}}{\overset{k_{on}}{\rightleftharpoons}} P{\cdot}L$$

At equilibrium	P_{eq}	L_{eq}	B_{eq}
At time t	$P_{eq} - x(t)$	$L_{eq} - x(t)$	$B_{eq} + x(t)$

$$\frac{dB}{dt} = \frac{dx}{dt} = k_{on}(P_{eq} - x)(L_{eq} - x) - k_{off}(B_{eq} + x)$$

$$= k_{on}(P_{eq} - x)^2 - k_{off}(B_{eq} + x)$$

Because both P and L came from the dissociation of the DNS-PBP2.ligand complex, P.L, I assume that, P ≈ L at any time. This allows us to simplify the expression to:

$$\int_0^x \frac{dx}{k_{on}(P_{eq} - x)^2 - k_{off}(B_{eq} + x)} = \int_0^t dt$$

If $m = \frac{2k_{on}a + k_{off}}{k_{on}}, n = \frac{k_{on}P_{eq}^2 - k_{off}B_{eq}}{k_{on}}; x_1 = \frac{m + \sqrt{m^2 - 4n}}{2}, x_2 = \frac{m - \sqrt{m^2 - 4n}}{2}$

I can get $\frac{x_2(x - x_2)}{x_1(x - x_1)} = e^{-k_{on}\sqrt{m^2 - 4n} \times t} = e^{-k_{app}t}$

Since n → 0, $x_2 \rightarrow 0$ and assume x is much smaller than x_1 which is close to K_d, I can get an approximation of

$$x = -\frac{x_1^2}{x_2} e^{-k_{app}t} = Ae^{-k_{app}t}$$

CHAPTER 3 MECHANISM UNDERLYING THE LIGAND SELECTIVITY OF LDISPBPS

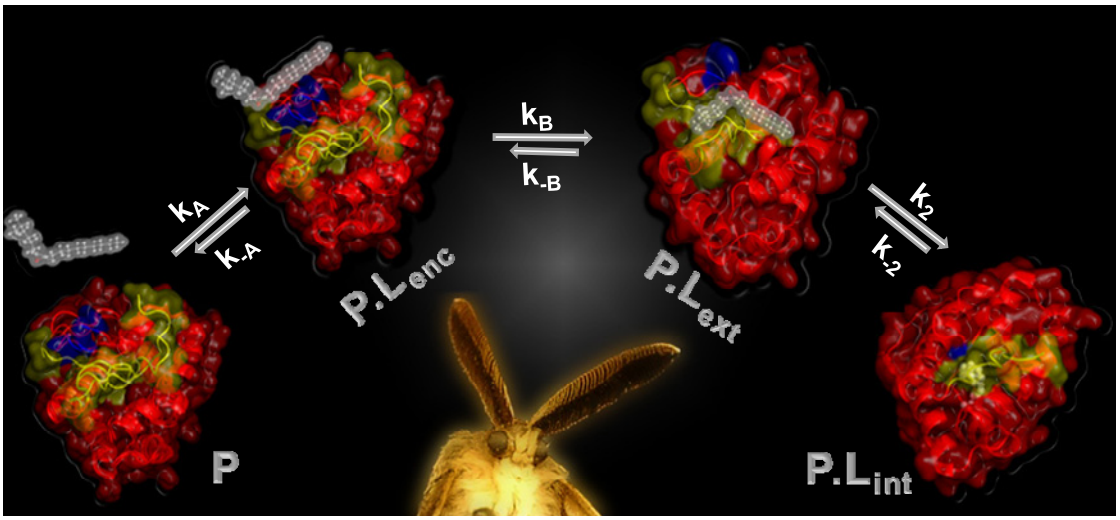

- The results of this chapter are adapted from the submitted paper to Biochemistry.
- This chapter depicts the continued kinetic studies of LdisPBPs. A fluorescent ligand and stopped-flow kinetics were involved.
- Both PBP1 and PBP2 interact with ligand in a stepwise manner. The diffusion-controlled collisional step was unveiled.
- Ligand-binding induced specific conformational changes around Trp37.

3.1 Introduction

I have proposed in Chapter 2 a two-step association mechanism based on the kinetic studies with PBP2. In this model, a ligand will associate with the protein on an external site before entering the internal binding pocket. In other words, there are two binding states of a ligand on the protein, externally bound ($P.L_{ext}$) and internally bound ($P.L_{int}$). A hydrophobic patch on the protein surface could be a potential external binding site, and I have suggested a region composed of the loop connecting helices 2 and 3 and the C-terminal segment for this site. Because of the limitations of the technique I have used before, a different method was needed to study the external binding process as well as the kinetics of PBP1. In this Chapter, I have used a fluorescent compound, N-phenyl-1-naphthylamine (NPN, Figure 1-10, 15) as a surrogate to study the ligand interaction kinetics of both PBP1 and PBP2, and their truncated forms which are lacking the C-terminal segment: TPBP1 and TPBP2. NPN is a very good fluorescent reporter. When present in a hydrophobic environment, its fluorescence increases dramatically, compared to its fluorescence in an aqueous environment. A similar compound, 8-anilino-1-naphtalenesulphonic acid (ANS, 14), has been crystallized in the internal cavity of LmaPBP [99]. I believe that the NPN can also enter the internal pocket of PBP and the study of NPN-PBP interaction kinetics can provide us with more insight into the dynamics of PBPs in solution.

In this work, I present the stopped-flow kinetic data for the two PBPs and TPBPs with NPN. In addition, I have monitored the conformational changes in

these proteins, by monitoring quenching of the tryptophan fluorescence, in the presence of the pheromone of the gypsy moth ((+)-disparlure), or of NPN. The results suggest that the relevant pheromone ligand induces a different local conformation around Trp37 from what is induced by the non-relevant ligand.

3.2 Experimental Procedures

3.2.1 Protein Production and CD Spectra

Recombinant PBPs were expressed and purified as previously described [104]. The C-terminally truncated PBPs (TPBPs) were constructed by a PCR based approach to delete the C-terminal fragment from Trp129 to Gln145 for TPBP2 and from Trp128 to Thr143 for TPBP1 [30].

CD spectra of PBPs and TPBPs in 20 mM Tris buffer, pH 7.4, at protein concentration 10 μM were acquired on a JASCO J-810 spectropolarimeter equipped with a Peltier type PFD-425S constant temperature cell holder. Far UV measurements were made between 190 and 260 nm at 25 °C using a quartz cell with 0.1 cm light path length. Data were recorded using three accumulations, each at a scan rate of 200 nm/min, with a response time of 0.1 s. A baseline was subtracted from all spectra. Secondary structure contents of each protein were determined by the CDPro program (http://lamar.colostate.edu/~sreeram/CDPro/main.html) using two methods: SELCON3 and CONTINLL. Two sets of reference proteins were used for

secondary structure calculation: 43 proteins and 56 proteins. The average values from four quantities (two methods and two reference sets) are presented.

3.2.2 Different Binding Affinities between Proteins

The dissociation constants of PBP.NPN complexes were obtained with two methods. First, a separation of the unbound NPN from the protein-bound NPN by a size exclusion mini column was followed by GC-MS based quantification of the NPN amount. This is a slightly modified procedure from previous ones [30,104]. Tests were done at room temperature for equilibrated 4 μM protein and 8 μM NPN in 20 mM Tris buffer, pH 7.4. A mini column filled with Sephadex G-10 powder (instead of the P-2 gel, Bio Rad, we have used previously) was used to remove the free NPN for each sample. Four replicates were conducted for each condition.

A second method was based on the increase in the NPN fluorescence when the NPN molecule is located in a hydrophobic environment. A series of NPN/MeOH stock solutions were prediluted from 2 mM stock to final concentrations of 0, 0.1, 0.2, 0.3, 0.6, 0.9, 1.2, and 1.5 mM. Then 2 μL of the prediluted solutions was added to 200 μL 4 μM PBP solutions in corresponding wells on 96-well plate. Protein solutions were prepared in 50 mM phosphate buffer, pH 7.0. There were three replicates for each protein. Controls in the phosphate buffer without PBPs were conducted on the same plate. Plates were

then scanned at 385 nm with Cary Eclipse Fluorimeter when excited at 337 nm. Each plate was scanned after 1 h incubation.

3.2.3 Stopped-Flow Kinetics for PBP/NPN Association

NPN as a surrogate ligand in this study is a good fluorescence reporter for ligand binding. It fluoresces stably and significantly in protein solutions (Figure 3-1) and dissolves well in aqueous buffer up to 30 μM (Figure 3-2).

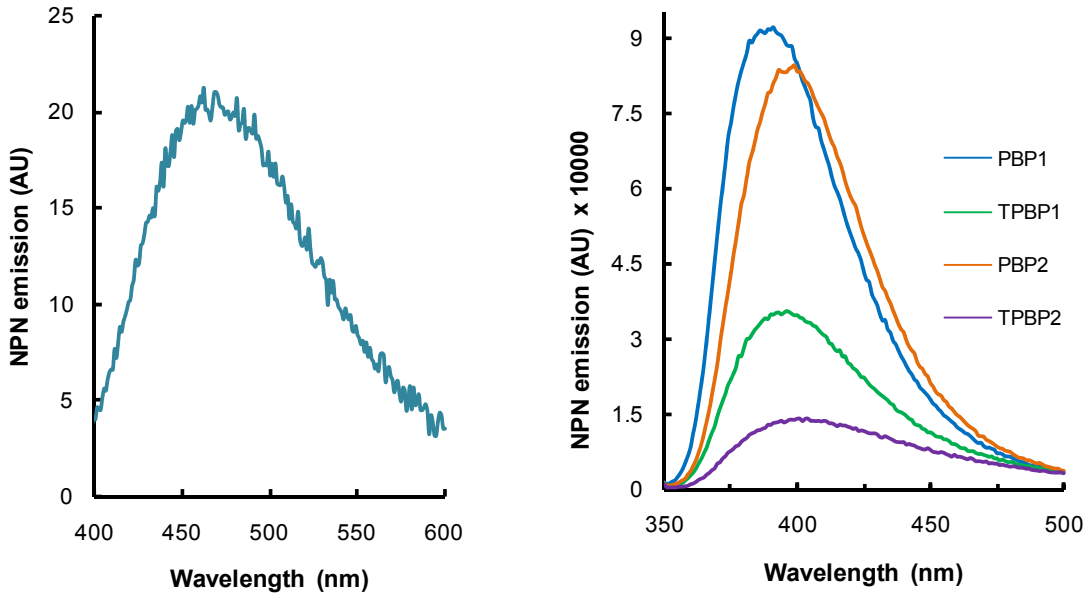

Figure 3-1 NPN fluoresces much more strongly in protein solutions.

Left: in 20 mM Tris buffer, pH 7.4; right: NPN bound to PBP1 (blue), PBP2 (orange), TPBP1 (green) and TPBP2 (purple). The concentrations for both protein and NPN were 2 μM. Samples were excited at 337 nm.

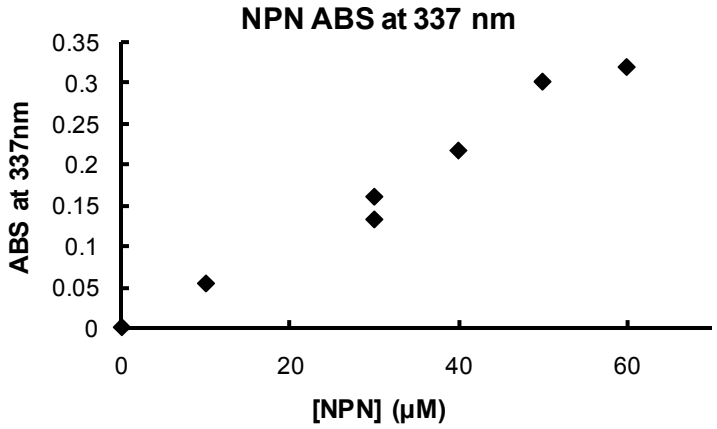

Figure 3-2 Absorbance of NPN at 337 nm in 20 mM Tris buffer, pH 7.4, at room temperature. Linear behavior was observed below 50 μM.

The stopped-flow kinetics experiment was conducted by Mr. H. Tang in Dr. C. Bohne's lab (Department of Chemistry, U. of Victoria). An SX20 stopped flow system from Applied Photophysics Ltd. was employed to measure the kinetics of NPN binding with PBPs. The excitation wavelength was adjusted to 337 nm by an excitation monochromator with a slit width corresponding to a bandwidth of 2 nm. The fluorescence emission was collected at 396 nm which was set by an emission monochromator with a bandwidth of 8 nm. Protein solutions (1 μM, 1.5 μM, 2 μM, 2.5 μM and 3 μM) and NPN solutions (0.25 μM) were prepared by dissolving the appropriate amounts of protein and NPN stock solutions into 20 mM Tris buffer, pH 7.4, respectively. The protein solution was contained in one syringe while the NPN solution was contained in the second syringe and the two solutions were mixed in a 1:1 ratio. Therefore the final concentrations of NPN and protein are half of the concentrations stated above. Samples were thermostated at 20.0 ± 0.1 °C for at least 15 min using a circulating water bath before

experiments were performed. The kinetic data were collected for 0.2 s or 0.5 s and the mixing time was 1 ms. For each experiment 20 individual traces were averaged.

The averaged kinetic traces were analyzed using the Pro-Kineticist II software from Applied Photophysics. In the case of PBP1, fits of the kinetic data to a mono-exponential function showed non-random residuals between the calculated and experimental values indicating that more than one kinetic process was present for PBP1 (Figure 3-3A). In the case of PBP2, TPBP1 and TPBP2, the residuals were the same and random for a fit to a mono-exponential function or to the sum of two exponentials (Figure 3-3B for TPBP1). For these three proteins the kinetic data were fit to a mono-exponential function (Figure 3-3 and Figure 3-4, see section 3-6 for details on other fits tried). Global fits were performed where all the kinetic traces recovered for each protein at different protein concentrations were fit simultaneously. The protein was assumed not to contribute to the fluorescence intensity, since no emission from the protein was observed for the experimental conditions of the stopped-flow experiment. Reactions A and B were considered for the fit of the kinetic data acquired for PBP1. However, the first relaxation process is fast and close to the time-resolution of the experiment. For this reason, a series of global fits were performed in which the values for k_A were fixed to incremental values between 1 × 10^9 $M^{-1}s^{-1}$ and 1 × 10^6 $M^{-1}s^{-1}$. Random residuals and similar standard deviations were observed for k_A values between 1 × 10^8 $M^{-1}s^{-1}$ and 4 × 10^7 $M^{-1}s^{-1}$ (Table 3-3). These led to an upper limit for k_{-A} of 25 s^{-1}. Reaction B corresponds

to a unimolecular relaxation process. The observed rate constant for this process ($k_{obs,B}$) is equal to the sum of k_B and k_{-B}. In the case of PBP1, the fits converged to a value of zero for k_{-B}. Simulations of the kinetics indicated that a value of k_{-B} corresponding to 10% of k_B would be discernable for the signal-to-noise ratio of the kinetic measurements with PBP1 (see details in the section 3-6). These simulations led to an upper limit for k_{-B} of 6 s^{-1}.

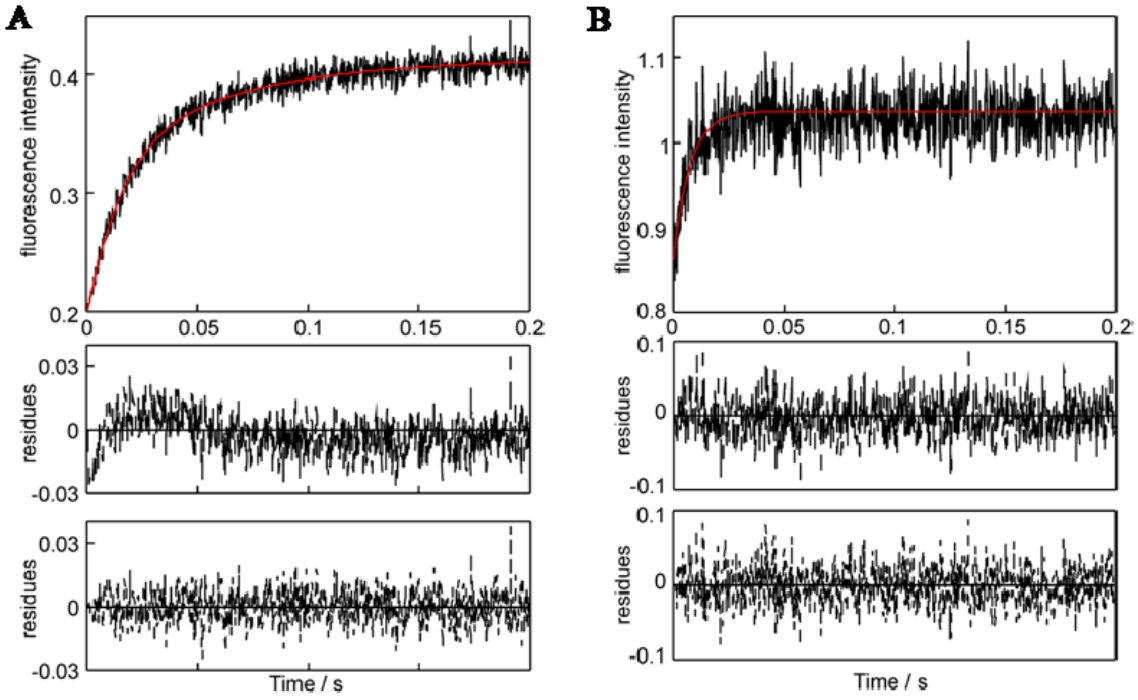

Figure 3-3 Stopped-flow kinetic traces for PBP1 and TPBP1 binding to NPN can be fit to the sum of two exponentials and mono-exponential function, respectively. Top: Kinetics for the mixing of PBP1 (A) and TPBP1 (B) ([PBP] = 0.5 μM) with NPN ([NPN] = 0.125 μM). The fit to a sum of two exponentials corresponding to the model in reactions A and B is shown in red for PBP1 and the fit to a mono-exponential function is shown in red for TPBP1. Middle: residuals for a fit to a mono-exponential function. Bottom: residuals for the fit of this individual kinetic trace to the sum of two exponentials.

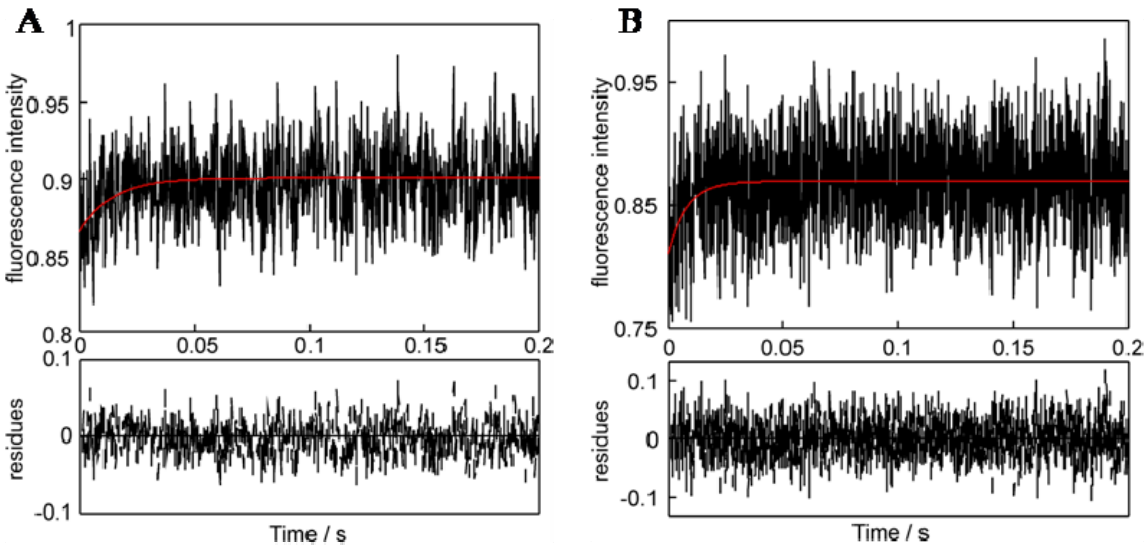

Figure 3-4 Stopped-flow kinetic traces for PBP2 and TPBP2 binding to NPN can be fit to a mono-exponential function. Top: Kinetics for the mixing of PBP2 (A) and TPBP (B) ([PBP] = 0.5 μM) with NPN ([NPN] = 0.125 μM). The fit to a mono-exponential function corresponding to the model in reaction 2 is shown in red. Bottom: residuals for a fit to a mono-exponential function.

Reactions A and B correspond to a model where an encounter complex is formed in a bimolecular reaction followed by the unimolecular relocation of the ligand. The observed rate constant measured by stopped-flow for PBP2, TPBP1 and TPBP2 did not depend on the protein concentration and therefore the kinetics corresponds to the unimolecular step of reaction B while reaction A occurs on a time scale faster than the time-resolution of the stopped-flow (1 ms). Only $k_{obs,B}$ could be determined. However, the similarity between the k_B value for PBP1 and $k_{obs,B}$ for PBP2 suggests that the major contribution to the observed rate constant was probably from k_B, for the two proteins.

$$P + L \underset{k_{-A}}{\overset{k_A}{\rightleftharpoons}} P.L_{enc} \qquad \text{(reaction A)}$$

$$P.L_{enc} \underset{k_{-B}}{\overset{k_B}{\rightleftharpoons}} P.L_{total} \qquad \text{(reaction B)}$$

3.2.4 Fluorescence Quenching Studies

Portions of 5 mM quencher (potassium iodide or acrylamide) stock solutions were added consecutively to 500 µL 2 µM protein samples either without or with ligand. To estimate the exposure of the Trp residue in the PBP.ligand complex, 10 µM (+)-disparlure were used for all the proteins, 8 µM and 40 µM NPN were used for PBP1/TPBP1 and PBP2/TPBP2, respectively. The high concentration of NPN used for PBP2 and TPBP2 ensured a good percentage of PBP.NPN complexes. The PBP and ligand mixtures were incubated for at least 2 h before each test. Three independent samples under each condition were used. For the short-time incubated PBP2.(+)-disparlure sample, ligand stock was added to the protein solution with the desired quencher concentration. The mixture was quickly shaken and scanned within 25 s. Each point represents the average of three replicates. Samples were excited at 295 nm and data was collected from 310 to 350 nm on a PTI fluorimeter equipped with 814 photomultiplier detection system at 20 ºC.

3.3 Results

3.3.1 Truncation Has Little Effect on PBP Core Structure

Figure 3-5 shows the far-UV CD spectra of PBP1, TPBP1, PBP2 and TPBP2. The shapes of the spectra are characteristic of proteins with a high percentage of helical structure. The spectrum of TPBPs overlaps very well with that of the corresponding PBPs in both the shape and the amplitude, except that there is an ~8% decrease in the amplitude of the negative 222-nm and 208-nm bands for TPBP1 and ~7% and 11% increases for each band, respectively, for TPBP2. The secondary structure fractions calculated from CD spectra in Figure 3-5 are listed in Table 3-1. The average values from four calculations and the standard deviations between calculations are presented for each type of secondary structure. Overall, consistent with the reported structures of PBPs from other insects [92,97-100,107], all the proteins tested here contain more than 90% helical structures. The truncation did not affect the protein structures on the secondary level and based on the high resemblance of the CD spectra, I assume that the tertiary core structures of PBP1 and PBP2 are preserved in their truncated forms.

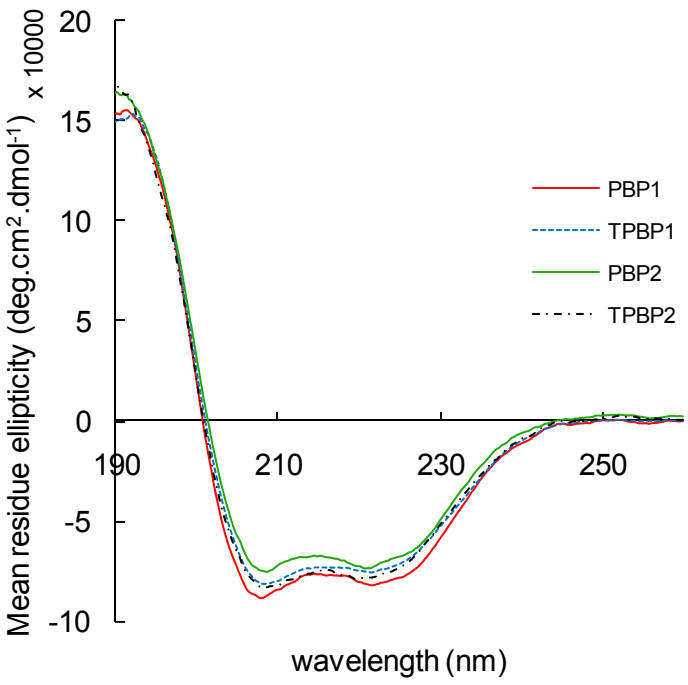

Figure 3-5 Far-UV CD spectra of full-length and truncated PBPs indicate similar secondary structure. The indicated proteins (10 μM) were prepared in 20 mM Tris buffer, pH 7.4. CD scans recorded as described in the experimental section.

Table 3-1 Secondary structure components of PBPs/TPBPs from the analysis of CD spectra in Figure 3-5 with the CDPro program.[a]

Protein	H(r)	H(d)	S(r)	S(d)	T	Unrd
PBP1	71 ± 4	25.1 ± 0.7	0	0.1 ± 0.9	3 ± 2	7 ± 5
PBP2	74 ± 6	21 ± 4	0	0.6 ± 0.2	4 ± 3	10 ± 6
TPBP1	70 ± 4	23.9 ± 0.9	0	0.8 ± 0.5	4 ± 3	9 ± 6
TPBP2	79 ± 9	16 ± 6	0	0.3 ± 0.4	4 ± 3	8 ± 5

[a] Numbers indicate the percentage of each component. Two methods and two sets of reference proteins are used (± S.E.). H: helices; S: strands; T: turns; Unrd: unordered; r: regular; d: distorted.

I also notice that the pair of PBP2 and TPBP2 has a slightly higher content of regular helix than the pair of PBP1 and TPBP1. The tertiary structure predicted by the CLUSTER program [150] for the first pair of proteins is in the all-α class and for the latter one, it is in the α+β class. The difference may also be represented

by a slight difference in the shape of the 190-nm band. And the shape of the specific band for PBP2/TPBP2 is similar to the reported one for BmorPBP [148]. Unfortunately, there are no structures available for PBP1 and PBP2 yet. PBP1 and PBP2 share 55% similarity in the amino acid sequence. I expect a subtle but possibly important difference between their structures based on the limited information provided by the CD spectra of the secondary structure.

3.3.2 Different Binding Affinities of the Proteins for NPN

The binding affinities of PBPs with NPN have been evaluated by two methods: first, the GC technique and second, fluorescence titration (Figure 3-6). Different K_d values were obtained from each method. However, consistently, the binding affinities from the strongest to the weakest were: PBP1 ≈ TPBP1 > PBP2 ≥ TPBP2 (Table 3-2). Consistent with previous observations, losing the C-terminal peptide has weakened the binding affinity of PBP2 in the GC assay [30], but not the fluorescence assay. Interestingly, the binding affinity of PBP1 is not affected by the truncation, as detected with either method.

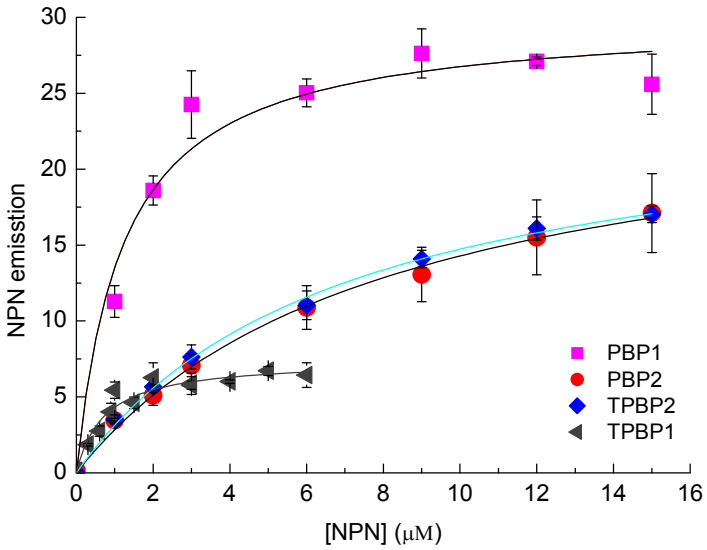

Figure 3-6 Binding of NPN to PBPs/TPBPs indicated by the fluorescence increase.

NPN/MeOH solution (2 mM) was titrated into 4 μM PBP solution in 50 mM phosphate buffer, pH 7, to final concentrations of 0-15 μM. λ_{ex}=337 nm. Bars indicate standard error of three replicates. NPN bound to TPBP1 showed weaker fluorescence intensity than that bound to PBP1, but in both cases, NPN had a similar binding affinity to the PBP. PBP2 and TPBP2 pair looked very similar.

Table 3-2 The dissociation constants of PBPs/TPBPs with NPN.[a]

Protein	K_d (μM)	
	GC	Fluorescence
PBP1	7 ± 4	1.3 ± 0.3
PBP2	66 ± 8	8.6 ± 0.6
TPBP1	6 ± 2	1.0 ± 0.2
TPBP2	300 ± 164	7.7 ± 0.8

[a] For the GC results, data is reported as the average of four replicates ± S.E.; for the fluorescence results, data is obtained from the one-site binding model fit of curves in Figure 3-6, errors represent the fitting error.

The K_d values from the fluorescence assay were overall smaller than those from the GC assay. Especially for TPBP2, two K_ds differ by a factor of 40. Both the GC and fluorescence assays were done at 4 μM PBP concentration,

and the same range of NPN concentration was used, so this should not be a result of binding enhancement induced by PBP multimerization at high ligand: protein ratio [47]. From the analysis of the stopped-flow data in Table 3-3 for PBP1 where $k_B/k_{-B} > 10$, the concentration of $P.L_{total}$ is much larger than that of $P.L_{enc}$. This might be true for the other three PBPs as well. Therefore, the existence of the $P.L_{enc}$ could not be the reason for the difference in K_d between two assays. I hypothesize that there are two binding modes of the ligand in the protein: externally bound and internally bound (Figure 3-10). The latter is more stable than the former, and also the encounter complex. All three species fluoresce. Therefore, there are two possibilities for the differences between the K_d values by GC and fluorescence experiments: 1) GC measures $P.L_{int}$ but neither $P.L_{enc}$ nor $P.L_{ext}$ and fluorescence measures all three; or 2) GC measures $P.L_{int}$ + $P.L_{ext}$ but not $P.L_{enc}$ and fluorescence measures all three species. The former might be more plausible considering that the concentration of $P.L_{enc}$ is low.

3.3.3 Stopped-Flow Kinetics for PBP/NPN Association

A final NPN concentration of 0.125 μM was chosen in order to work with an excess of protein (≥ 0.5 μM, Figure 3-7). A qualitative comparison of the kinetics for PBP1 and TPBP1 shows that equilibration is faster for TPBP1 than for PBP1 (Figure 3-7). For PBP1 the formation of $P.L_{enc}$ is slow enough to be observed on the time-scale of stopped-flow experiments. The time constant for the generation of $P.L_{enc}$ is equal to the sum of the association and dissociation processes (k_A[protein] + k_{-A}). For the other three proteins the kinetics was

adequately fit to a mono-exponential function and the kinetics was not dependent on the protein concentration indicating that the formation of $P.L_{enc}$ occurred with a time constant higher than 10^3 s^{-1}. Since the k_A value for PBP1 is close to a diffusion-controlled ligand-protein encounters (normally ~10^7 $M^{-1}s^{-1}$) [151], the higher time constant for the other three proteins is dictated by a much higher value for k_{-A}, i.e. the dissociation of $P.L_{enc}$. The second process, which is related to the incorporation of the ligand into the protein was shown to be similar for PBP1 and PBP2 or TPBP1 and TPBP2, where higher values for $k_{obs,B}$ were observed for the latter two proteins.

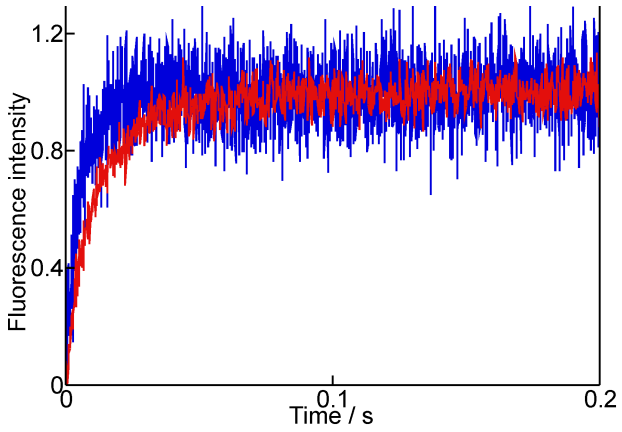

Figure 3-7 PBP1 (red) equilibrates more slowly than TPBP1 (blue).
Normalized kinetic traces for protein binding with NPN at 1.5 µM PBP and 0.125 µM NPN (T=20 °C).

The obvious disadvantage of using NPN to study the PBP-ligand interaction kinetics is that NPN is non-natural, but nevertheless, the results provide us with three new insights (Table 3-3).

First, the kinetic traces for PBP1 can be fit with a sum of two exponentials, consistent with the stopped-flow results of BmorPBP binding with its cognate ligand [113]. These results support and further expand the model that a ligand, whether natural [30] or not (NPN), is introduced into the protein binding pocket in a stepwise manner. Although the kinetics for PBP2, TPBP1 and TPBP2 do not show the fast first binding, such a process to generate $P.L_{enc}$ must occur because the observed relaxation kinetics did not show a dependence on the protein concentration, indicating that it corresponded to a unimolecular reaction.

Table 3-3 Kinetic parameters for the interaction between PBPs/TPBPs and NPN

Protein	k_A ($\times 10^7$ M^{-1} s^{-1})	k_{-A} (s^{-1})	$k_{obs,B}$ (s^{-1})
PBP1	4 – 10[a]	< 25	61 ± 9[b,c]
PBP2	nd[d]	nd	56 ± 4[c]
TPBP1	nd	nd	168 ± 3[c]
TPBP2	nd	nd	133 ± 8[c]

[a] Values for k_A were fixed and for the range of k_A values stated random residuals were observed for the fit and experimental data.
[b] This value corresponds to k_B, and k_{-B} was estimated to be smaller than 6 s^{-1}.
[c] Errors correspond to the errors recovered from the global fit analysis of the Pro-Kineticist II software from Applied Photophysics.
[d] nd = Not detected. The formation of $P.L_{enc}$ was faster than the time-resolution of the stopped-flow instrument, but must have taken place because $k_{obs,B}$ was independent of protein concentration (see text).

Second, PBP1 and PBP2 show different binding modes at the initial encounter, with a faster process being observed for PBP2. Since PBP1 and PBP2 should have k_A values in the same magnitude (diffusion-controlled step), the faster relaxation process for PBP2 is due to a higher k_{-A} leading to a higher K_d value for the formation of $P.L_{enc}$ in the case of PBP2. Although PBP1 and

PBP2 have similar k_B value, the larger k_{-A} value for PBP2, which competes with the forward reaction, led to an overall slower reaction rate for PBP2.

Third, loss of the C-terminal peptide leads to a faster relaxation process for the relocation of the non-natural ligand, NPN. The values of $k_{obs,B}$ correspond to the sum of the relocation of the ligand into the protein and dissociation of the ligand back to the first encounter complex, and one or both of these rate constants increased with the removal of the C-terminal peptide when compared to the full-length PBPs. This result supports the idea that the C-terminal peptides of long-chain PBPs are gating the binding pocket.

3.3.4 Tryptophan Fluorescence Quenching Studies

Quenching of fluorescence can be used to measure the accessibility of a quencher to a fluorophore. I used a neutral quencher, acrylamide, and an anionic quencher, iodide, to determine if these quenchers had differential accessibility to Trp residues in the PBPs and TPBPs. There are two conserved tryptophan residues in LdisPBPs, Trp 37 and 129. The first one is on the α2/3 loop and the second one is on the C-terminus and connects the C-terminus to the 6th helix of the protein, as predicted from the threaded structures of these proteins. It is eliminated in both TPBP1 and TPBP2 [30].

Fluorescence quenching is measured as a decrease of the fluorescence intensity in the presence of quencher (F) when compared to the intensity in the absence of quencher (F_0), where a linear relationship with the quencher concentration is expected (Eq. 3.1, Figure 3-8) [152].

$$\frac{F_0}{F} = 1 + K_{sv}[\mathrm{Q}] \quad \textbf{(3.1)}$$

K_{SV} is defined as the Stern-Volmer constant which carries the unit of M^{-1} and its value is equal to the product of the quenching rate constant (k_q, $M^{-1}s^{-1}$) and the lifetime of the chromophore, in this case Trp, in the absence of quencher (τ_0, s) ($K_{SV} = k_q\tau_0$). The accessibility of the quencher to the Trp is related to the values of k_q. Previous studies showed that the lifetime of Trp varied when ligands were bound (unpublished data), and therefore, the Stern-Volmer constants cannot be directly related to the accessibility of the quenchers when comparing free vs. ligand-bound PBPs. However, for each ligand the ratio of the Stern-Volmer constant for acrylamide ($\mathrm{K_{SV}^{Acr}}$) and iodide anions ($\mathrm{K_{SV}^{I}}$) is equal to the ratio of the k_q values (Eq. 3.2). A change in this ratio indicates that the environment around Trp is different, and it changes either the accessibility of the neutral quencher or the ionic quencher or both (Table 3-6).

$$\frac{K_{sv}^{Acr}}{K_{sv}^{I}} = \frac{k_q^{Acr}\ \tau_0^x}{k_q^{I}\ \tau_0^x} = \frac{k_q^{Acr}}{k_q^{I}} \quad \textbf{(3.2)}$$

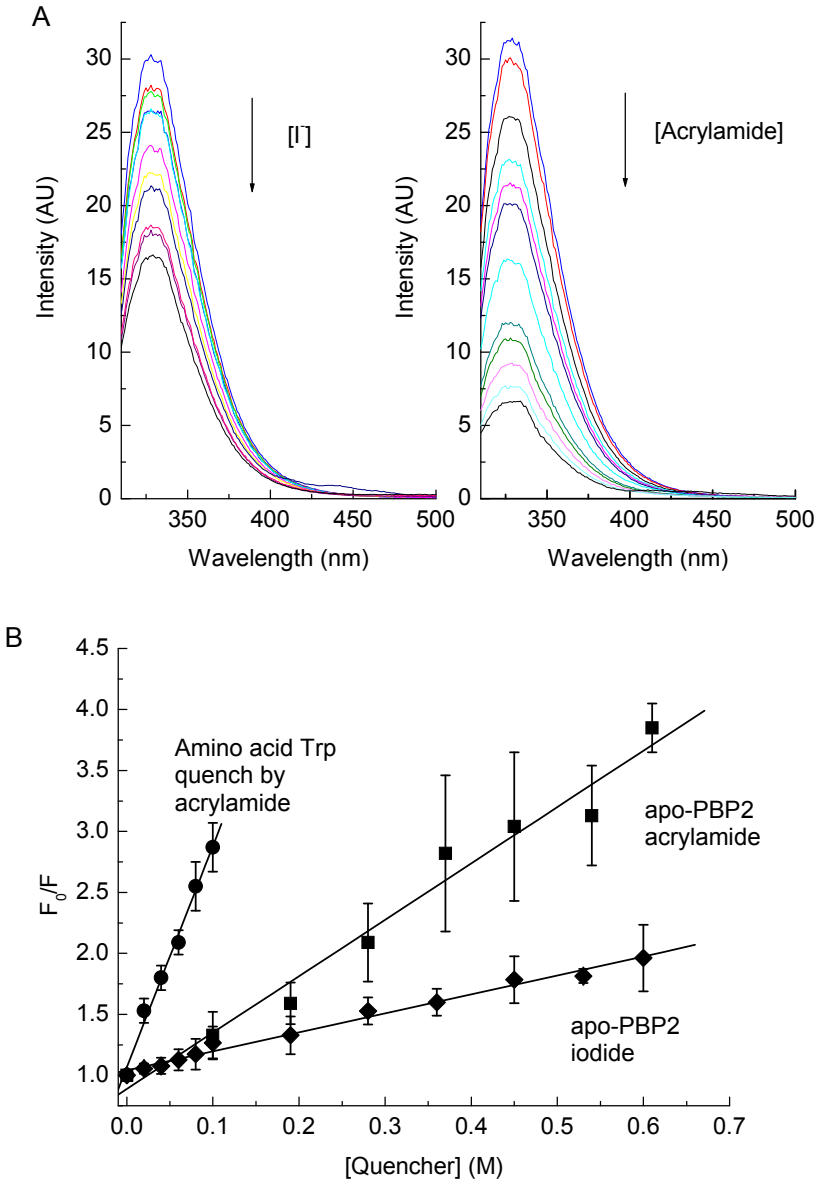

Figure 3-8 Examples of fluorescence quenching.

A. Fluorescence emission spectra (λ_{ex} = 295 nm) of PBP2 as a function of increasing concentrations (0−0.7 M) of iodide (left) and acrylamide (right). PBP2 concentration was 2 μM. Samples were in 20 mM Tris buffer, pH 7.4, at 20 °C. B. Stern-Volmer plots for apo-PBP2 and free tryptophan. (diamonds: PBP2 quenched by iodide; squares: PBP2 quenched by acrylamide; circles: free tryptophan quenched by acrylamide. Bars indicate standard error for three replicates.)

In order to understand the meaning of the ratio of the Stern-Volmer constants better, we have to realize that there is a difference between the intrinsic capabilities of acrylamide and iodide to quench the excited indole ring. Acrylamide has been indicated as an effective and potent quencher for tryptophan fluorescence through collisional processes [153]. Its quenching efficiency is mostly affected by the steric hindrance around the Trp residue. The highly hydrated and charged iodide ion does not quench the tryptophan fluorescence as effectively as acrylamide. Under the test conditions (pH 7.4, 20 mM Tris buffer), the K_{SV} constants for iodide and acrylamide to quench the free tryptophan are 8.6 M^{-1} and 18.1 M^{-1}, respectively, giving a ratio of 2.1 ± 0.2 (Table 3-5). Moreover, the electronic environment around a tryptophan residue also affects the quenching efficiency of iodide. A positively charged environment around Trp can increase significantly the quenching degree by an anionic quencher [154]. Therefore, the ratio of the Stern-Volmer constants represents the overall environment around the residue Trp37 in my case, including the steric and electronic factors.

Table 3-4 Stern-Volmer constants, K_{SV} (M^{-1}), for quenching of tryptophan fluorescence.[a]

Protein	Quencher	Ligand			
		None	(+)-disp	(-)-disp	NPN
PBP1	Iodide	1.44 ± 0.09	2.8 ± 0.2	3.7 ± 0.4	1.5 ± 0.1
	Acrylamide	3.5 ± 0.2	3.6 ± 0.2	3.7 ± 0.2	1.4 ± 0.2
TPBP1	Iodide	3.0 ± 0.2	5.4 ± 0.3	10.8 ± 0.5	4.0 ± 0.3
	Acrylamide	4.7 ± 0.6	4.4 ± 0.3	3.7 ± 0.2	1.5 ± 0.1
PBP2	Iodide	1.56 ± 0.05	3.0 ± 0.2	4.5 ± 0.4	1.4 ± 0.2
	Acrylamide	4.6 ± 0.3	3.2 ± 0.3	3.4 ± 0.2	2.3 ± 0.1
TPBP2	Iodide	2.8 ± 0.2	3.6 ± 0.1	6.7 ± 0.2	1.8 ± 0.2
	Acrylamide	5.2 ± 0.3	4.1 ± 0.2	5.1 ± 0.3	2.2 ± 0.1

[a] Trp quenching in apo-PBPs/TPBPs and in the complexes with different ligands (K_{SV} ± fitting error). See Figure 3-8 for an example of the data. Data were obtained with 8-12 points per line and three replicates per point. [Protein] = 2 μM; [disparlure] = 10 μM; [NPN] = 8 μM for PBP1/TPBP1 and 40 μM for PBP2/TPBP2.

Table 3-5 Stern-Volmer constants, K_{SV} (M^{-1}), for fluorescence quenching by acrylamide and iodide of amino acid tryptophan, and proteins incubated with ligand (either (+)-disparlure or NPN) for a short time.

Quencher	**Testing conditions**			
	Free Trp	PBP1 with (+)-disp[a]	PBP2 with (+)-disp[a]	PBP2 with NPN[a]
Iodide	8.6 ± 0.8	3.5 ± 0.2	3.9 ± 0.5	1.2 ± 0.2
Acrylamide	18.1 ± 0.8	3.6 ± 0.2	3.8 ± 0.3	2.4 ± 0.2

[a] [Protein] = 2 μM; [(+)-disparlure] = 10 μM; [NPN] = 40 μM.

If the Trp residue in a protein is exposed to the solvent and is not in the vicinity of any charged residues, it should have a ratio of Stern-Volmer constants for the two quenchers close to the ratio observed for free Trp. A larger ratio indicates a more negative environment around Trp (smaller K_{SV}^{I}), and a smaller ratio may imply either a more positive (larger K_{SV}^{I}) or a more sterically hindered (smaller K_{SV}^{Acr}) environment around Trp. Thus, bigger ratios observed for apo-

PBP1 and apo-PBP2 have indicated that the Trp37 in both proteins is solvent-exposed and in the proximity of some negative residues (Table 3-6).

Table 3-6 Ratio of the Stern-Volmer constants for the quenching of the fluorescence of Trp by acrylamide (K_{SV}^{Acr}) and iodide anions (K_{SV}^{I}). [a]

Protein	Ligand			
	None	(+)-disp	(-)-disp	NPN
PBP1	2.4 ± 0.2	1.3 ± 0.1	1.0 ± 0.1	0.9 ± 0.1
PBP2	2.9 ± 0.2	1.1 ± 0.1	0.76 ± 0.08	1.6 ± 0.2
TPBP1	1.6 ± 0.2	0.81 ± 0.07	0.34 ± 0.02	0.38 ± 0.04
TPBP2	1.9 ± 0.2	1.14 ± 0.06	0.76 ± 0.05	1.2 ± 0.1

[a] Data were obtained for apo-PBPs/TPBPs and protein complexes with different ligands. The Ksv values are shown in Table 3-4 and the errors correspond to the error propagation from the errors for the individual Ksv values.

The reasons why I mostly refer to Trp37 in the discussion and interpretation of the results about the environment of tryptophan residue(s) in the proteins are as follows. First, previous studies have shown that Trp129 in two other moth PBPs does not contribute significantly to the protein tryptophan fluorescence [113,120]. Second, multi-tryptophan proteins have been loosely categorized into three groups based on the curvature of their Stern-Volmer plots. 1) Upward curving: all residues nearly equally accessible or one single residue dominating. 2) Downward curving: heterogeneous fluorescence residues having a widely different accessibility to quencher. 3) Linear plot: heterogeneous fluorescence residues differing slightly in accessibility [153]. I have carefully examined all of the plots and none of them falls into the second category. This means either the fluorescence is dominated by Trp37 or both tryptophan residues

have similar accessibility. The first one is a more likely scenario. Third, TPBPs only have one tryptophan (Trp37). Therefore, I would expect that any decrease in Trp fluorescence from quenching should primarily come from Trp37 in all proteins tested here.

For all the proteins the ratio of the Stern-Volmer constants decreased when ligands were bound, suggesting a change in the environment around the Trp leading to either a decrease in the acrylamide accessibility or an increase in the accessibility of the negative iodide anion. This change is ligand-specific for both PBPs between relevant ((+)-disparlure) and non-relevant ((-)-disparlure and NPN) ligands, and differs between PBP1 and PBP2. Binding with (+)-disparlure induced a 62% decrease in the ratio for PBP2 and 46% decrease for PBP1 only (Table 3-6). Truncation of the C-termini also shows different effects on the change pattern. Take the same ligand as an example. Binding with (+)-disparlure induced a smaller decrease in the ratio for TPBP2 (40%) and a comparable decrease for TPBP1 (49%), when compared with the corresponding intact PBPs. It is worth to mention that, overall, TPBPs have smaller ratios of the Stern-Volmer constants than that of PBPs. This might be a direct result of the elimination of the negative residues on the C-terminal peptide. It is also very interesting that after binding with a ligand, TPBP2 and PBP2 have similar ratios. Actually the same numbers are obtained for (+)- and (-)-disparlure (Table 3-6), indicating that the tryptophan in ligand-bound TPBP2 and PBP2 might be in the same environment, no matter if there is a C-terminal peptide or not.

Based on these results from the quenching study, I can draw two conclusions. First, the C-terminal peptide may play different roles in different PBPs. Second, ligand-binding can induce different conformational changes from ligand to ligand and between PBP1 and PBP2. Specifically, I have followed the environmental change around Trp37, which is predicted to be on the α2/α3 loop of the protein. This change is clearly ligand specific and not directly related to the binding constant of the ligand. For example, PBP1 and (+)-disparlure have a K_d value of 7.1 μM [104] and a Stern-Volmer ratio of 1.3. PBP1 and NPN also have a K_d of 7 μM but a ratio of 0.9. Similarly, TPBP1 and NPN have a K_d of 6 μM and a much smaller ratio of 0.38 (Table 3-2 and Table 3-6). Interaction with different ligands results in subtly different conformations of the protein. Another consistent observation is that PBP1 and PBP2 had different pH profiles with (+)- and (-)-disparlure [117], suggesting that different ionisable groups are exposed with different ligands.

To determine if the stepwise binding would be apparent in the change of the ratio of the Stern-Volmer constants, I obtained the ratios for PBP1 and PBP2 in different complexes at short incubation lengths (< 25 s). The results show that the ratio decreases immediately after the protein and ligand are mixed, to the same level as that of the fully incubated mixture (Figure 3-9).

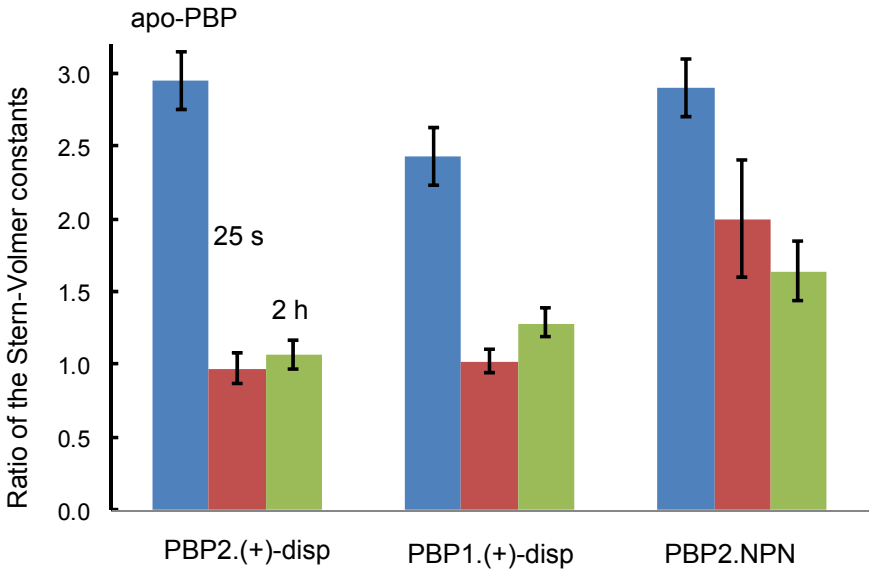

Figure 3-9 Ligand-binding induced change in the ratio of the Stern-Volmer constants of intrinsic Trp. The two K_{SV} values were obtained with acrylamide and iodide, and the ratio shown here is K_{SV}(acrylamide)/K_{SV}(iodide). The reason for comparing these ratios rather than the individual K_{SV} values is that in the ratio, the fluorophor lifetimes cancel and these ratios are equal to the ratio of the two quenching rate constants. See text page 99. Bars indicate the error propagation from the errors for the individual Ksv values.

3.4 Discussion

3.4.1 Stepwise Association of a Ligand on the PBP

I proposed a two-step binding mechanism for the association of PBP2 with (+)-disparlure and with (-)-disparlure [30]: a ligand is bound externally before it is docked into the internal binding pocket (Figure 3-10). This study has provided further evidence for a stepwise binding mechanism. The traces of stopped-flow fluorescence for the association of PBP1 with NPN fit best to a model of two sequential reactions (Figure 3-3). The first one is a diffusion-controlled bimolecular reaction and the second one is a unimolecular reaction (Table 3-3).

When compared with the previous study, binding of PBP with NPN is much faster than with disparlure. The latter has a k_2 value in the magnitude of 10^{-4} s^{-1}, whereas k_B (the rate constant for reaction B) for PBP1/NPN binding is 61 s^{-1}. Different techniques and/or different ligands can be reasons for this. It is also possible that the k_2 value I have measured before describes a different process from the reaction B here. In the previous work, I found that the mixing of dansylated PBP2 with (+)-disparlure led to an immediate loss in the dansyl fluorescence intensity (≤ 5 s), followed by a slow decrease of the fluorescence. The first decrease was attributed to a rapid interaction between the protein and the ligand, and I suggested an external binding site for that interaction. The exact position of the external binding site was unknown and the word “external” was used to distinguish it from the internal binding site that binds ligand stably. The difference in K_d values between the GC and the fluorescence assay suggests the existence of two binding sites, one binding the ligand more stably than the other. If the conversion of the bound ligand from the external binding site to the internal binding site takes a long time, longer than the time-resolution of the stopped-flow fluorimeter, such a process will not be detected. Another possibility is that the natural ligand goes into the internal site while NPN does not. That is why the k_2 step is not detected here. Overall, I suggest a third step following the two relaxation processes observed in this work, the conversion of the bound ligand from the less stable to the more stable binding mode. This step is characterized by the parameters k_2 and k_{-2}. For the interaction between PBP2 and (+)-

disparlure, the k_2 value is 4.3×10^{-4} s^{-1} [30]. The parameter k_1 in the previous work is most likely a composite of k_A and k_B from this work.

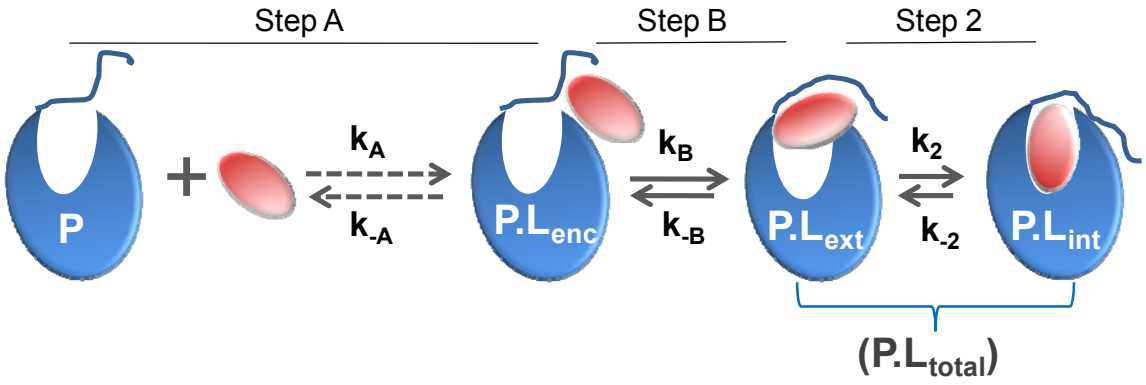

Figure 3-10 Illustration of stepwise association of a ligand with PBP.

This is the expanded model based on the previous model (solid arrows) [30]. The ligand (ellipse) first collides with the protein in a diffusion-controlled step (dashed arrows, from this work), forming an encounter complex, $P.L_{enc}$ which may decay to a relatively stable complex, $P.L_{ext}$. The C-terminal peptide (random coil) of the PBP may be involved. In the last step, the ligand is slowly internalized. In the previous study (Chapter 2), the first two steps were unresolved. In this work, I have followed the formation of $P.L_{total}$.

3.4.2 Activation of PBPs

The PBP-ligand complex can activate the olfactory signalling cascade, provided a relevant ligand is bound [29]. This means that ligand-induced specific local conformational changes on the PBP can be recognized by membrane-localized components. In the medium-chain PBP, LUSH, two binding modes of the ligand to the protein are observed and one of them effectively triggers the active PBP conformation (conformer B). The characteristics of the active conformation include a significant conformational shift of the loop connecting helices 2 and 3 and a salt bridge breaking between a residue on the C-terminal

region, Asp118, and another residue Lys87 [29]. In the long-chain PBPs, different conformations of the cognate ligand are also observed in the binding pocket [92]. I hypothesize that it is also true for the long-chain PBPs that the active conformation only involves local but ligand-specific conformational changes in a similar region.

I have proposed that a ligand is taken into the binding pocket progressively. A complement to a two-site model for ligand binding is the idea that the ligand capture and relocation concur with conformational changes. In this work, the Stern-Volmer constant has provided us with a unique method to probe the local conformational changes around Trp37, which is on the α2/α3 loop. I have found that the conformational changes around Trp37 are ligand-specific (Table 3-6) and are finished in 25 s (Figure 3-9). This may indicate that the PBP is activated within 25 s, before the complex $P.L_{int}$ is formed.

With all the information above, I suggest a slight modification to the model. In step A, PBP and ligand collide with each other randomly. A properly oriented ligand on the protein surface (L in $P.L_{enc}$) can turn into the externally bound ligand (L in $P.L_{ext}$) in step B. In this step, the PBP may be activated by the relevant ligand. Key residues have been shifted (salt bridge or hydrogen bond making or breaking) and the local environment close to Trp37 has been rearranged (milliseconds or faster). In the last step, step 2, the global protein conformation changes slowly to embed the ligand and force it to a more stable binding mode (seconds). The ligand in the external binding mode is neither well stabilized nor strongly bound by the protein. $P.L_{ext}$ may dissociate quickly during

the gel filtration in a GC assay and this can explain why GC assay has revealed relatively smaller binding affinities than the fluorescence assay for PBP-NPN interaction (Table 3-2).

3.4.3 Ligand Discrimination by PBP1 and PBP2

PBP1 and PBP2 differ significantly in primary sequence (Figure 2-11), binding affinities with structurally related ligands [47,104] and pH profiles of ligand binding [117]. However, in terms of overall structure, the proteins are very similar ([95] and Figure 3-5). I am curious about the reason why the moth produces two PBPs and wish to explore the possible connections between the PBP binding and the selectivity in the pheromone sensing of insects. It is reported that PBPs are capable of binding many different compounds, natural or unnatural[91,92,98,99,109,155]. It is found that the dissociation constants of various compounds are not directly related to their biological function (unpublished data and (Honson et al. 2003)[47]). Two explanations are possible: either PBPs do not discriminate and the selectivity of the olfactory system only comes from the downstream component such as the odorant receptors, or PBPs discriminate ligand in a subtle but elegant way.

Recent literature has drawn our attention to the importance of the C-terminal peptide of PBPs and the local conformational change of PBPs induced by a biofunctional ligand [29,91]. This suggests that PBPs contribute to ligand discrimination through their elaborate conformational changes, seen only with biologically relevant ligands. Our group has probed this kind of conformational

change before by testing the pH profiles of PBP1 and PBP2 with different ligands [117]. The pH profile indicates the environment of the residues being titrated and therefore reflects indirectly the local conformational changes in each case.

In this study, I have shown different local conformational changes induced by ligand association by the ratios of the Stern-Volmer constants (Table 3-6). It is apparent that different ligands will induce different changes in the local environment in one PBP, and in different PBPs, different conformational changes are induced by the same ligand. A change in the ratio of the Stern-Volmer constants indicates that the environment around Trp is different, either electronically or sterically or both. Binding of PBP2 with (+)-disparlure has decreased the ratio by 62% but only by 45% for binding with NPN. On the other side, association with NPN has induced the biggest decrease of the ratio for PBP1. Besides the difference in the ligand-induced conformational change, kinetically, PBP1 interacts with ligand differently from PBP2. The backward reaction of step A between NPN and PBP2 is much faster than with PBP1.

The C-terminal peptide is important for PBP1 and PBP2 function. The effect of C-terminal elimination for PBP1 is that the k_{-A} value increased for TPBP1. A similar comparison is not possible for PBP2 and TPBP2 because for both proteins the external binding was faster than the time-resolution of the experiment. Elimination of the C-terminal peptide results in a faster relaxation process for step B (Table 3-3, larger $k_{obs,B}$). In the previous paper, lacking the C-terminal peptide has slowed down the internalization process for PBP2 and (+)-disparlure binding (smaller k_2) [30]. PBP1 and TPBP1 have similar binding affinities

for NPN, but TPBP2 consistently binds ligand more weakly than PBP2 (Table 3-2). PBP1 and TPBP1 exhibit different ratios of Stern-Volmer constants in different complexes while PBP2 and TPBP2 have very similar ratios. This indicates that the C-terminal peptide plays different roles in PBP1 and PBP2. It is possible that the C-terminal peptide may also contribute to the PBP selectivity.

3.5 Summary

I have studied the interaction kinetics of PBP1 and PBP2 with one surrogate ligand, NPN. The results have provided further evidence of the stepwise interaction between PBP and a ligand and shown the possibility of a three-step binding model. The difference in affinity of NPN binding to PBPs between two different methods supports the hypothesis of the existence of a weaker binding site on the PBP, the external binding site. Through the quenching study of the intrinsic fluorescence of Trp37 with two quenchers of different inherent properties, I notice that the quenching profiles of PBPs with different ligands are unique (Table 3-6) and the change of the local environment around that residue happens immediately after the PBP and ligand are mixed (Figure 3-9). I suggest that the external binding mode of the relevant ligand to the PBP may represent the active form of the PBP. By comparing the binding properties of intact PBPs and TPBPs, I am able to further identify the importance of the C-terminal peptide of the long-chain PBPs. Besides acting as a gate and a step stone for the ligand, it is also a distinct component of the PBP and may primarily help to discriminate ligands.

3.6 Supporting Information

3.6.1 Supporting Data for Stopped-Flow Assay

The kinetics for PBP1s could not be fit to a mono-exponential function and was adequately fit to the sum of two exponentials (Figure 3-3A). This result shows that both reactions A and B have to be included in the fitting procedure. For PBP1 all rate constants were set as free parameters and the initial concentrations of P and L were explicitly included in the global fit. The same values for k_A, k_{-A} and k_B were recovered when k_{-B} was included or absent in the model, i.e. k_{-B} converged to zero. Simulations were performed by fixing values of k_A and k_{-A} and by setting $k_B = 47\ s^{-1}$ or $k_B + k_{-B} = 47\ s^{-1}$ and varying the values for k_B and k_{-B}. For the typical signal-to-noise ratio seen in Figure S1A, a k_{-B} value of 10% of k_B would have been resolved in the data analysis.

In the case of TPBP1, PBP2 and TPBP2 (Figure 3-3B and Figure 3-4) the kinetics was adequately fit to a mono-exponential function, and the value for the observed rate constant did not vary with protein concentration. Three types of fits were performed: 1) Reaction 1 was included as a fast equilibrium with equilibrium constant K_1, 2) the kinetics was modeled with one relaxation constant $k_{obs,B}$ and 3) the reaction was modeled with k_B and k_{-B}. Fits (1) and (2) led to the recovery of similar values for $k_{obs,B}$ but unrealistically high K_1 values, showing that the kinetic traces did not reflect any information for the formation of $P.L_{enc}$. Fit (3) was unsuccessful because the recovered values for k_B and k_{-B} had very large errors. Therefore, fit (2) was used to determine the values of $k_{obs,B}$.

CHAPTER 4 OLFACTION INHIBITION AND PBP FUNCTIONS IN THE GYPSY MOTH

4.1 PBP Binding and Its Function

Aiming to develop an effective method for screening of inhibitors of pheromone perception in gypsy moths, I have tested the PBP binding with sets of aromatic compounds and correlated the binding data with data from electroantenogram (EAG) recordings. Our group has synthesized five classes of compounds derived from or inspired by aromatic (phenolic) odorants from plants [140]. I have picked out three classes of compounds for my test: dialkoxybenzenes (**3** series), monoalkoxy allyl phenols (**4** series), and dialkoxyallylbenzenes (**5** series) (Figure 4-1). In some cases, pure compounds were tested, while in some cases, mini libraries were tested. A mini library was a mixture of compounds with the same substituent R_1 and varied substituent R_2.

The experiments were originally designed two years ago based on the assumption that PBPs bound the pheromone in the only binding pocket, transported the pheromone to the OR and then the pheromone activated the OR. At that time, the active PBP conformation was not discovered yet. According to this model, a compound which binds strongly to PBP (in the same range of K_d as the cognate pheromone ligands) should compete and interfere with pheromone binding to PBP. This, in turn, should have some effect on the EAG response. In our EAG experiments, several stimuli were puffed over the antenna sequentially: i) clean air, ii) pure (+)-disparlure (100 ng), iii) (+)-disparlure (100 ng) + test compound (1 µg), iv) (+)-disparlure (100 ng) + test compound (10 µg), v) (+)-disparlure (100 ng) + test compound (100 µg), vi) pure (+)-disparlure (100 ng) (Figure 4-2). There were three different effects the test compounds had on the

EAG waves of the mixed puffs (iii-v) or on the last pure (+)-disparlure puff (vi) relative to the first one (ii). First, the depth of depolarization of the mixed puffs could be either enhanced or inhibited. We termed this short-term inhibition (STI). Second, the width at the base of the signal of the mixed puffs could be increased by certain compounds. We termed this peak broadening (PB). Third, the depth of the depolarization of the last pure (+)-disparlure puff (vi) relative to the first (+)-disparlure puff (ii) could be diminished. We termed this long-term inhibition (LTI).

I did not observe any correlation between the PBP binding affinities and STI/LTI. As our knowledge towards the understanding of the perireceptor events grew, it became clear that, for PBPs, it may not be the binding strength but the conformation induced by ligand binding that is important. The complex of PBP with the biological compound can activate the OR [29], and thus a compound that binds strongly may not trigger the active PBP conformation, and may be ineffective in stimulating a pheromone response. Kinetic studies have suggested many binding modes of the ligand. I have reached the same conclusion that the behavioral responses of a compound did not correlate with the binding affinity of the PBP for that ligand [47,138,139,156]. Some correlation was seen between PB and the blend effect between the PB compounds and (+)-disparlure, with PBP1. Correlation of PB with the ratio of the Stern-Volmer constants of **3c** compounds indicates a connection between PB and the active PBP conformation. I will summarize all my results here, as well as some interpretations, for reference in future work.

4.2 Experimental Procedures

4.2.1 EAG Experiment

The EAG recordings were done by Ms. R. Gries (Department of Biological Sciences, SFU). The detailed procedures and the synthesis of the compounds tested have been described previously [140]. Structures and corresponding nomenclature are shown in Figure 4-1, and these follow Paduraru's nomenclature [140].

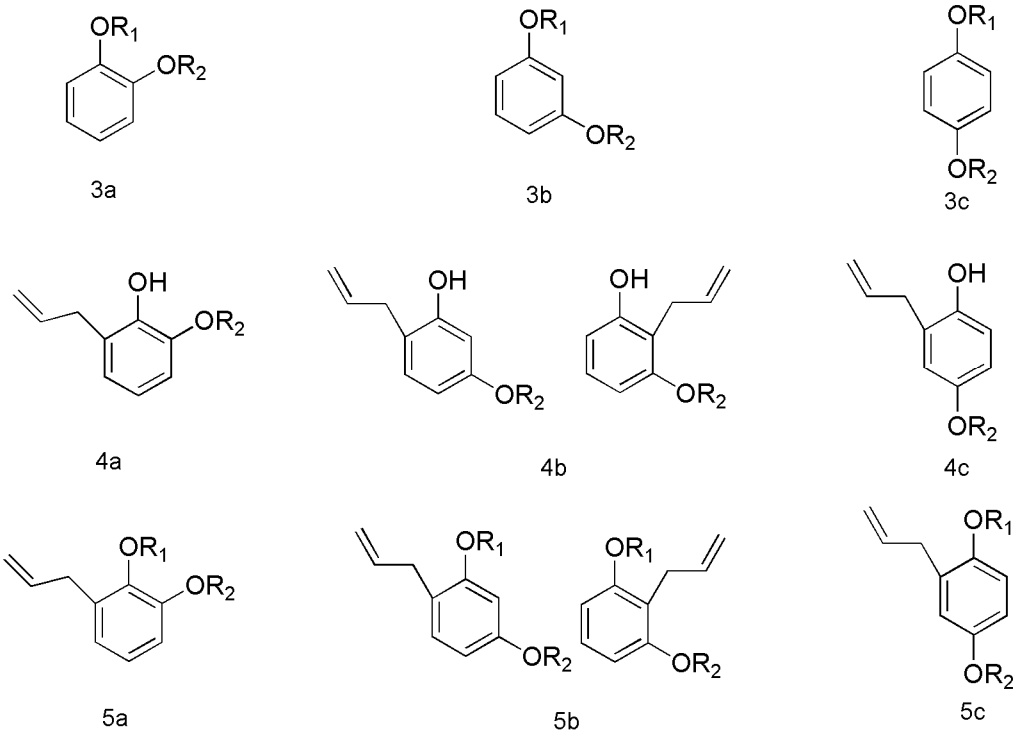

Figure 4-1 Structures of the aromatic compounds.

R_1 or R_2 = CH_3 (Me), CH_2CH_3 (Et), $(CH_2)_2CH_3$ (Pr), $(CH_2)_3CH_3$ (Bu), $(CH_2)_2CH(CH_3)_2$ (iPent) and allyl group. This coding scheme has been taken from [140].

The EAG data were analyzed by Dr. E. Plettner, using the various phases of the EAG signal as shown in Figure 4-2.

$$STI = 100 \times \Delta d_{iii}/d_{net} \quad \textbf{(4.1)}$$

$$LTI = 100 \times \Delta d_{vi}/d_{net} \quad \textbf{(4.2)}$$

$$PB = 100 \times (\Delta t_{v} - \Delta t_{ii})/\Delta t_{ii} \quad \textbf{(4.3)}$$

Where d are depolarizations in mV and t are times in s, and the subscripts refer to either a puff number (see above) or a net value (Figure 4-2).

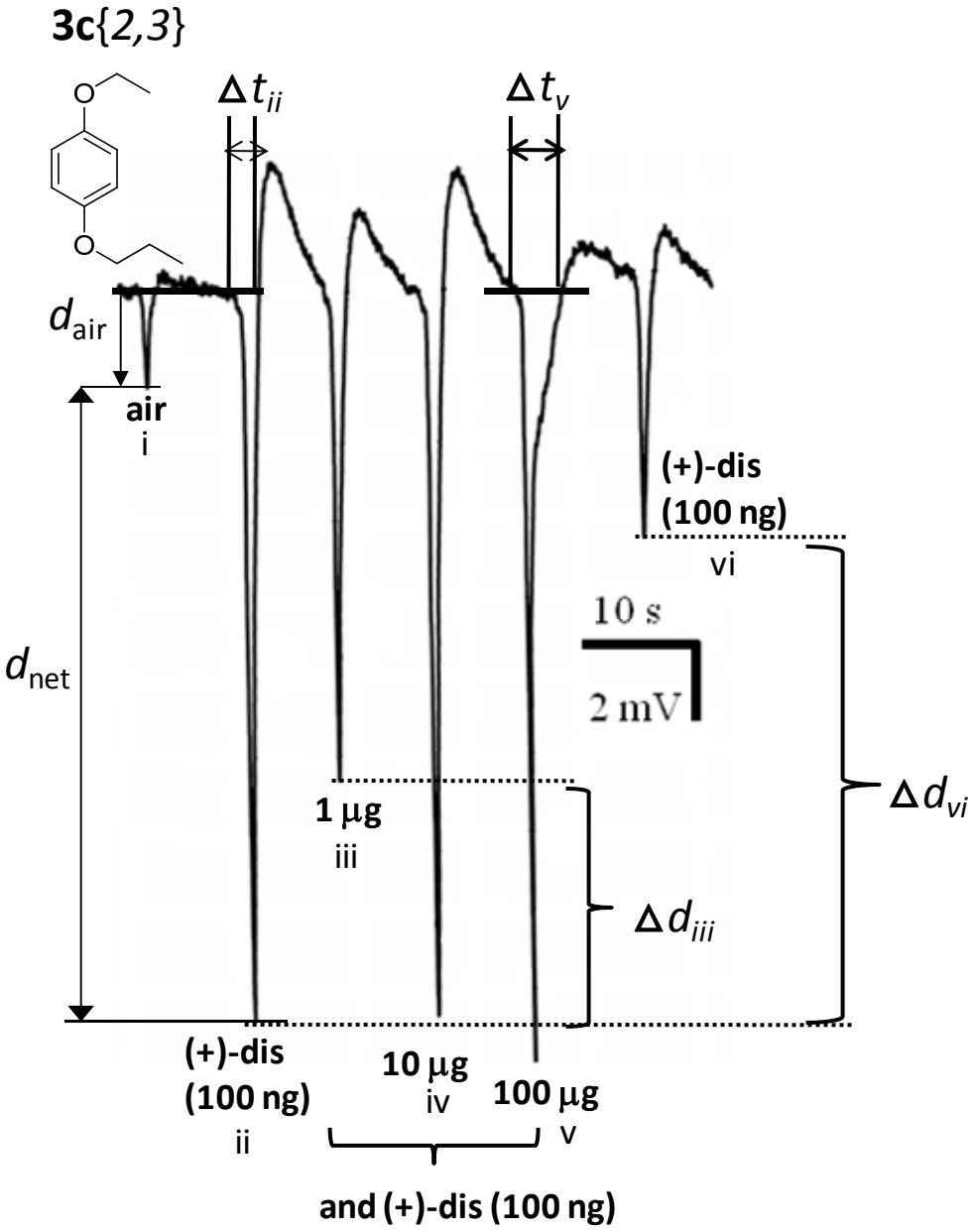

Figure 4-2 A EAG trace for compound 3c{2,3} with six puffs.

Six puffs were recorded: clean air (i), pure (+)-disparlure (100 ng) (ii), mixture of 1 µg of the compound with the pheromone (iii), mixture of 10 µg of the compound with the pheromone (iv), mixture of 100 µg of the compound with the pheromone (v), and pure (+)-disparlure(100 ng) (vi).

4.2.2 Binding of Aromatic Compounds to PBPs

The binding affinities of the aromatic compounds were measured with both the GC assays and a fluorescence-based displacement experiment. The GC assays followed the P2 gel filtration method (Chapter 2). Details were listed in the paper [140].

The fluorescence tests were conducted in a 96-well plate. All the compounds were dissolved in distilled MeOH to a final concentration of 2 mg/mL first and then were diluted further to 0.14 mg/mL. On a preloading plate ,the concentrations of each compound were 0, 2.3, 4.7, 7, 9.3, 12.8, 17.5, 35 μg/mL from row A to H. PBPs (4 μM) were incubated with excess NPN (12 μM for PBP1 and 40 μM for PBP2) in 50 mM phosphate buffer, pH 7.0, for a half hour. The PBP/NPN mixtures were distributed into each well, 200 μL/well. NPN was prepared as a 2 mM stock in MeOH. Then, 4 μL solutions from the preloading plate were pipetted into the corresponding well. Each PBP.ligand combination was run in 4 replicates. Plates were then scanned at 385 nm with Cary Eclipse Fluorimeter excited at 337 nm. The data were analyzed with GraphPad Pritsm, nonlinear regression fitting with one-site competitive binding equation to get K_i values (Eq. 4.4, see section 4.3.2).

4.2.3 Measurement of Blend Effects

A blend effect measures the pheromone binding to the protein in the presence of a second compound. Blend effects have been detected previously, for example, the racemic disparlure binds less strongly than either enantiomer [104],

and (-)-disparlure/(Z)-2-methyloctadec-7-ene bind more strongly than either component [47]. In a mixture of 4 μM PBP and 5 μM (+)-disparlure, 5 μM aromatic compound was added. The incubation was then analyzed using the GC assay. The detailed procedure can be found in Chapter 2. The blend effect is represented by ΔK_d, which is the difference between the K_ds of (+)-disparlure in the absence and in the presence of the aromatic compound ($K_{d(absence)}$ - $K_{d(presence)}$). A positive blend effect has a positive ΔK_d value, meaning that the aromatic compound has enhanced the binding affinity of (+)-disparlure with PBP.

4.2.4 Stern-Volmer Constants Measurement

The same procedure was followed as listed in section 3.2.4. The concentration of each compound was 10 μM. Compounds from the **3c** series were tested.

4.3 Results and Discussion

4.3.1 EAG Responses Altered by a Compound

Figure 4-2 shows a typical EAG experimental trace. The following three parameters were measured with this experiment, as shown in the figure: STI, LTI and PB. STI represents the effect of the compound on the pheromone perception when it is applied simultaneously with pheromone. LTI represents the long-term effect of the compound and pheromone mixture on the antennal response to pure pheromone. Both STI and LTI can depict either an antagonist (positive value) or

an agonist (negative value) effect. PB manifests in a broadened shape in the recovery phase of the EAG signal. A good example of broadening can be seen in puff v in Figure 4-2. The structure-activity-relationship for PB of EAG showed clearly the size requirements of the compounds that cause PB (Figure 4-3). I correlated these three parameters with the binding affinity of each compound. Part of the results is summarized in Table 4-1.

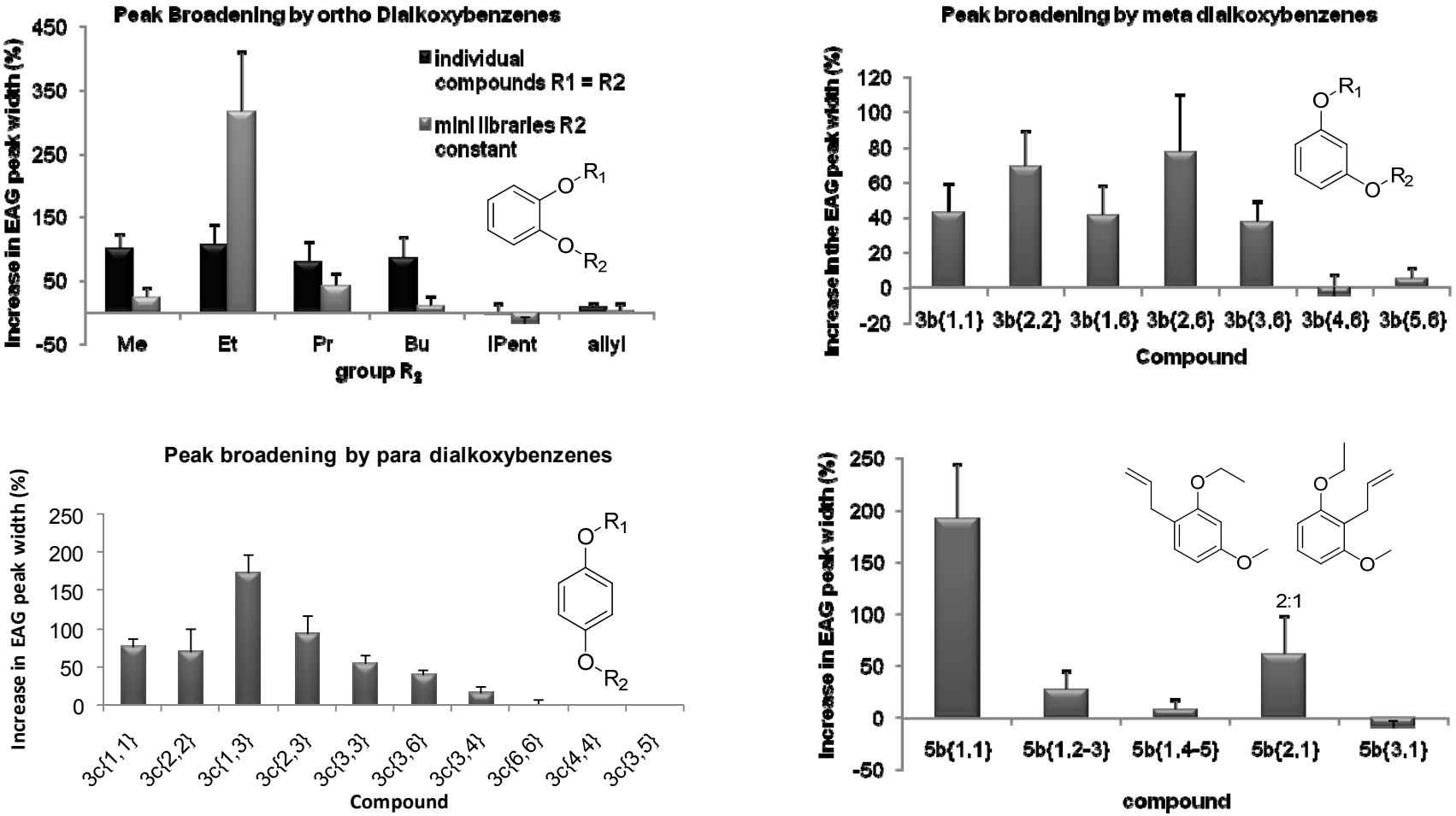

Figure 4-3 Structure-activity-relationship of peak broadening.
These plots were made by Dr. E. Plettner. The other EAG effects measured (STI and LTI) also showed structure-activity relationships. They are not shown here because they did not correlate with PBP binding (see below).

Table 4-1 EAG inhibition activity and binding affinity with PBPs of bis-phenol diethers*.

Compound		Long-term inhibition (%)	Short-term inhibition (%)	Peak broadening(%)	K_d (μM)		K_i (μM)		ΔK_d (μM)	
					PBP1	PBP2	PBP1	PBP2	PBP1	PBP2
3a	1	18 ± 13	(-)8 ± 77	99 ± 25	NA[a]	0.9	3.3	3.5	NA	NA
	2	15 ± 11	(-)22 ± 69	106 ± 32	NA	NA	3.7	4.2	NA	NA
	3	36 ± 9	(-)11 ± 36	80 ± 31	NA	NA	2.5	2.5	NA	NA
	4	49 ± 12	27 ± 29	86 ± 32	NA	NA	1.7	1.8	NA	NA
	5	(-)78 ± 80	(-)193 ± 107	(-)1 ± 15	0.2	63	2.6	1.1	-27.9	2.8
	6	17 ± 28	(-)27 ± 48	9 ± 5	NA	NA	1.3	1.2	NA	NA
3a lib	1	26 ± 6	(-)33 ± 50	23 ± 16	NA	NA	1.8	7.4	NA	NA
	2	15 ± 4	71 ± 7	316 ± 94	NA	NA	2.2	0.1	NA	NA
	3	18 ± 6	(-)35 ± 57	42 ± 18	NA	NA	4.2	0.6	NA	NA
	4	15 ± 11	38 ±10	10 ± 14	NA	NA	3.2	2.6	NA	NA
	5	10 ± 7	39 ± 9	(-)16 ± 8	NA	NA	0.7	0.4	NA	NA
	6	9 ± 5	53 ± 10	3 ± 11	NA	NA	NA	NA	NA	NA
3b	1	1 ± 8	44 ± 36	43 ± 16	NA	900	0.4	0.2	10.9	1
	2	39 ± 6	63 ± 65	69 ± 20	NA	NA	0.04	0.04	-27.4	2.2
	3	45 ± 12	(-)2 ± 34	19 ± 33	NA	NA	0.005	0.04	2.9	1.7
	4	8 ± 9	(-)42 ± 93	78 ± 38	87	64	0.05	0.05	4.5	1.7
3c	1	(-)7 ± 10	15 ± 25	77 ± 12	2.6	13	NA	NA	NA	NA
	2	17 ± 11	(-)27 ± 15	71 ± 30	5	8.1	0.8	5	-17.1	2.4
	3	29 ± 13	(-)100 ± 40	55 ± 12	11	38	1.7	1.6	NA	NA
	4	7 ± 14	(-)205 ± 115	0 ± 0	48	22	0.5	0.4	NA	NA
	5	7 ± 4	50 ± 9	0 ± 0	20	24	NA	NA	NA	NA
	6	4 ± 6	41 ± 8	0 ± 0	NA	NA	0.05	0.04	NA	NA
3c lib	1	0 ± 10	72 ± 17	53 ± 45	NA	NA	4.3	5.4	NA	NA
	2	10 ± 12	50 ± 19	62 ± 53	NA	NA	0.4	0.3	NA	NA
	3	71 ± 13	105 ± 11	116 ± 47	NA	NA	0.1	0.3	-11.3	0.2
	4	57 ± 11	87 ± 6	74 ± 44	NA	NA	0.2	0.2	8	-2.3
	5	50 ± 11	71 ± 9	86 ± 61	NA	NA	1.3	1.2	7.6	-3.8

*1 = Me
2 = Et
3 = Pr
4 = Bu
5 = iPent
6 = allyl
In the single compound, R_1=R_2; in the library, the number indicates R_1 (Figure 4-1).
[a] NA = not measured
The Kd and ΔKd values were measured with GC assay and Ki values were obtained by fluorescence test (NPN displacement).
Details on page 121

4.3.2 PBP Binding and EAG

Correlation between K_i and K_d

The K_i value for each compound or set was obtained by fitting the data to a one-site competitive binding equation:

$$K_i = \frac{EC_{50}}{1+\frac{[ligand]}{K_d}} \quad (4.4)$$

EC_{50} is the concentration of the compound that competes for half the specific binding; K_d is the dissociation constant of the PBP complex with the reporter compound (NPN in my case). Normally, the smaller the K_i value is, the stronger the binding of the compound with the PBP. Paradoxically, correlation between the available K_i and K_d values shows a negative slope (Figure 4-4). This means that the compounds that competed better than the NPN for binding to the PBP are those, which by themselves did not bind PBP very strongly in the GC assay. This raises an important caveat for previous studies, in which only fluorophore displacement K_i values were used to make inferences about PBP binding selectivities [121,124].

My previous work (chapters 2 and 3) suggests that the K_d values obtained in GC assays reflect the most stable internal binding of the ligand and that the increase in the NPN fluorescence intensity in PBP.NPN complexes reflects both internally and externally bound NPN. Externally bound NPN is probably easier to displace by another ligand than internally bound NPN, given the multi-step

mechanism of ligand binding and release proposed in Chapter 3. Finally, previous studies and my own work with mini-libraries of aromatic compounds (Appendix B) have shown blend effects when multiple ligands are competing in the multi-step binding mechanism of PBPs. Therefore, the fluorophore displacement constants, K_i, reflect only the ability of a competing compound to displace the bound NPN.

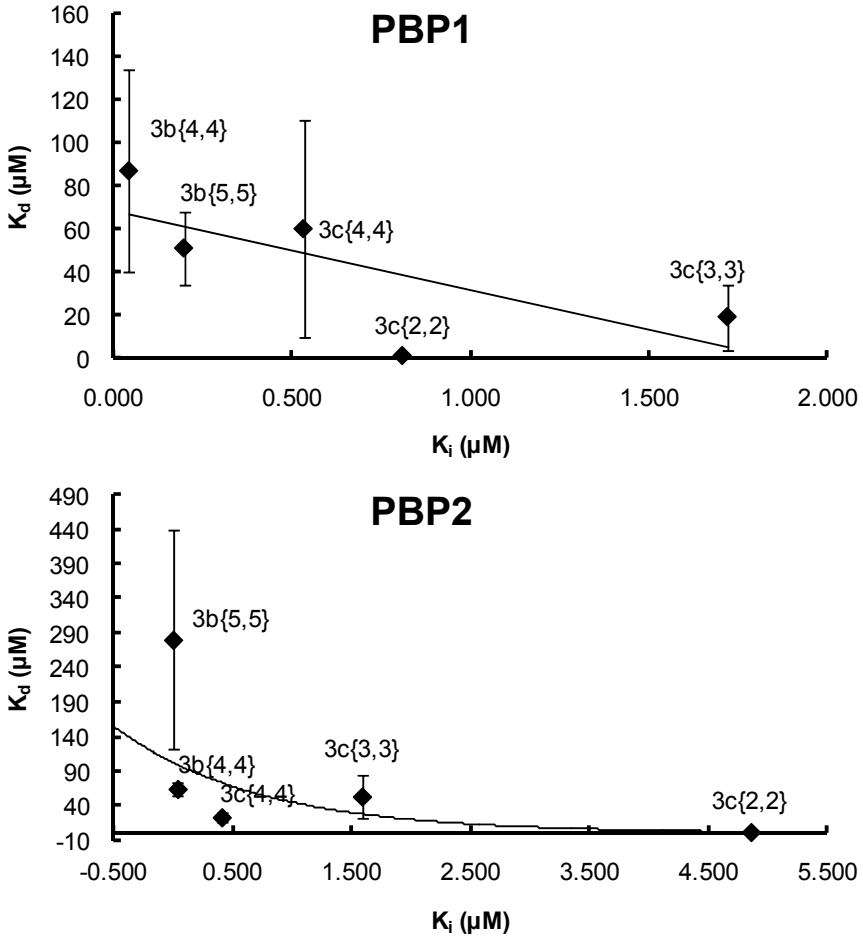

Figure 4-4 Binding affinities from two methods show negative correlation.

K_d was measured directly by the GC assay and K_i was obtained from the NPN displacement experiment. Lines represent the trend of the data.

Correlation between K_i and LTI

LTI values from all tested compounds were plotted against corresponding K_i values in Figure 4-5 (see Appendix B for values). The correlation was weak but overall, the strongest LTI effect came from the compounds with smaller K_is with both PBPs. Overall, a small K_i is necessary but not the only condition that leads to strong long-term inhibition of the pheromone signal. If plots of K_i vs. LTI for each Individual series of compounds are compared, it is impossible to reach a conclusion (Figure 4-6). For some series of compounds, for example, individual **3b** compounds, **3c** library and **5c** library series, K_i values correlate negatively with the LTI. For some other series of compounds, the plots show positive correlation (individual **3c** compounds and **5a/5b** library series). Plots of K_i vs. LTI for both PBP1 and PBP2 are similar and only those for PBP1 are shown here. From these analyses, we can not predict the LTI effect of a compound from its ability to displace NPN from the binding pocket of PBPs.

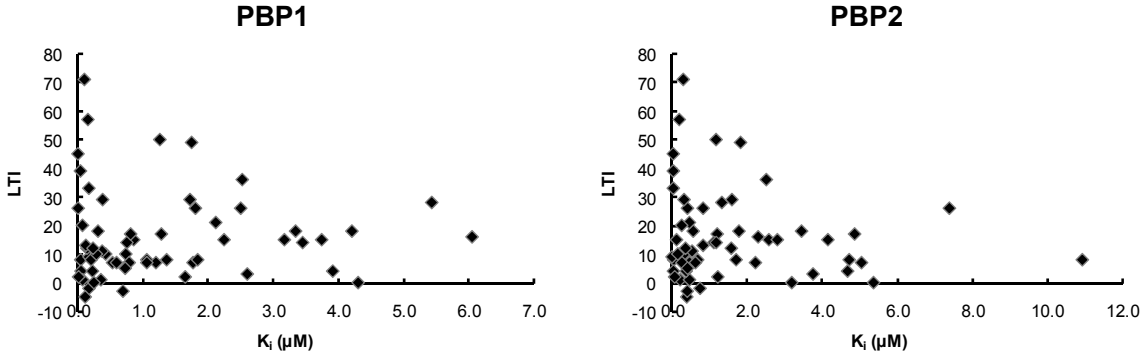

Figure 4-5 PBP binding does not correlate with LTI for all tested compounds.

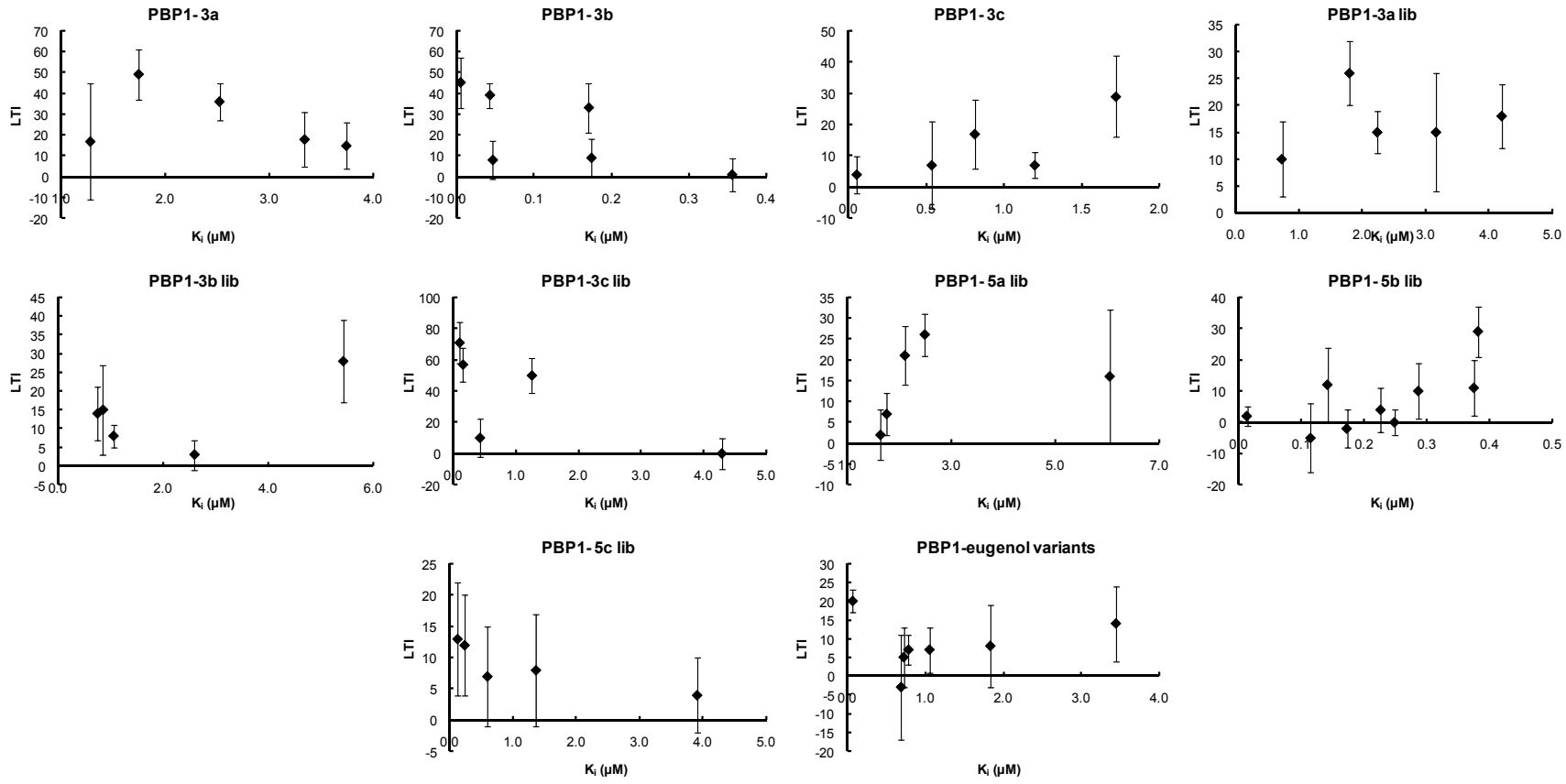

Figure 4-6 PBP binding correlates randomly with LTI for compounds from individual series.
Both positive and negative correlations are present. NPN displacement data for PBP1 are used here.

Correlation between K_i and Peak Broadening

As indicated in Figure 4-7, there was no correlation between K_i and PB.

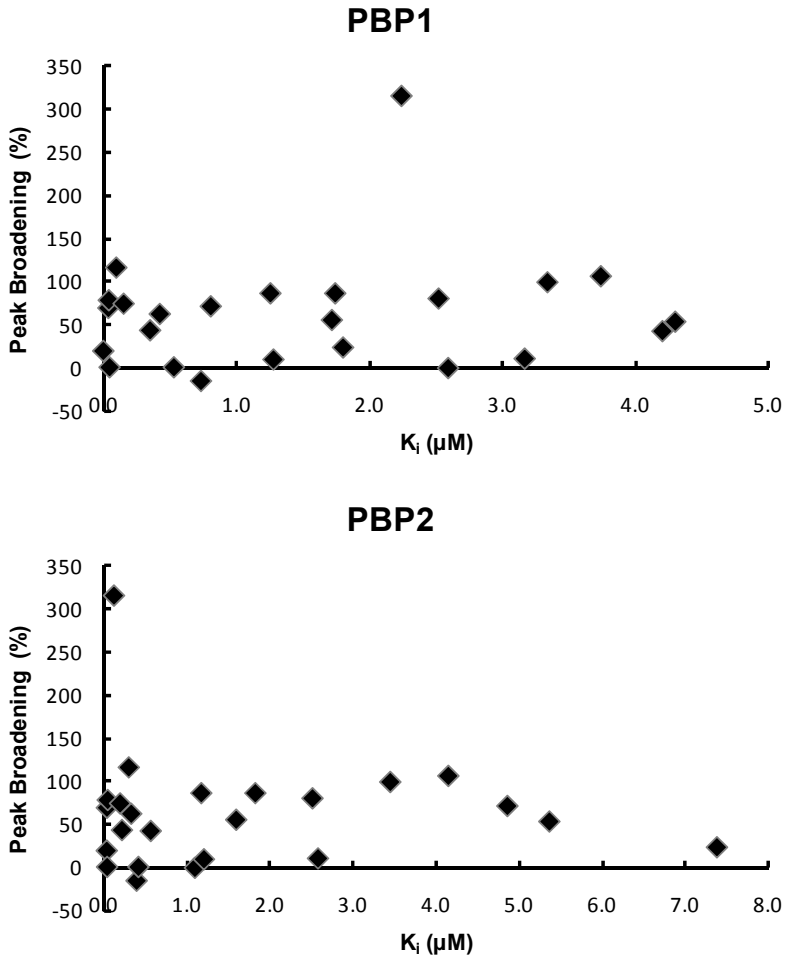

Figure 4-7 No correlation between PBP binding and Peak Broadening (PB).

Correlation between ΔK_d and Peak Broadening

With the purpose of finding a correlation between the blend effect and the LTI effect of an aromatic compound, compounds that had induced a strong LTI were chosen to test, by the GC assay, for a blend effect with (+)-disparlure. No

connection was found between the LTI and the blend effect. Instead, Dr. E. Plettner and I have found that for PBP1, ΔK_d was related to PB. For PBP1, the compounds I have tested can be categorized into two series: series 1 inducing positive blend effect and series 2 inducing negative blend effect. The strongest PB comes from the compounds with either the strongest positive blend effect (series 1) or the weakest negative blend effect (series 2) (Figure 4-8). In both cases, that represents the strongest possible binding of (+)-disparlure with PBP1 in the presence of that series of compounds.

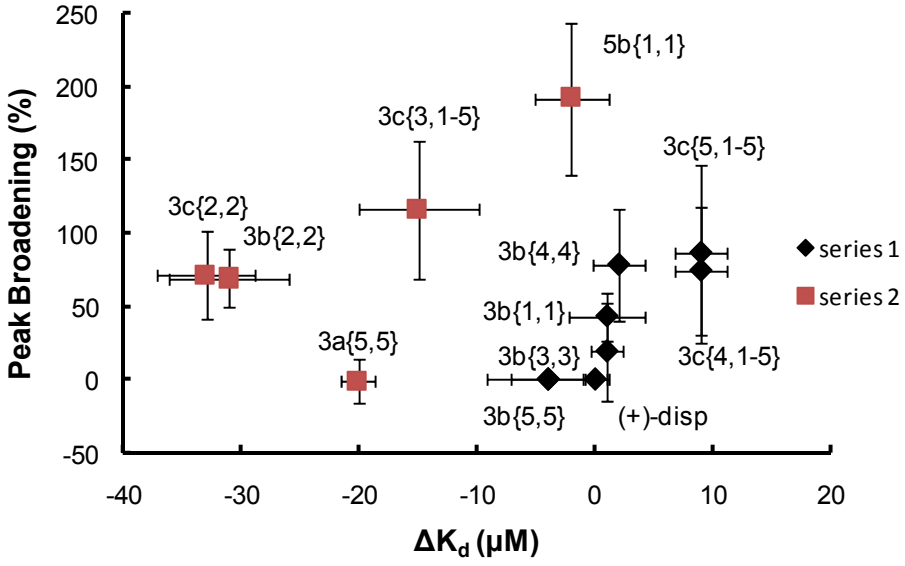

Figure 4-8 Correlation between PB and the blend effect on PBP1 binding with (+)-disparlure.

Correlation between ratio of Stern-Volmer constants and Peak Broadening

I have obtained the ratio of the Stern-Vomer constants of the **3c** compounds (3c{1,1}, 3c {2,2}, 3c {1,3}, 3c{3,3} and 3c{3,5}), for both PBPs.

Overall, smaller compounds gave bigger ratios (Figure 4-9). A very important result is shown in Figure 4-10. Compounds that have a similar ratio of the Stern-Volmer constants as (+)-disparlure show relatively larger PB. This is consistent with our hypothesis that the PB might be related, in some way, to the active conformation of the protein induced by a ligand.

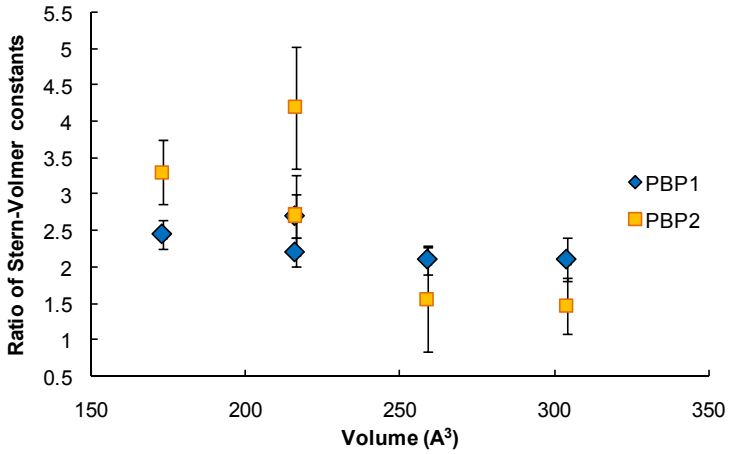

Figure 4-9 Structure-activity-relationship of ratio of the Stern-Volmer constants for both PBPs.

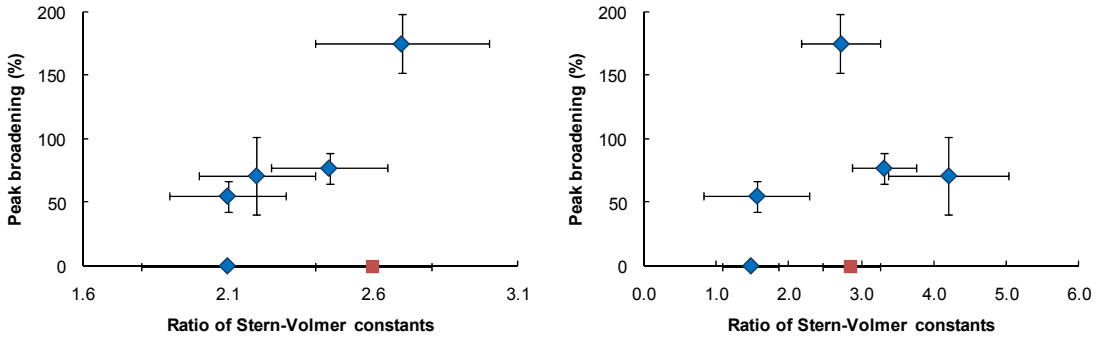

Figure 4-10 Correlation between PB and ratio of the Stern-Volmer constants.

Left: PBP1; right: PBP2. Blue diamonds: 3c compounds; red square: (+)-dispalure. Bars indicated the S.E. for PB and the propagated error from the fitting errors for the ratio of the Stern-Volmer constants.

4.4 Summary

It is very difficult to link the PBP binding directly to EAG responses. Part of this problem is due to the complexity of EAG signals. An EAG peak represents the overall electrophysiological behavior of the whole moth antenna. Along with the other perineuronal and neuronal events, PBP binding is only one step of the signal transduction process in portions of sensory hairs. However, we did observe some correlation between PBP binding and the PB of an EAG signal. Two sets of compound altered the binding affinities of (+)-disparlure with PBP1, and this behavior correlated o PB. I also found in 3c compounds a correlation between PB and the ratio of the Stern-Volmer constants. The ratio of the Stern-Volmer constants reflects the local conformation of the intrinsic Trp in PBPs. Both results indicate that a certain conformation of the PBP, induced by the interaction with a ligand, is related to the PB observed in EAG responses.

CHAPTER 5 SUMMARY AND PERSPECTIVES

5.1 Concluding Remarks

Aiming to understand the molecular basis of the biological function of PBPs, this thesis has systematically explored the kinetics of PBP-ligand interactions. As the major contribution, I have proposed a three-step binding mechanism and successfully dissected the PBP-ligand association process. My current hypothesis is that PBPs might be multifunctional and each of the kinetic phases could be related to a different function. The insect olfactory system has a broad range of sensitivity, from 10 to 10^8 molecules.s^{-1}.sensillum^{-1}. Wicher et al. suggested two activation pathways of insect ORs: one rapid ionotropic pathway that may function at high pheromone concentrations and one slow but highly sensitive pathway involving G-protein-mediated signal amplification [64]. If this is true, correspondingly, there should be different ways of transferring the message from the pheromone to the ORs at high or low pheromone concentrations as well. Therefore, insect PBPs need to act differently at high and low ligand concentrations. In addition, different roles of PBPs may take place in different time regimes.

Kinetic studies are powerful tools for the dissection of reaction mechanisms, but they are also technically difficult. Challenges with the PBPs are: 1) the multiple steps and 2) the reversibility of those steps. It is technically demanding to isolate these steps from each other (with PBP1/disparlure, and the GC assay, this was not possible), and therefore, to interpret the results. Taking into account the validations and limitations of the techniques used, my work is the first to articulate the multi-step binding mechanism of insect PBPs.

I have also tried to understand the multimerization of PBPs and ligand-specific conformational changes. The technical challenges in my search for answers have increased my appreciation of the brilliant and delicate system of insect olfaction. In the future, there are three major questions I feel should be addressed:

First, is PBP aggregation biologically relevant?

Second, what is the mechanism (kinetics) of the local conformational rearrangement in the step of PBP activation?

Third, how can we effectively find a good inhibitor for the antenna response of the gypsy moth?

5.2 Future Directions

5.2.1 Resolving the 3D Structures of LdisPBPs

Successful crystallization of apo-LdisPBPs or LdisPBPs with carefully chosen ligands or ligand mixtures would help to answer most of the questions. By comparing the crystal structures of apo-LdisPBP and complexes of LdisPBP.(+)-disparlure and LdisPBP.non-natural ligand (NPN for example), we can identify the active conformation, the key residues involved in ligand recognition and the residues in the interface between two monomers of the LdisPBP dimer. To answer the first question, we can produce LdisPBP mutants, LdisPBP^{mono}, which can not dimerize. By comparing the ligand binding kinetics or affinities of LdisPBP^{mono} with native PBPs, we can tell whether the aggregation is important

or not. In the future, when the conditions mature, we can also investigate the effect of the PBP aggregation *in vivo* by studying the single sensillum responses of a gypsy moth mutant, which expresses LdisPBP^{mono} in its sensilla. If the dimerization of PBPs is related to a scavenger function at high doses of ligands, we would expect a lower saturation concentration of the sensillum response curve in the gypsy moth mutant.

5.2.2 Kinetics of PBP Activation

The activation of insect PBPs is related to the local conformational changes on the C-terminal area. I have hypothesized that the PBPs are activated in the first binding mode, where a ligand is bound externally. It is difficult to measure the rate constant for this step in my case, especially for the interaction between LdisPBPs and the cognate ligand, (+)-disparlure. Because association of LdisPBPs with (+)-disparlure does not induce any intrinsic fluorescence change of the protein, we need structural information to strategically mutate the protein if we still want to measure the kinetics based on the fluorescence technique (stopped-flow for example). An alternative is the NMR technique, which is very powerful in investigating protein conformational changes and obtaining detailed information about molecular rearrangements on the millisecond to microsecond timescale.

My work has built a basic understanding of the process of PBP-ligand interaction. Any information on the kinetics of the C-terminal peptide

conformational change in association with ligand binding would expand this picture. Furthermore, I look forward to seeing if there is any kinetic selectivity of the PBPs. In other words, would the cognate ligand activate the PBP more quickly than an irrelevant ligand, and is there any relationship between the k_1 values and the ligand activity? If so, this can be developed as another strategy for PBP inhibitor screening.

5.2.3 Influence of Potassium Ion on NPN Dissociation

I have done several tests regarding salt effects on PBP binding (Appendix C). During fluorescence measurements on 96-well plates, I noticed that the fluorescence of NPN was much more stable in potassium phosphate buffer than in Tris buffer. In most cases in a Tris buffer, it seemed that the bound NPN cannot be displaced by a second ligand and the NPN fluorescence did not decrease, but the same ligand could displace the bound NPN from PBPs in a potassium phosphate buffer. Kowcun et al. has suggested a potassium-binding site on PBPs [117]. There is high concentration of K^+ in the sensillum lymph. Potassium ions may help to stabilize certain conformers of PBPs. To test this hypothesis, kinetic experiments and solving the protein NMR structures at different potassium concentrations may help to elucidate ion effects on insect PBPs.

5.2.4 Investigation of Inhibitors of Gypsy Moth's Electrophysiological Response

After vast investigation of the relationship between PBP binding and the inhibitory effect of certain compounds to the gypsy moth electrophysiology, I have concluded that a direct relationship does not exist. The inhibition to the PBP binding is not necessarily related to the inhibition (short-term or long-term) of the response to pheromone stimuli of moth antennae. It is possible that similar to the methodology used by PBPs to activate the olfactory neurons, the inhibition of the electrophysiological response of the antenna is regulated through subtle conformational changes on the PBPs. Following this line, instead of measuring the binding affinities of the candidate compounds, we have to monitor different conformational changes induced by an inhibitor. In this case, the measurement of the ratio of the Stern-Volmer constants in various PBP.ligand complexes could be a rapid screening method. I have tested a few compounds and found some correlation between peak broadening (=prologation) of EAG signals and conformational changes (Figure 4-10). More compounds need to be tested to get further conclusions. The Stern-Volmer method can be developed to measure the kinetics of the conformational changes as well. It is easy and can be completed without further modification of the protein.

In the long-term, I think the best way to find a good inhibitor is to isolate the LdisORs and work on their binding selectivity.

APPENDICES

APPENDIX A:
ADDED STRUCTUAL STUDIES OF INSECT PBPS SINCE 2003

	Species [a]	*Major pheromone component*	*PBPs*	*Research and reference*	*Accession number*
Dictyoptera	*Leucophaea maderae* Cockroach	3-hydroxyl-2-butanone	LmaPBP	Cloning &binding[123]	AY116618
				Crystal structure[99]	
Hymenoptera	*Apis mellifera* Honey bee	(E)-9-oxodec-2-enoic acid	ASP1	Crystal structure[91]	
Lepidoptera	*Agrotis ipsilon* Black cutworm	(Z)-7-dodecenyl acetate	AipsPBP1 AipsPBP2	Cloning[157]	AY973627, AY973626
	Helicoverpa armigera Cotton bollworm	(Z)-11-hexadecenal	HarmPBP	Cloning & insect distribution [158]	AJ278992
	Sesamia nonagrioides Corn stalk borer	(Z)-11-hexadecenyl acetate	SnonPBP1 SnonPBP2	Cloning & insect distribution[159]	AY485219; AY485220
	Spodoptera exigua Beet armyworm	(Z,E)-9,12-tetradecadienyl acetate	SexiPBP1 SexiPBP2	Cloning[160]	AY743352; AY743351
	Spodoptera litura Tobacco cutworm	(Z,E)-9,11-tetradecadienyl acetate	SlitPBP1 SlitPBP2	Cloning[161]	DQ004497, DQ114219

[a] This table is the extension of the summary in the reference [162].

APPENDIX B:
LIST OF K_I AND LTI VALUES OF THE AROMATIC COMPOUNDS

Compound	*Ki (μM)*		*LTI*
	PBP1	*PBP2*	*(%)*
3a{1,1}	3.3	3.5	18
3a{2,2}	3.7	4.2	15
3a{3,3}	2.5	2.5	36
3a{4,4}	1.7	1.8	49
3a{5,5}	2.6	1.1	-78
3a{6,6}	1.3	1.2	17
3a{1,1-5}	1.8	7.4	26
3a{2,1-5}	2.2	0.1	15
3a{3,1-5}	4.2	0.6	18
3a{4,1-5}	3.2	2.6	15
3a{5,1-5}	0.7	0.4	10
3b{1,1}	0.4	0.2	1
3b{2,2}	0.04	0.04	39
3b{3,3}	0.05	0.04	45
3b{4,4}	0.05	0.05	8
3b{5,5}	0.2	0.01	9
3b{6,6}	0.2	0.04	33
3b{1,1-5}	5.4	1.3	28
3b{2,1-5}	2.6	3.8	3
3b{3,1-5}	0.9	2.8	15
3b{4,1-5}	1.1	0.7	8
3b{5,1-5}	0.8	1.1	14
3c{2,2}	0.8	4.9	17
3c{3,3}	1.7	1.6	29
3c{4,4}	0.5	0.4	7
3c{5,5}	1.2	0.5	7
3c{6,6}	0.1	0.04	4
3c{1,1-5}	4.3	5.4	0
3c{2,1-5}	0.4	0.3	10
3c{3,1-5}	0.1	0.3	71
3c{4,1-5}	0.2	0.2	I7
3c{5,1-5}	1.3	1.2	50

Compound	*Ki (μM)*		*LTI*
	PBP1	*PBP2*	*(%)*
4a{1-5}	0.01	0.8	26
4b{2-3}	0.2	10.9	8
4b{4-5}	0.1	0.5	1
4c{1-5}	0.3	1.8	18
5a{1,1-5}	6.1	2.3	16
5a{2,1-5}	2.5	0.4	26
5a{3,1-5}	2.1	0.5	21
5a{4,1-5}	1.8	5.0	7
5a{5,1-5}	1.6	1.2	2
5b{1,2-3}	0.4	0.2	29
5b{1,4-5}	0.4	0.3	11
5b{2,2-3}	0.3	0.5	10
5b{2,4-5}	0.2	0.7	-2
5b{3,2-3}	0.2	0.4	4
5b{3,4-5}	0.01	0.08	2
5b{4,2-3}	0.2	3.2	0
5b{4,4-5}	0.1	0.4	-5
5b{5,2-3}	0.1	0.4	12
5b{5,4-5}	0.7	0.2	-18
5c{1,1-5}	0.1	0.8	13
5c{2,1-5}	1.4	4.7	8
5c{3,1-5}	0.6	2.2	7
5c{4,1-5}	0.2	1.6	12
5c{5,1-5}	3.9	4.7	4
eugenol	3.5	1.2	14
Me eugenol	1.8	1.7	8
Et eugenol	0.07	0.3	20
Pr eugenol	1.1	0.3	7
Bu eugenol	0.8	0.6	7
iPent eugenol	0.7	0.4	5
Allyl eugenol	0.7	0.4	-3

APPENDIX C:
EFFECTS OF IONS ON PBP BINDING

In the lymph of olfactory sensilla in moths, there are 25 mM Na^+, 200 mM K^+ and 3 mM Mg^{2+} [163]. The effect of ions on PBP binding with disparlure was measured with the 96-well plate experiment (see Chapter 4 for details). NPN was displaced by disparlure at various ion concentrations, giving the binding affinities (K_i) of disparlure with PBPs under each condition (Figure 5-1). Cations from the subgroups Ia and IIa metals were tested. The tests were carried out accidentally in 50 mM potassium phosphate buffer, originally, with additional cation concentrations ranging from 6 to 400 mM. Overall, the displacement under these conditions worked very well. The R^2 value for each fit was above 0.9.

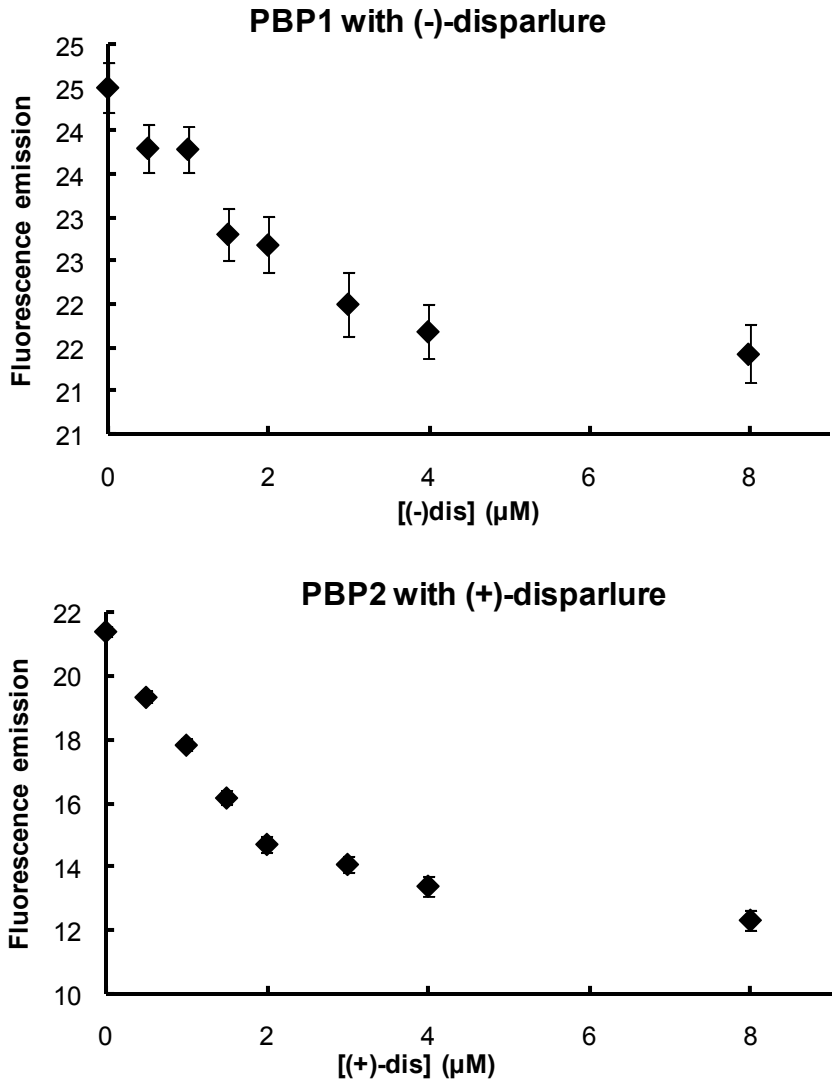

Figure 5-1 NPN displacement by disparlure in 50 mM phosphate buffer

NPN that is bound to the PBP can be displaced by disparlure, manifest in a decrease in the fluorescence emission. Here I show two examples of such an experiment. Data were obtained in the absence of the testing cation. Four μM PBP1 and PBP2 were equilibrated with 12 and 40 μM NPN, respectively, before adding disparlure. Each point represents the average of 40 replicates ± S.E.

As shown in Figure 5-2 it seems that PBP2 binds (+)-disparlure most strongly at either low (<10 mM) or very high (>300 mM) concentrations of ions. The patterns of PBP1 binding with (-)-disparlure at different cation concentrations

are a little bit random (Figure 5-3). However, it is very interesting to notice that for the effect of K^+ ions, the strongest binding between PBP1 and (-)-disparlure is achieved at a medium concentration of K^+ (~40 mM).

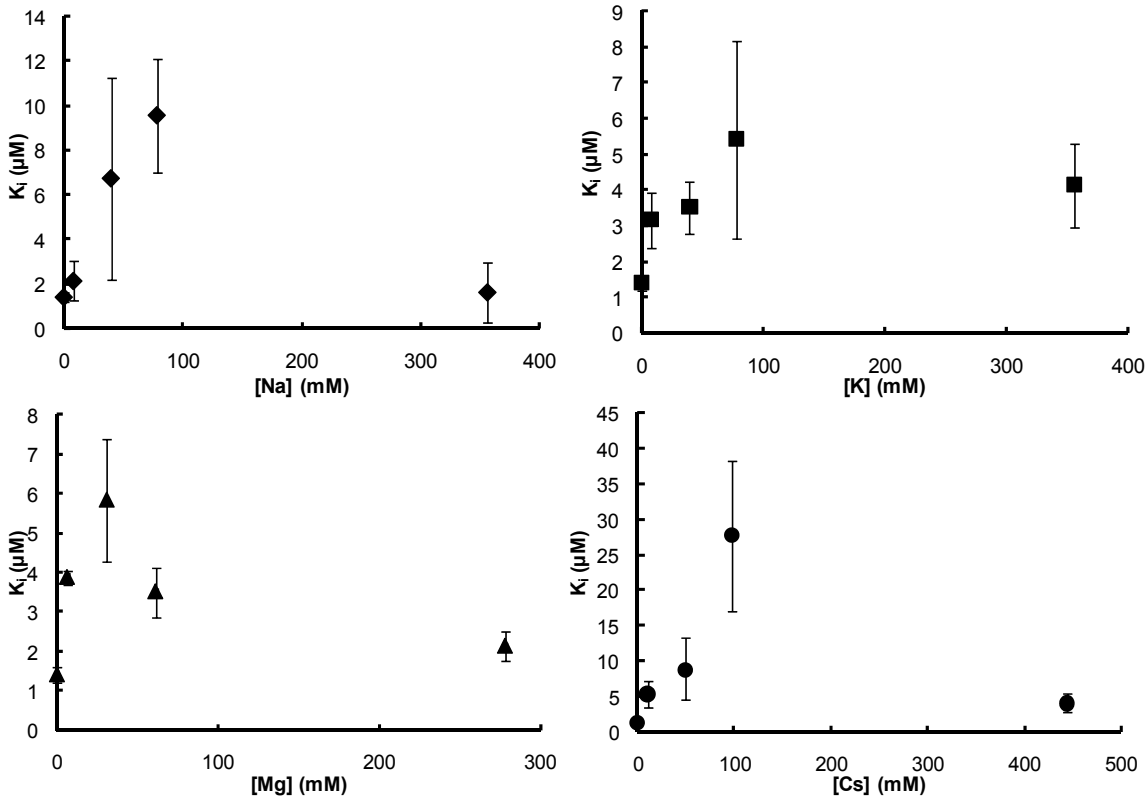

Figure 5-2 Ion effect on the binding affinities of PBP2 with (+)-disparlure.

The strongest binding is achieved at medium concentrations of ions. Tests were done in 50 mM phosphate buffer. Each point represents the average of three replicates ± S.E.

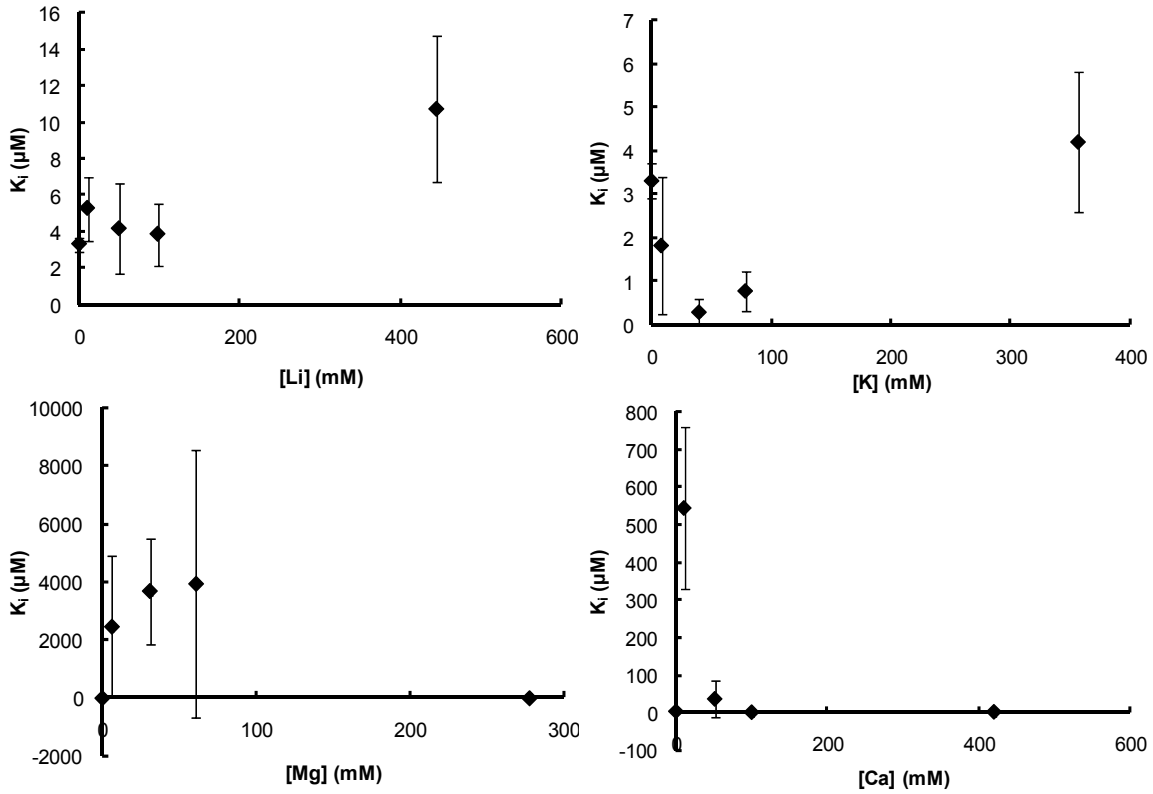

Figure 5-3 Ion effect on the binding affinities of PBP1 with (-)-disparlure.

Diverse effects were observed with different ions. Tests were done in 50 mM phosphate buffer. Each point represents the average of three replicates ± S.E.

Later, I switched the buffer to Tris (pH 7) and MES (pH 6). Interestingly, it seemed that NPN can not be displaced easily any more (Figure 5-4). It could be that the potassium ion is involved in stabilizing a certain conformation of the PBP, or that the absence of potassium ion has elongated the time needed for the NPN displacement, or simply that the potassium ion affects the NPN fluorescence. This experiment is not complete and more tests need to be done to find out the reason for this phenomenon.

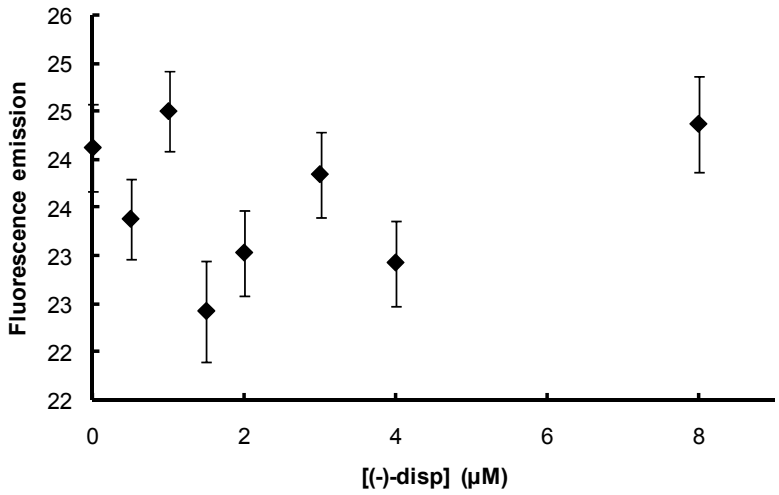

Figure 5-4 Unsuccessful displacement of NPN by disparlure in 50 mM Tris buffer, pH 7

Here I show one test of PBP1 binding using (-)-disparlure to displace bound NPN. Tris buffer is not a good solvent for the displacement experiment. Each point is the average of three replicates ± S.E.

REFERENCE LIST

1. Wyatt, T.D. *Pheromones and Animal Behaviour: Communication by Smell and Taste*, (Cambridge University Press, Cambridge, 2003).
2. Landolt, P.J. & Phillips, T.W. Host plant influences on sex pheromone behavior of phytophagous insects. *Annual Review of Entomology* **42**, 371-391 (1997).
3. Ryan, M.F. Plant chemicals. in *Insect Chemoreception. Fundamental and Applied* (Springer, New York, 2002).
4. Butenandt, A., Beckmann, R., Stamm, D. & Hecker, E. Uber den sexual-lockstoff des Seidenspinners *Bombyx Mori* - Reindarstellung und konstitution. *Zeitschrift Fur Naturforschung Part B-Chemie Biochemie Biophysik Biologie Und Verwandten Gebiete* **14**, 283-284 (1959).
5. Kochansky, J. et al. Sex pheromone of moth, *Antheraea polyphemus* (Lepidoptera saturniidae). *Journal of Insect Physiology* **21**, 1977-1983 (1975).
6. Sirugue, D., Bonnard, O., Lequere, J.L., Farine, J.P. & Brossut, R. 2-Methylthiazolidine and 4-ethylguaiacol, male sex pheromone components of the cockroach *Nauphoeta cinerea* (Dictyoptera, Blaberidae) - A reinvestigation. *Journal of Chemical Ecology* **18**, 2261-2276 (1992).
7. Plettner, E. Insect pheromone olfaction: New targets for the design of species-selective pest control agents. *Current Medicinal Chemistry* **9**, 1075-1085 (2002).
8. Chapman, O.L., Mattes, K.C., Sheridan, R.S. & Klun, J.A. Stereochemical evidence of dual chemoreceptors for an achiral sex-pheromone in Lepidoptera. *Journal of the American Chemical Society* **100**, 4878-4884 (1978).
9. Liljefors, T., Thelin, B., Vanderpers, J.N.C. & Lofstedt, C. Chain-elongated analogs of a pheromone component of the turnip moth, *Agrotis segetum* - A structure activity study using molecular mechanics. *Journal of the Chemical Society-Perkin Transactions 2*, 1957-1962 (1985).
10. Norinder, U., Gustavsson, A.L. & Liljefors, T. A 3D-QSAR study of analogs of (Z)-5-decenyl acetate, a pheromone component of the turnip moth, *Agrotis segetum*. *Journal of Chemical Ecology* **23**, 2917-2934 (1997).
11. Charlton, R.E. et al. Sex-pheromone for the brownbanded cockroach is an unusual dialkyl-substitured alpha-pyrone. *Proceedings of the National Academy of Sciences of the United States of America* **90**, 10202-10205 (1993).

12. Leal, W.S., Shi, X.W., Liang, D.S., Schal, C. & Meinwald, J. Application of chiral gas chromatography with electroantennographic detection to the determination of the stereochemistry of a cockroach sex pheromone. *Proceedings of the National Academy of Sciences of the United States of America* **92**, 1033-1037 (1995).

13. Gries, G. et al. Specificity of nun and gypsy moth sexual communication through multiple-component pheromone blends. *Naturwissenschaften* **83**, 382-385 (1996).

14. Miller, J.R., Mori, K. & Roelofs, W.L. Gypsy moth (Lepidoptera Lymantriidae) field trapping and electroantennogram studies with pheromone enantiomers. *Journal of Insect Physiology* **23**, 1447-1453 (1977).

15. Mori, K. Significance of chirality in pheromone science. *Bioorganic & Medicinal Chemistry* **15**, 7505-7523 (2007).

16. Haniotakis, G., Francke, W., Mori, K., Redlich, H. & Schurig, V. Sex-specific activity of (R)-(-) and (S)-(+)-1,7-dioxaspiro[5.5]undecane, the major pheromone of *Dacus oleae* (Diptera, Tephritidae). *Journal of Chemical Ecology* **12**, 1559-1568 (1986).

17. Adams, M.D. et al. The genome sequence of *Drosophila melanogaster*. *Science* **287**, 2185-2195 (2000).

18. Kreher, S.A., Kwon, J.Y. & Carlson, J.R. The molecular basis of odor coding in the Drosophila larva. *Neuron* **46**, 445-456 (2005).

19. de Bruyne, M., Foster, K. & Carlson, J.R. Odor coding in the Drosophila antenna. *Neuron* **30**, 537-552 (2001).

20. de Bruyne, M., Clyne, P.J. & Carlson, J.R. Odor coding in a model olfactory organ: The Drosophila maxillary palp. *Journal of Neuroscience* **19**, 4520-4532 (1999).

21. Carde, R.T. & Minks, A.K. Control of moth pests by mating disruption - Successes and constraints. *Annual Review of Entomology* **40**, 559-585 (1995).

22. Cook, S.M., Khan, Z.R. & Pickett, J.A. The use of push-pull strategies in integrated pest management. *Annual Review of Entomology* **52**, 375-400 (2007).

23. Rau, P. & Rau, N. *Trans. Acad. Sci. St Louis* **26**, 83-221 (1929).

24. Shuker, K.P.N. *The Hidden Powers of Animals: Uncovering the Secrets fo Nature*, (Marshall Editions Ltd., London, 2001).

25. Schneider, D., Kasang, G. & Kaissling, K.E. Determination of scent threshold of *Bombyx mori* with tritium-labeled bombydol. *Naturwissenschaften* **55**, 395 (1968).

26. Kanaujia, S. & Kaissling, K.E. Interactions of pheromone with moth antennae - Adsorption, desorption and transport. *Journal of Insect Physiology* **31**, 71-81 (1985).

27. Honson, N. Simon Fraser University (2006).

28. Benton, R., Vannice, K.S. & Vosshall, L.B. An essential role for a CD36-related receptor in pheromone detection in Drosophila. *Nature* **450**, 289-U13 (2007).

29. Laughlin, J.D., Ha, T.S., Jones, D.N.M. & Smith, D.P. Activation of pheromone-sensitive neurons is mediated by conformational activation of pheromone-binding protein. *Cell* **133**, 1255-1265 (2008).

30. Gong, Y. et al. Ligand-interaction kinetics of the pheromone- binding protein from the gypsy moth, *L. dispar*: Insights into the mechanism of binding and release. *Chemistry & Biology* **16**, 162-172 (2009).

31. Getchell, T.V., Margolis, F.L. & Getchell, M.L. Perireceptor and receptor events in vertebrate olfaction. *Progress in Neurobiology* **23**, 317-345 (1984).

32. Pelosi, P. Perireceptor events in olfaction. *Journal of Neurobiology* **30**, 3-19 (1996).

33. Keil, T.A. Contacts of pore tubules and sensory dendrites in antennal chemosensilla of a silkmoth - Demonstration of a possible pathway for olfactory molecules. *Tissue & Cell* **14**, 451-462 (1982).

34. Steinbrecht, R.A. Pore structures in insect olfactory sensilla: A review of data and concepts. *International Journal of Insect Morphology & Embryology* **26**, 229-245 (1997).

35. Fadamiro, H.Y., Cosse, A.A. & Baker, T.C. Fine-scale resolution of closely spaced pheromone and antagonist filaments by flying male *Helicoverpa zea*. *Journal of Comparative Physiology a-Sensory Neural and Behavioral Physiology* **185**, 131-141 (1999).

36. Vogt, R.G., Riddiford, L.M. & Prestwich, G.D. Kinetic-properties of a sex pheromone-degrading enzyme - The sensillar esterase of *Antheraea polyphemus*. *Proceedings of the National Academy of Sciences of the United States of America* **82**, 8827-8831 (1985).

37. Kasang, G. Bombykol reception and metabolism on the antennae of the silkmoth *Bombys mori*. in *Gustation and Olfaction* (eds. Ohloff, G. & Thomas, A.) 245-250 (Academic Press, London/New York, 1971).

38. Kasang, G., Knauer, B. & Beroza, M. Uptake of Sex Attractant H-3 Disparlure by Male Gypsy Moth Antennae (Lymantria-Dispar) [=Porthetria-Dispar]. *Experientia* **30**, 147-148 (1974).

39. Kasang, G., Vonproff, L. & Nicholls, M. Enzymatic conversion and degradation of sex pheromones in antennae of the male silkworm moth

Antheraea polyphemus. *Zeitschrift Fur Naturforschung C-a Journal of Biosciences* **43**, 275-284 (1988).

40. Steinbrecht, R.A. & Muller, B. Stimulus conducting structures in insect olfactory receptors. *Zeitschrift Fur Zellforschung Und Mikroskopische Anatomie* **117**, 570-575 (1971).

41. Kaissling, K.E. Sensory transduction in insect olfactory receptors. in *Biochemistry of Sensory Functions* (ed. Jaenicke, L.) 243-273 (Springer-Verlag, Berlin, 1974).

42. Kaissling, K.E. Chemo-electrical transduction in insect olfactory receptors. *Annual Review of Neuroscience* **9**, 121-145 (1986).

43. Maida, R., Ziegelberger, G. & Kaissling, K.E. Esterase-activity in the olfactory sensilla of the silkmoth *Antheraea polyphemus*. *Neuroreport* **6**, 822-824 (1995).

44. Vogt, R.G. & Riddiford, L.M. Pheromone reception: A kinetic equilibrium. in *Mechanisms in Insect Olfaction* (eds. Payne, T.L., Birch, M.C. & Kennedy, C.E.J.) 201-208 (Oxford Univeresity Press, London/New York, 1986).

45. Riddiford, L.M. Antennal proteins of Saturniid moths - Their possible role in olfaction. *Journal of Insect Physiology* **16**, 653-660 (1970).

46. Honson, N., Gong, Y. & Plettner, E. Structure and function of insect odorant and pheromone-binding proteins (OBPs and PBPs) and chemosensory-specific proteins (CSPs). in *Chemical Ecology and Phytochemistry of Forest Ecosystems* (ed. Romeo, J.T.) 227-268 (Elsevier Ltd, Oxford, 2005).

47. Honson, N., Johnson, M.A., Oliver, J.E., Prestwich, G.D. & Plettner, E. Structure-activity studies with pheromone-binding proteins of the gypsy moth, *Lymantria dispar*. *Chemical Senses* **28**, 479-489 (2003).

48. Vogt, R.G. & Riddiford, L.M. Pheromone binding and inactivation by moth antennae. *Nature* **293**, 161-163 (1981).

49. Vogt, R.G. Biochemical diversity of odor detection: OBPs, ODEs and SNMPs. in *Insect Pheromone Biochemistry and Molecular Biology: The biosynthesis and detection of pheromones and plant volatiles* (eds. Blomquist, G.J. & Vogt, R.G.) 391-445 (Elsevier Academic Press, London, 2003).

50. Ishida, Y. & Leal, W.S. Rapid inactivation of a moth pheromone. *Proceedings of the National Academy of Sciences of the United States of America* **102**, 14075-14079 (2005).

51. Rybczynski, R., Reagan, J. & Lerner, M.R. A pheromone-degrading aldehyde oxidase in the antennae of the moth *Manduca sexta*. *Journal of Neuroscience* **9**, 1341-1353 (1989).

52. Rybczynski, R., Vogt, R.G. & Lerner, M.R. Antennal-specific pheromone-degrading aldehyde oxidases from the moths *Antheraea polyphemus* and *Bombyx mori*. *Journal of Biological Chemistry* **265**, 19712-19715 (1990).

53. Tumlinson, J.H., Klein, M.G., Doolittle, R.E., Ladd, T.L. & Proveaux, A.T. Identification of female Japanese beetle sex pheromone - Inhibition of male response by an enantiomer. *Science* **197**, 789-792 (1977).

54. Leal, W.S. Chemical communication in scarab beetles: Reciprocal behavioral agonist-antagonist activities of chiral pheromones. *Proceedings of the National Academy of Sciences of the United States of America* **93**, 12112-12115 (1996).

55. Ishida, Y. & Leal, W.S. Chiral discrimination of the Japanese beetle sex pheromone and a behavioral antagonist by a pheromone-degrading enzyme. *Proceedings of the National Academy of Sciences of the United States of America* **105**, 9076-9080 (2008).

56. Graham, S.M. & Prestwich, G.D. Tissue distribution and substrate-specificity of an epoxide hydrase in the gypsy moth, *Lymantria dispar*. *Experientia* **48**, 19-21 (1992).

57. Prestwich, G.D. Chemistry of pheromone and hormone metabolism in insects. *Science* **237**, 999-1006 (1987).

58. Buck, L. & Axel, R. A novel multigene family may encode odorant receptors - A molecular basis for odor recognition. *Cell* **65**, 175-187 (1991).

59. Clyne, P.J. et al. A novel family of divergent seven-transmembrane proteins: Candidate odorant receptors in Drosophila. *Neuron* **22**, 327-338 (1999).

60. Gao, Q. & Chess, A. Identification of candidate Drosophila olfactory receptors from genomic DNA sequence. *Genomics* **60**, 31-39 (1999).

61. Vosshall, L.B., Amrein, H., Morozov, P.S., Rzhetsky, A. & Axel, R. A spatial map of olfactory receptor expression in the Drosophila antenna. *Cell* **96**, 725-736 (1999).

62. Benton, R., Sachse, S., Michnick, S.W. & Vosshall, L.B. Atypical membrane topology and heteromeric function of Drosophila odorant receptors in vivo. *Plos Biology* **4**, 240-257 (2006).

63. Sato, K., Pellegrino, M., Nakagawa, T., Vosshall, L.B. & Touhara, K. Insect olfactory receptors are heteromeric ligand-gated ion channels. *Nature* **452**, 1002-U9 (2008).

64. Wicher, D. et al. Drosophila odorant receptors are both ligand-gated and cyclic-nucleotide-activated cation channels. *Nature* **452**, 1007-U10 (2008).

65. Touhara, K. & Vosshall, L.B. Sensing odorants and pheromones with chemosensory receptors. *Annual Review of Physiology* **71**, 307-332 (2009).

66. Laue, M., Maida, R. & Redkozubov, A. G-protein activation, identification and immunolocalization in pheromone-sensitive sensilla trichodea of moths. *Cell and Tissue Research* **288**, 149-158 (1997).

67. Hallem, E.A., Ho, M.G. & Carlson, J.R. The molecular basis of odor coding in the drosophila antenna. *Cell* **117**, 965-979 (2004).

68. Wang, J.W., Wong, A.M., Flores, J., Vosshall, L.B. & Axel, R. Two-photon calcium imaging reveals an odor-evoked map of activity in the fly brain. *Cell* **112**, 271-282 (2003).

69. Hansson, B.S., Ljungberg, H., Hallberg, E. & Lofstedt, C. Functional specialization of olfactory glomeruli in a moth. *Science* **256**, 1313-1315 (1992).

70. Kanzaki, R., Soo, K., Seki, Y. & Wada, S. Projections to higher olfactory centers from subdivisions of the antennal lobe macroglomerular complex of the male silkmoth. *Chemical Senses* **28**, 113-130 (2003).

71. Kaissling, K.E. & Kasang, G. New pheromone of silkworm moth *Bombyx mori* - Sensory pathway and behavioral effect. *Naturwissenschaften* **65**, 382-384 (1978).

72. Nakagawa, T., Sakurai, T., Nishioka, T. & Touhara, K. Insect sex-pheromone signals mediated by specific combinations of olfactory receptors. *Science* **307**, 1638-1642 (2005).

73. Grosse-Wilde, E., Gohl, T., Bouche, E., Breer, H. & Krieger, J. Candidate pheromone receptors provide the basis for the response of distinct antennal neurons to pheromonal compounds. *European Journal of Neuroscience* **25**, 2364-2373 (2007).

74. Grosse-Wilde, E., Svatos, A. & Krieger, J. A pheromone-binding protein mediates the bombykol-induced activation of a pheromone receptor in vitro. *Chemical Senses* **31**, 547-555 (2006).

75. Krieger, J., Klink, O., Mohl, C., Raming, K. & Breer, H. A candidate olfactory receptor subtype highly conserved across different insect orders. *Journal of Comparative Physiology a-Neuroethology Sensory Neural and Behavioral Physiology* **189**, 519-526 (2003).

76. Larsson, M.C. et al. Or83b encodes a broadly expressed odorant receptor essential for Drosophila olfaction. *Neuron* **43**, 703-714 (2004).

77. Calvo, D., Gomez-Coronado, D., Suarez, Y., Lasuncion, M.A. & Vega, M.A. Human CD36 is a high affinity receptor for the native lipoproteins HDL, LDL, and VLDL. *Journal of Lipid Research* **39**, 777-788 (1998).

78. Baillie, A.G.S., Coburn, C.T. & Abumrad, N.A. Reversible binding of long-chain fatty acids to purified FAT, the adipose CD36 homolog. *Journal of Membrane Biology* **153**, 75-81 (1996).

79. Jin, X., Ha, T.S. & Smith, D.P. SNMP is a signaling component required for pheromone sensitivity in Drosophila. *Proceedings of the National*

Academy of Sciences of the United States of America **105**, 10996-11001 (2008).

80. Nichols, Z. & Vogt, R.G. The SNMP/CD36 gene family in Diptera, Hymenoptera and Coleoptera: *Drosophila melanogaster, D. pseudoobscura, Anopheles gambiae, Aedes aegypti, Apis mellifera,* and *Tribolium castaneum*. *Insect Biochemistry and Molecular Biology* **38**, 398-415 (2008).

81. Rogers, M.E., Steinbrecht, R.A. & Vogt, R.G. Expression of SNMP-1 in olfactory neurons and sensilla of male and female antennae of the silkmoth *Antheraea polyphemus*. *Cell and Tissue Research* **303**, 433-446 (2001).

82. Rogers, M.E., Sun, M., Lerner, M.R. & Vogt, R.G. SNMP-1, a novel membrane protein of olfactory neurons of the silk moth *Antheraea polyphemus* with homology to the CD36 family of membrane proteins. *Journal of Biological Chemistry* **272**, 14792-14799 (1997).

83. Forstner, M. et al. Differential expression of SNMP-1 and SNMP-2 proteins in pheromone-sensitive hairs of moths. *Chemical Senses* **33**, 291-299 (2008).

84. Breer, H., Krieger, J. & Raming, K. A novel class of binding-proteins in the antennae of the silk moth *Antheraea pernyi*. *Insect Biochemistry* **20**, 735-740 (1990).

85. Krieger, J., vonNickischRosenegk, E., Mameli, M., Pelosi, P. & Breer, H. Binding proteins from the antennae of *Bombyx mori*. *Insect Biochemistry and Molecular Biology* **26**, 297-307 (1996).

86. Vogt, R.G., Prestwich, G.D. & Lerner, M.R. Odorant-binding protein subfamilies associate with distinct classes of olfactory receptor neurons in insects. *Journal of Neurobiology* **22**, 74-84 (1991).

87. Maida, R., Krieger, J., Gebauer, T., Lange, U. & Ziegelberger, G. Three pheromone-binding proteins in olfactory sensilla of the two silkmoth species *Antheraea polyphemus* and *Antheraea pernyi*. *European Journal of Biochemistry* **267**, 2899-2908 (2000).

88. NagnanLeMeillour, P., Huet, J.C., Maibeche, M., Pernollet, J.C. & Descoins, C. Purification and characterization of multiple forms of odorant/pheromone binding proteins in the antennae of *Mamestra brassicae* (Noctuidae). *Insect Biochemistry and Molecular Biology* **26**, 59-67 (1996).

89. Vogt, R.G., Kohne, A.C., Dubnau, J.T. & Prestwich, G.D. Expression of pheromone binding-proteins during antennal development in the gypsy moth *Lymantria dispar*. *Journal of Neuroscience* **9**, 3332-3346 (1989).

90. Klein, U. Sensillum-lymph proteins from antennal olfactory hairs of the moth *Antheraea polyphemus* (Saturniidae). *Insect Biochemistry* **17**, 1193-1204 (1987).

91. Pesenti, M.E. et al. Structural basis of the honey bee PBP pheromone and pH-induced conformational change. *Journal of Molecular Biology* **380**, 158-169 (2008).

92. Sandler, B.H., Nikonova, L., Leal, W.S. & Clardy, J. Sexual attraction in the silkworm moth: Structure of the pheromone-binding-protein-bombykol complex. *Chemistry & Biology* **7**, 143-151 (2000).

93. Briand, L., Nespoulous, C., Huet, J.C. & Pernollet, J.C. Disulfide pairing and secondary structure of ASP(1), an olfactory-binding protein from honeybee (*Apis mellifera* L). *Journal of Peptide Research* **58**, 540-545 (2001).

94. Briand, L., Nespoulous, C., Huet, J.C., Takahashi, M. & Pernollet, J.C. Ligand binding and physico-chemical properties of ASP2, a recombinant odorant-binding protein from honeybee (*Apis mellifera* L.). *European Journal of Biochemistry* **268**, 752-760 (2001).

95. Honson, N.S. & Plettner, E. Disulfide connectivity and reduction in pheromone-binding proteins of the gypsy moth, *Lymantria dispar*. *Naturwissenschaften* **93**, 267-277 (2006).

96. Leal, W.S., Nikonova, L. & Peng, G.H. Disulfide structure of the pheromone binding protein from the silkworm moth, *Bombyx mori*. *Febs Letters* **464**, 85-90 (1999).

97. Lartigue, A. et al. Sulfur single-wavelength anomalous diffraction crystal structure of a pheromone-binding protein from the honeybee *Apis mellifera* L. *Journal of Biological Chemistry* **279**, 4459-4464 (2004).

98. Kruse, S.W., Zhao, R., Smith, D.P. & Jones, D.N.M. Structure of a specific alcohol-binding site defined by the odorant binding protein LUSH from *Drosophila melanogaster*. *Nature Structural Biology* **10**, 694-700 (2003).

99. Lartigue, A. et al. The crystal structure of a cockroach pheromone-binding protein suggests a new ligand binding and release mechanism. *Journal of Biological Chemistry* **278**, 30213-30218 (2003).

100. Wogulis, M., Morgan, T., Ishida, Y., Leal, W.S. & Wilson, D.K. The crystal structure of an odorant binding protein from *Anopheles gambiae*: Evidence for a common ligand release mechanism. *Biochemical and Biophysical Research Communications* **339**, 157-164 (2006).

101. Campanacci, V., Longhi, S., Nagnan-Le Meillour, P., Cambillau, C. & Tegoni, M. Recombinant pheromone binding protein 1 from *Mamestra brassicae* (MbraPBP1) - Functional and structural characterization. *European Journal of Biochemistry* **264**, 707-716 (1999).

102. Danty, E. et al. Cloning and expression of a queen pheromone-binding protein in the honeybee: an olfactory-specific, developmentally regulated protein. *Journal of Neuroscience* **19**, 7468-7475 (1999).

103. Maida, R., Proebstl, T. & Laue, M. Heterogeneity of odorant-binding proteins in the antennae of *Bombyx mori*. *Chemical Senses* **22**, 503-515 (1997).

104. Plettner, E., Lazar, J., Prestwich, E.G. & Prestwich, G.D. Discrimination of pheromone enantiomers by two pheromone binding proteins from the gypsy moth *Lymantria dispar*. *Biochemistry* **39**, 8953-8962 (2000).

105. Leal, W.S. Duality monomer-dimer of the pheromone-binding protein from *Bombyx mori*. *Biochemical and Biophysical Research Communications* **268**, 521-529 (2000).

106. Lee, D. et al. NMR structure of the unliganded *Bombyx mori* pheromone-binding protein at physiological pH. *Febs Letters* **531**, 314-318 (2002).

107. Mohanty, S., Zubkov, S. & Gronenborn, A.M. The solution NMR structure of *Antheraea polyphemus* PBP provides new insight into pheromone recognition by pheromone-binding proteins. *Journal of Molecular Biology* **337**, 443-451 (2004).

108. Horst, R. et al. NMR structure reveals intramolecular regulation mechanism for pheromone binding and release. *Proceedings of the National Academy of Sciences of the United States of America* **98**, 14374-14379 (2001).

109. Lautenschlager, C., Leal, W.S. & Clardy, J. *Bombyx mori* pheromone-binding protein binding nonpheromone ligands: Implications for pheromone recognition. *Structure* **15**, 1148-1154 (2007).

110. Zubkov, S., Gronenborn, A.M., Byeon, I.J.L. & Mohanty, S. Structural consequences of the pH-induced conformational switch in *A. polyphemus* pheromone-binding protein: Mechanisms of ligand release. *Journal of Molecular Biology* **354**, 1081-1090 (2005).

111. Lautenschlager, C., Leal, W.S. & Clardy, J. Coil-to-helix transition and ligand release of *Bombyx mori* pheromone-binding protein. *Biochemical and Biophysical Research Communications* **335**, 1044-1050 (2005).

112. Brylinski, M. & Skolnick, J. What is the relationship between the global structures of apo and holo proteins? *Proteins-Structure Function and Bioinformatics* **70**, 363-377 (2008).

113. Leal, W.S. et al. Kinetics and molecular properties of pheromone binding and release. *Proceedings of the National Academy of Sciences of the United States of America* **102**, 5386-5391 (2005).

114. Prestwich, G.D. Bacterial expression and photoaffinity-labeling of a pheromone-binding protein. *Protein Science* **2**, 420-428 (1993).

115. Damberger, F.F., Ishida, Y., Leal, W.S. & Wuethrich, K. Structural basis of ligand binding and release in insect pheromone-binding proteins: NMR structure of *Antheraea polyphemus* PBP1 at pH 4.5. *Journal of Molecular Biology* **373**, 811-819 (2007).

116. McLaughlin, S. The electrostatic properties of membranes. *Annual Review of Biophysics and Biophysical Chemistry* **18**, 113-136 (1989).

117. Kowcun, A., Honson, N. & Plettner, E. Olfaction in the gypsy moth, *Lymantria dispar* - Effect of pH, ionic strength, and reductants on pheromone transport by pheromone-binding proteins. *Journal of Biological Chemistry* **276**, 44770-44776 (2001).

118. Kim, M.S., Repp, A. & Smith, D.P. LUSH odorant-binding protein mediates chemosensory responses to alcohols in *Drosophila melanogaster*. *Genetics* **150**, 711-721 (1998).

119. Bohbot, J., Sobrio, F., Lucas, P. & Nagnan-Le Meillour, P. Functional characterization of a new class of odorant-binding proteins in the moth *Mamestra brassicae*. *Biochemical and Biophysical Research Communications* **253**, 489-494 (1998).

120. Bette, S., Breer, H. & Krieger, J. Probing a pheromone binding protein of the silkmoth *Antheraea polyphemus* by endogenous tryptophan fluorescence. *Insect Biochemistry and Molecular Biology* **32**, 241-246 (2002).

121. Campanacci, V. et al. Revisiting the specificity of *Mamestra brassicae* and *Antheraea polyphemus* pheromone-binding proteins with a fluorescence binding assay. *Journal of Biological Chemistry* **276**, 20078-20084 (2001).

122. Inkster, J.A.H. et al. Synthesis of disparlure analogues, using resolution on microcrystalline cellulose triacetate-I. *Tetrahedron-Asymmetry* **16**, 3773-3784 (2005).

123. Riviere, S. et al. A pheromone-binding protein from the cockroach *Leucophaea maderae*: cloning, expression and pheromone binding. *Biochemical Journal* **371**, 573-579 (2003).

124. Zhou, J.J. et al. Revisiting the odorant-binding protein LUSH of *Drosophila melanogaster*: evidence for odour recognition and discrimination. *Febs Letters* **558**, 23-26 (2004).

125. Du, G.H. & Prestwich, G.D. Protein structure encodes the ligand-binding specificity in pheromone-binding-proteins. *Biochemistry* **34**, 8726-8732 (1995).

126. van den Berg, M.J. & Ziegelberger, G. On the function of the pheromone-binding protein in the olfactory hairs of *Antheraea polyphemus*. *Journal of Insect Physiology* **37**, 79-85 (1991).

127. Syed, Z., Ishida, Y., Taylor, K., Kimbrell, D.A. & Leal, W.S. Pheromone reception in fruit flies expressing a moth's odorant receptor. *Proceedings of the National Academy of Sciences of the United States of America* **103**, 16538-16543 (2006).

128. Pophof, B. Moth pheromone binding proteins contribute to the excitation of olfactory receptor cells. *Naturwissenschaften* **89**, 515-518 (2002).

129. Mitsuno, H. et al. Identification of receptors of main sex-pheromone components of three Lepidopteran species. *European Journal of Neuroscience* **28**, 893-902 (2008).

130. Xu, P.X., Atkinson, R., Jones, D.N.M. & Smith, D.P. Drosophila OBP LUSH is required for activity of pheromone-sensitive neurons. *Neuron* **45**, 193-200 (2005).

131. Krieger, J. & Breer, H. Olfactory reception in invertebrates. *Science* **286**, 720-723 (1999).

132. Pelosi, P. Odorant-binding proteins. *Critical Reviews in Biochemistry and Molecular Biology* **29**, 199-228 (1994).

133. Krieger, J., Raming, K. & Breer, H. Cloning of genomic and complementary-DNA encoding insect pheromone-binding proteins - Evidence for microdiversity. *Biochimica Et Biophysica Acta* **1088**, 277-284 (1991).

134. Adler, V.E., Bierl, B.A., Beroza, M. & Sarmient.R. Electroantennograms and field attraction of gypsy moth *Lepidoptera Lymantriidae* sex attractant disparlure and related compounds. *Journal of Economic Entomology* **65**, 679-680 (1972).

135. Bierl, B.A., Beroza, M. & Collier, C.W. Potent sex attractant of gypsy moth - Its isolation, identification, and synthesis. *Science* **170**, 87-89 (1970).

136. Bierl, B.A., Beroza, M. & Collier, C.W. Isolation, identification, and synthesis of gypsy moth *Lepidoptera lymantriidae* sex attractant. *Journal of Economic Entomology* **65**, 659-664 (1972).

137. Vite, J.P., Klimetzek, D., Loskant, G., Hedden, R. & Mori, K. Chirality of insect pheromones - Response interruption by inactive antipodes. *Naturwissenschaften* **63**, 582-583 (1976).

138. Hansen, K. Discrimination and production of disparlure enantiomers by the gypsy moth and the nun moth. *Physiological Entomology* **9**, 9-18 (1984).

139. Grant, G.G., Langevin, D., Liska, J., Kapitola, P. & Chong, J.M. Olefin inhibitor of gypsy moth, *Lymantria dispar*, is a synergistic pheromone component of nun moth, *L. monacha*. *Naturwissenschaften* **83**, 328-330 (1996).

140. Paduraru, P.A. et al. Synthesis of substituted alkoxy benzene minilibraries, for the discovery of new insect olfaction or gustation inhibitors. *Journal of Combinatorial Chemistry* **10**, 123-134 (2008).

141. Pace, C.N., Vajdos, F., Fee, L., Grimsley, G. & Gray, T. How to measure and predict the molar absorption-coefficient of a protein. *Protein Science* **4**, 2411-2423 (1995).

142. Flecha, F.L.G. & Levi, V. Determination of the molecular size of BSA by fluorescence anisotropy. *Biochemistry and Molecular Biology Education* **31**, 319-322 (2003).

143. Kublickas, R., Jariene, G. & Lasas, L. Investigation of the monomeric and oligomeric molecular forms of human growth hormone and poly-L-lysine using fluorescence anisotropy measurement method. *Polymer Bulletin* **56**, 193-199 (2006).

144. Tanford, C. *Physical Chemistry of Macromolecules*, 317-456 (John Wiley & Sons, Inc., New York, 1961).

145. Kuntz, I.D. & Kauzmann, W. Hydration of proteins and polypeptides. in *Advances in Protein Chemistry*, Vol. 28 239-345 (Academic Press, New York, 1974).

146. Perkins, S.J. Protein volumes and hydration effects - The calculations of partial specific volumes, neutron-scattering matchpoints and 280-nm absorption-coefficients for proteins and glycoproteins from amino-acid-sequences. *European Journal of Biochemistry* **157**, 169-180 (1986).

147. Valeur, B. *Molecular fluorescence : principles and applications*, xiv, 387 p. (Wiley-VCH, Weinheim ; New York, 2002).

148. Wojtasek, H. & Leal, W.S. Conformational change in the pheromone-binding protein from Bombyx mori induced by pH and by interaction with membranes. *Journal of Biological Chemistry* **274**, 30950-30956 (1999).

149. Isin, E.M. & Guengerich, F.P. Multiple sequential steps involved in the binding of inhibitors to cytochrome p450 3A4. *Journal of Biological Chemistry* **282**, 6863-6874 (2007).

150. Venyaminov, S.Y. & Vassilenko, K.S. Determination of protein tertiary structure class from circular-dichroism spectra. *Analytical Biochemistry* **222**, 176-184 (1994).

151. Fersht, A. *Structure and mechanism in protein science : a guide to enzyme catalysis and protein folding*, xxi, 631 p. (W.H. Freeman, New York, 1999).

152. Birks, J.B. *Photophysics of aromatic molecules*, (Wiley-Interscience, New York, 1970).

153. Eftink, M.R. & Ghiron, C.A. Exposure of tryptophanyl residues in proteis - Quantitative determination by fluorescence quenching studies. *Biochemistry* **15**, 672-680 (1976).

154. Lehrer, S.S. Solute perturbation of protein fluorescence - Quenching of tryptophyl fluorescence of model compounds and of lysozyme by iodide ion. *Biochemistry* **10**, 3254-3263 (1971).

155. Thode, A.B., Kruse, S.W., Nix, J.C. & Jones, D.N.M. The role of multiple hydrogen-bonding groups in specific alcohol binding sites in proteins: Insights from structural studies of LUSH. *Journal of Molecular Biology* **376**, 1360-1376 (2008).

156. Dickens, J.C., Oliver, J.E. & Mastro, V.C. Response and adaptation to analogs of disparlure by specialist antennal receptor neurons of gypsy

moth, *Lymantria dispar*. *Journal of Chemical Ecology* **23**, 2197-2210 (1997).

157. Abraham, D., Lofstedt, C. & Picimbon, J.F. Molecular characterization and evolution of pheromone binding protein genes in Agrotis moths. *Insect Biochemistry and Molecular Biology* **35**, 1100-1111 (2005).

158. Wang, G.R., Wu, K.M. & Guo, Y.Y.N. Molecular cloning and bacterial expression of pheromone binding protein in the antennae of *Helicoverpa armigera* (Hubner). *Archives of Insect Biochemistry and Physiology* **57**, 15-27 (2004).

159. de Santis, F. et al. Molecular cloning and in situ expression patterns of two new pheromone-binding proteins from the corn stemborer *Sesamia nonagrioides*. *Journal of Chemical Ecology* **32**, 1703-1717 (2006).

160. Xiu, W.M. & Dong, S.L. Molecular characterization of two pheromone binding proteins and quantitative analysis of their expression in the beet armyworm, *Spodoptera exigua* Hubner. *Journal of Chemical Ecology* **33**, 947-961 (2007).

161. Xiu, W.M., Zhou, Y.Z. & Dong, S.L. Molecular characterization and expression pattern of two pheromone-binding proteins from *Spodoptera litura* (Fabricius). *Journal of Chemical Ecology* **34**, 487-498 (2008).

162. Plettner, E. The peripheral pheromone olfactory system in insects: targets for species-selective insect control agents. in *Insect Pheromone Biochemistry and Molecular Biology: The biosynthesis and detection of pheromones and plant volatiles* (eds. Bolmquist, G.J. & Vogt, R.G.) 477-507 (Elsevier Academic Press, London, 2003).

163. Kaissling, K.E. & Thorson, J. *Insect olfactory sensilla: structural, chemical and electrical aspects of the functional organization*, (Elsevier/North-Holland Biomedical Press, Amsterdam, 1980).